Karlsruhe Institute of Technology

Tritium Laboratory Karlsruhe

First measurement of the tritium viscosity in a temperature range from 100 K to 300 K

Zur Erlangung des akademischen Grades eines

Doktors der Naturwissenschaften (Dr. rer. nat.)

von der KIT-Fakultät für Physik
des Karlsruher Instituts für Technologie (KIT)

angenommene

Dissertation

von

M. Sc. Johanna Maria Wydra geb. Renner

aus Bad Friedrichshall

Erste Gutachterin: Prof. Dr. Kathrin Valerius
Zweiter Gutachter: Prof. Dr. Ulrich Husemann
Tag der mündlichen Prüfung: 24. Januar 2025

Abstract

The viscosity of tritium is a crucial material property needed for a wide range of theoretical and technological scientific fields, starting from fluid dynamics including vacuum science, over astroparticle physics experiment like the Karlsruhe Tritium Neutrino Experiment (KATRIN) to nuclear fusion for energy. Values found in literature are either ab initio calculated by a classical approach neglecting quantum mechanical effects [Son16], or extrapolated from hydrogen (H_2) or deuterium (D_2) by the square root of the mass ratios [Kuc18], both with uncertainties of 2 % to 10 %. The lack of measurement data on material properties of tritium is caused by the combination of it being an isotopologue of hydrogen, the smallest existing molecule, which permeates even through metal, and its radioactive nature, causing not only safety issues which have to be solved, but also radiolytic reactions. For the measurement of the viscosity of tritium, a laboratory is needed with the license to handle a significant amount of tritium. The Tritium Laboratory Karlsruhe (TLK) is a unique facility in Europe with a license to handle 40 g of tritium with the ability to purify tritium up to 99 %, enabling the measurement of material properties such as the viscosity of tritium. Within this work, the viscosity of T_2 in the zero-density limit is measured with an accuracy of 2.5 % in a temperature range from 100 K to 300 K. These measurements first enable a test of the trueness of the aforementioned calculations, and second enlarge the testbed for ab initio calculations regarding small non-spherical molecules including plasmas, caused by the radioactivity of T_2.

Zusammenfassung

Die Viskosität von Tritium ist für viele Bereiche unerlässlich, sei es ein allgemeines Forschungsgebiet wie die Fluiddynamik oder die Vakuumtechnik, oder auch spezifische Forschungsbereiche wie die Fusionsforschung zur Energieerzeugung sowie große Teilchenphysik-Experimente wie das Karlsruhe Tritium Neutrino Experiment (KATRIN). In der Literatur lassen sich derzeit Werte finden, die auf zwei verschiedene Arten berechnet werden: Im ersten Fall handelt es sich um die Extrapolation der Viskosität von Wasserstoff (H_2) oder Deuterium (D_2) über eine Skalierung durch das Massenverhältnis der Moleküle. Im zweiten Fall handelt es sich um tatsächliche ab-initio-Berechnungen, die jedoch auf klassischer Mechanik basieren. Dadurch ignorieren sie quantenmechanische Effekte, die vor allem bei Temperaturen unterhalb von 300 K relevant werden. Für die Berechnungen werden Unsicherheiten von 2 % bis 10 % angegeben, die für die extrapolierten Werte allerdings nur geschätzt werden. Teil dieser Arbeit ist es, ergänzend die Viskosität von T_2 zu messen, um die theoretischen Werte zu validieren. Zusätzlich wird an die Messergebnisse eine Funktion angepasst, mit der der Temperaturverlauf der Viskosität beschrieben werden kann.

In Kapitel 2 wird herausgearbeitet, wie die Viskosität Einfluss auf aktuelle Forschung nimmt. Hierbei wird gezeigt, dass die Viskosität von T_2 in der Vakuumtechnik Anwendung findet, vor allem bei der Erweiterung des Testdatensatzes zur Überprüfung theoretischer Berechnungen zu Flusseigenschaften verdünnter Gase.
Des Weiteren wird die Viskosität in der Fusionsforschung benötigt, zum einen, um tritiumführende Komponenten, vor allem Pumpen und Destillationskolonnen, optimieren zu können. Zum anderen ist hier die Bilanzierung von äußerster Wichtigkeit. Da es für ein Fusionskraftwerk weder wirtschaftlich noch technisch umsetzbar ist, in regelmäßigen Abständen alles an T_2 zu sammeln und zu vermessen, um die vorhandene Menge an Tritium zu bestimmen, ist es wichtig, möglichst viele Informationen über T_2 zu sammeln, um Berechnungen zur Bilanzierung zu verbessern.
Das KATRIN-Experiment hat das Ziel, die Masse des Elektron-Antineutrinos mit bisher unerreichter Genauigkeit zu messen. Dazu wird der Betazerfall von Tritium ausgenutzt, bei dem ein Elektron sowie ein Elektron-Antineutrino entstehen. Da das Neutrino kaum Wechselwirkungen eingeht, wird das Energiespektrum des Zerfallselektrons gemessen, um daraus auf die Masse des Neutrinos zu schließen. Die dafür benötigte hochstabile Tritiumquelle ist in Form eines 10 m langen Strahlrohrs realisiert, in dessen Mitte T_2 eingespeist und an beiden Enden abgepumpt wird. Das so zirkulierende T_2 bildet dabei eine konstante Dichteverteilung entlang der Quelle aus. Diese Dichteverteilung ist wichtig für die Datenanalyse, kann aber nur integral gemessen werden. Zur Bestimmung der Verteilung werden Simulationen benötigt, die wiederum die Viskosität von T_2 als Eingabewert erfordern.

In Kapitel 3 werden die Grundlagen der Strömungslehre verdünnter Gase kurz umrissen, bevor verschiedene Messmethoden zur Bestimmung der Viskosität von Fluiden erklärt werden. Aufgrund der Einschränkungen durch den anvisierten Temperatur- und Druckbereich sowie der Kompatibilität zu T_2 mit all seinen durch die Radioaktivität hervorgerufenen Anforderungen an Material und Sicherheit des Systems fällt die Wahl auf ein Rotationsvakuummeter, die Spinning Rotor Gauge (SRG). Um die späteren Messungen besser einordnen zu können, werden hier auch die bisherigen Messungen der Viskosität von H_2 und D_2 aufgeführt und genauer auf die Berechnungsart der bisherigen Literaturwerte für die Viskosität von Tritium eingegangen.

Im darauffolgenden Kapitel 4 wird der kryogene Viskositätsmessaufbau (Cryo-ViMA) beschrieben. Dabei werden zum einen die Arbeitsbereiche für Temperatur und Druck abgesteckt, zum anderen werden zwei unterschiedliche Messprozeduren vorgestellt. Hierbei wird unterschieden, ob die Temperatur konstant gehalten und der Druck zyklisch variiert wird, oder umgekehrt der Druck zu Anfang festgelegt wird und ein Temperaturzyklus durchlaufen wird. Beide Vorgehensweisen liefern gute Ergebnisse, mit dem Unterschied, dass Letzteres interessanter ist, wenn die Viskosität in Abhängigkeit von der Temperatur ermittelt werden soll, was im Fall dieser Arbeit das bevorzugte Vorgehen ist.

In Kapitel 5 werden die Unsicherheiten der einzelnen Messgrößen und deren Einfluss auf die Viskositätsmessung dargelegt. Es wird gezeigt, dass die beiden größten Unsicherheiten durch den Radius des Rotors der SRG und die Temperatur gegeben sind. Dabei beeinflusst der Radius den Wert der berechneten Viskosität, während die Temperatur zwar nicht direkt in der Analyse vorkommt, jedoch eine Rolle spielt, wenn die Viskositätswerte der Messtemperatur zugeordnet werden. Mit dem Wissen über die Messgenauigkeit wird Cryo-ViMA mit Helium kalibriert, um einen apparaturspezifischen Kalibrierfaktor zu bestimmen. Dabei wird gezeigt, dass dieser leicht mit der Temperatur variiert und in erster Näherung eine lineare Abhängigkeit angenommen werden kann.

In Kapitel 6 werden zunächst Messungen der Viskosität mit H_2 und D_2 durchgeführt und mit den jeweiligen Literaturdaten verglichen, um sicherzugehen, dass die vorigen Betrachtungen zur Messgenauigkeit gültig sind. Es wird gezeigt, dass die Messergebnisse im Rahmen ihrer Messgenauigkeit mit den Literaturdaten übereinstimmen. In einem zweiten Schritt wird Cryo-ViMA mit T_2 in Betrieb genommen. Hierzu wird zunächst T_2 mit einer Reinheit von etwa 95 % genutzt, da bei erstmaligem Kontakt mit T_2 eine höhere Verunreinigung durch radiolytische Reaktionen mit den Wänden des Messsystems zu erwarten ist. Erst nachdem das System vollständig in Betrieb genommen ist, wird eine finale Messung mit hochreinem T_2 (99 %) durchgeführt. Im Vergleich zu den bisherigen Literaturwerten zur Viskosität von T_2 liegen die Ergebnisse der Messung signifikant niedriger, wie in Abbildung 1 zu sehen ist. Die Abweichungen zwischen Literatur und Messung liegen je nach Literaturwert zwischen 5 % und 12 %. Damit wird gezeigt, dass eine einfache Extrapolation der Viskosität von H_2 oder D_2 nicht genügt. Außerdem liegt auch der ab-initio berechnete Wert für die Viskosität von T_2 knappe 10 % über dem Messwert, was vermuten lässt, dass die Abweichung zur gängigen Literatur nicht nur durch quantenmechanische Effekte zu erklären ist, sondern möglicherweise auch in der radioaktiven Natur von T_2 zu suchen ist. In einem letzten Schritt wird eine Funktion an

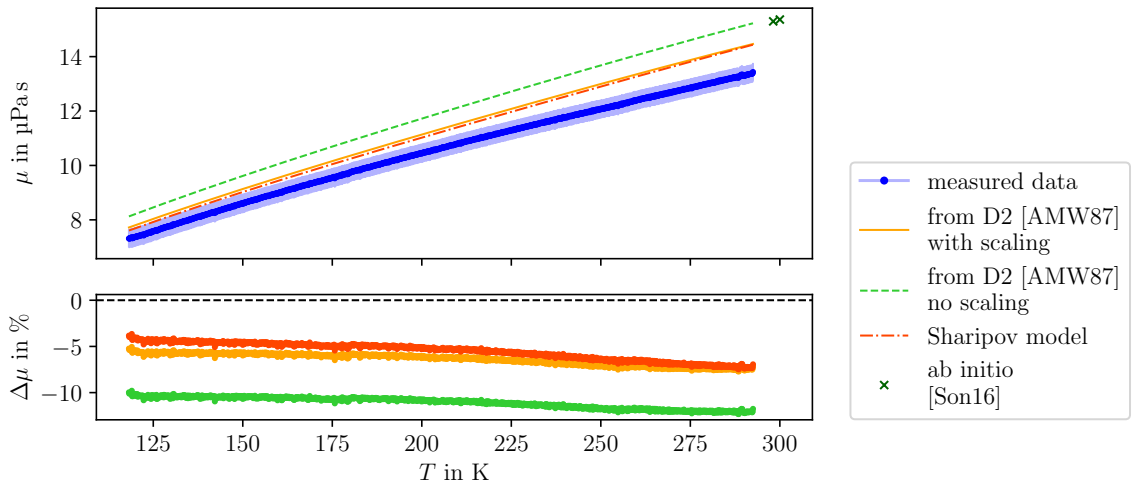

Abbildung 1.: Vergleich der Messergebnisse mit einer Auswahl an theoretisch berechneten Werten für die Viskosität von T_2. Hierbei gilt $\Delta\mu = \mu_{\text{mess}} - \mu_{\text{theo}}$.

die Messdaten angepasst, sodass die Viskosität μ von T_2 sich in Abhängigkeit von der Temperatur T beschreiben lässt als

$$\mu = 0.78\sqrt{T} + 0.009 \cdot T^{-2.26}\,. \tag{1}$$

Abschließend wird in Kapitel 7 nochmals auf den Einfluss dieser Messungen auf die aktuelle Forschung eingegangen und gezeigt, dass diese Ergebnisse nicht nur aktuelle Simulationen für Fusion und Teilchenphysik verbessern, sondern auch eine bessere Datenlage für künftige theoretische Berechnungen von Transportgrößen wie der Viskosität liefern.

Nach der Zusammenfassung in Kapitel 8 wird im Ausblick noch geschildert, dass mit Cryo-ViMA nicht nur die Viskosität von T_2 bis 100 K mit einer Messgenauigkeit von 2.5 % gemessen werden kann, sondern dass auch noch eine Modifikation geplant ist, mit der es möglich sein wird, auf eine Temperatur von 77 K zu kommen. Zusätzlich ermöglicht der Messaufbau die Untersuchung von Reaktionsgeschwindigkeiten über die Veränderung der Entschleunigungsrate bei Veränderung der Gaszusammensetzung und dadurch der Viskosität.

Diese Arbeit zeigt, dass zum einen die Viskosität von Tritium nicht einfach zu berechnen ist, die Messung jedoch akkurate Daten liefert mit einer Messgenauigkeit von 2.5 %. Zum anderen ist diese Arbeit auch ein gutes Beispiel dafür, wie aus einem Experiment für einen bestimmten Zweck weitere Möglichkeiten für weiterführende Untersuchungen geschaffen werden.

Contents

Abstract . . . . . **i**

Zusammenfassung . . . . . **iii**

List of Figures . . . . . **xi**

List of Tables . . . . . **xiii**

List of Acronyms . . . . . **xv**

List of Symbols . . . . . **xvii**

1. Introduction **1**

2. Necessity of the knowledge on tritium viscosity **3**
2.1. The viscosity of gases in vacuum science and technology 3
2.2. Tritium in Fusion 3
2.3. The tritium viscosity in the KATRIN experiment 5
2.3.1. KATRIN Working principle 5
2.3.2. The windowless gaseous tritium source 7
2.3.3. The influence of the tritium viscosity on the column density . . . 7
2.4. Tritium viscosity - the missing parameter 9

3. Viscosity of hydrogen isotopologues **11**
3.1. Fluid dynamics in vacuum technology 11
3.1.1. Parameters for the classification of a fluid system 11
3.1.2. Transport coefficients for gases in the transition regime 13
3.2. The viscometry of gases 14
3.3. Previous measurements on the viscosity of non-tritiated hydrogen isotopologues 17
3.4. Current values for the viscosity of tritium from theoretical calculations . 18
3.5. Goals of this work 20

4. Design of Cryo-ViMA - the Cryogenic VIscosity Measurement Apparatus 21
4.1. Design parameters for measuring the viscosity of tritium 21
4.1.1. Scientific design parameters 21
4.1.2. Technical design parameters 22
4.1.3. Temperature range 23

4.1.4. Pressure range . . . 23
4.2. The spinning rotor gauge (SRG) . . . 24
4.2.1. Measurement and analysis concept . . . 24
4.2.2. Technical description . . . 26
4.3. The Cryo-ViMA setup . . . 27
4.3.1. The primary system . . . 27
4.3.2. The cooling system . . . 27
4.3.3. Temperature instrumentation . . . 28
4.3.4. Pressure instrumentation . . . 29
4.3.5. Sample preparation with TriHyDe . . . 35
4.4. Measurement procedure . . . 35
4.4.1. Pressure cycling . . . 37
4.4.2. Temperature cycling . . . 38

5. Accuracy of the viscosity measurements with Cryo-ViMA . . . 41
5.1. Quantities influencing the accuracy of the Cryo-ViMA setup . . . 41
5.1.1. Isotopic purity . . . 42
5.1.2. Dimensions of the sphere and evacuated cylinder . . . 42
5.1.3. Angular deceleration rate . . . 43
5.1.4. Pressure . . . 43
5.1.5. Temperature . . . 44
5.1.6. Calibration factor C_0 . . . 46
5.2. Thermal simulations of the Cryo-ViMA primary system . . . 49
5.2.1. Thermal simulation of the SRG with ANSYS® . . . 50
5.2.2. Fluid simulation of the SRG with ANSYS® . . . 52
5.2.3. Influence of the temperature gradient on the viscosity . . . 54
5.3. Characterization and calibration of Cryo-ViMA with helium . . . 56

6. Experimental driven model development for the viscosity of T_2 . . . 59
6.1. Reference measurements with H_2 and D_2 . . . 59
6.1.1. Protium . . . 59
6.1.2. Deuterium . . . 62
6.2. Measurement of the viscosity of T_2 . . . 63
6.2.1. T_2 commissioning phase . . . 63
6.2.2. Measurement campaign with high purity T_2 . . . 67
6.3. Comparison of the measured T_2 viscosity to literature values . . . 68
6.4. Model development for the tritium viscosity at low pressures . . . 71

7. Impact of viscosity measurements on current and future science . . . 75
7.1. Impact on vacuum science . . . 75
7.2. Impact on fusion science . . . 76
7.3. Impact on the KATRIN experiment . . . 77

8. Summary and Outlook . . . 79

A. Appendix **83**
A.1. Reynolds number 83
A.2. Additional plots for the viscosity measurements 83
A.3. Velocity slip coefficient and tangential momentum accommodation coefficient 87

Bibliography **89**

List of Figures

1. Vergleich der Messergebnisse mit einer Auswahl an theoretisch berechneten Werten für die Viskosität von T_2. Hierbei gilt $\Delta\mu = \mu_{\text{mess}} - \mu_{\text{theo}}$. . . . v

2.1. Overview of fluid dynamics topics. . . . 4
2.2. The KATRIN experiment. . . . 6
2.3. The KATRIN Loops. . . . 8
2.4. The Column Density Profile of the WGTS. . . . 9

3.1. Different types of viscometry. . . . 15

4.1. KATRIN Loops parameters. . . . 30
4.2. Knudsen boarders for SRG-viscosity measurements. . . . 31
4.3. The SRG magnet system. . . . 32
4.4. Flow diagram of the Cryo-ViMA setup. . . . 32
4.5. CAD cut of the Cryo-ViMA setup. . . . 33
4.6. Thermal cycle of Cryo-ViMA. . . . 34
4.7. Block diagrams for pressure and temperature cycling measurements. . . . 36
4.8. Measurement cycle of the SRG. . . . 37
4.9. Pressure cycling with the SRG. . . . 40

5.1. Rotor speed of the SRG rotor during one thermal cycle. . . . 47
5.2. Simulated temperature difference for He, H_2 and D_2. . . . 48
5.3. Basic FEM problem 50
5.4. Geometry used for thermal simulation 50
5.5. Thermal simulation of the SRG. . . . 53
5.6. Gas flow around the rotating sphere 54
5.7. Calibration of the SRG. . . . 57

6.1. Viscosity of protium. . . . 61
6.2. Viscosity of deuterium. . . . 63
6.3. Commissioning phase of Cryo-ViMA. . . . 64
6.4. RGA measurement of Run031. . . . 65
6.5. Viscosity of tritium - first measurement. . . . 66
6.6. Viscosity of tritium. . . . 68
6.7. Comparison of extrapolated to measured values for the viscosity of tritium. 69
6.8. Theory comparison of the viscosity of tritium. . . . 73

7.1. The Column Density Profile of the WGTS. . . . 78

A.1. Viscosity of deuterium. . . . 84

A.2. Viscosity of tritium from directly measured C_0 values. 85
A.3. Comparison of the models for fitting the tritium viscosity. 86
A.4. Velocity slip coefficient and tangential momentum accommodation coefficient. 88

List of Tables

2.1. Properties of tritium 10

3.1. Summary of the basic features of the different viscometers 17

3.2. Previous measured values of the viscosity μ of He, H_2, D_2 and HD 18

4.1. Technical data of the MKS instruments SRG3 26

5.1. Uncertainties of the Cryo-ViMA setup 41

5.2. Calibration results of the temperature sensors used in the Cryo-ViMA setup. 45

5.3. Input parameters and results of thermal simulations 55

6.1. Fit results of the residuals for the H_2 and D_2 measurements. 62

6.2. Fit results for the empirical temperature dependent viscosity function . . 74

List of Acronyms

A-Loop analyzing loop.

BGA binary gas analyzer.

BIXS beta-induced X-ray spectrometry.

CD column density.

CPS cryogenic pumping section.

Cryo-ViMA Cryogenic Viscosity Measurement Apparatus.

DCR normalized deceleration rate.

DPS differential pumping section.

FEM finite elements method.

FPD focal plane detector.

HAZOP hazard and operability studies.

ISS isotope separation system.

KATRIN Karlsruhe Tritium Neutrino Experiment.

LARA LArge-RAman system.

MAC-E Filter magnetic adiabtic collimator and electrostatic filter.

P-Loop processing loop.

Pt100 platinum 100 Ω temperature sensor.

RGA residual gas analyzer.

SRG spinning rotor gauge.

TLK Tritium Laboratory Karlsruhe.

TriHyDe Tritium Hydrogen Deuterium experiment.

TTS tritium transfer system.

UHV ultra high vacuum.

WGTS windowless gaseous tritium source.

List of Symbols

C_0 Parameter describing the flow of a sphere rotating inside a cylinder with rotation axis perpendicular to the cylinder axis.

D Torque on the SRG rotor.

F Force.

I Moment of inertia of the SRG rotor.

K_n Knudsen-number.

M The molar mass of the investigated gas.

Q Heat of the rotating sphere.

Re Reynolds-number.

R Ideal gas constant.

T Temperature.

$\Delta(\frac{\mathrm{d}\Omega}{\mathrm{d}t}/\Omega)$ Deviation on the normalized deceleration rate of the SRG rotor.

ΔT Temperature difference.

$\Omega^{(2,2)^*}$ Collision integral.

Ω The angular velocity of the SRG rotor.

Φ_{ij} Weighting factor for the calculation of mixture viscosities.

α Thermal expansion coefficient of the SRG rotor.

β Angle between the relaxed and stressed tube.

$\dot{Q}$ Heat flux.

ϵ Well-depth of the potential.

$\frac{\Delta T}{dx}$ Temperature gradient.

$\frac{\Delta v}{dx}$ Velocity gradient.

λ_Q Thermal conductivity.

λ Mean-free path.

Pr Prandtl number.

μ_{mix} Viscosity of a gas mixture.

μ Viscosity.

$\frac{\mathrm{d}\Omega}{\mathrm{d}t}/\Omega$ Normalized deceleration rate of the SRG rotor.

$\overline{v}_r$ Average relative thermal speed of the gas particles in equilibrium.

$\overline{v}$ Average thermal speed of the gas particles in equilibrium.

ρ_g Density of the sample gas.

ρ Density of the SRG rotor.

σ_{tot} Total cross-section.

σ Interaction cross-section.

a_1 Radius of the SRG rotor.

a_2 Radius of the cylinder surrounding the SRG rotor.

a Scaling factor of the empirical fit function.

b Offset of the empirical fit function.

c_V Heat capacity at constant volume.

c_m Velocity slip coefficient.

c Specific heat of the SRG rotor.

d Diameter of a gas particle.

d Exponent of the empirical fit function.

k_B Boltzmann constant.

m_g The mass of the investigated gas.

m The mass of the SRG rotor.

p Pressure.

r Radius.

v Averaged velocity of the gas flow.

x_i Molar fraction of component i.

y_0 Offset of the linear fit to calculate the viscosity.

1. Introduction

The viscosity of tritium is a crucial property with applications across multiple fields of research, including nuclear fusion research and development, and astroparticle physics experiments like the Karlsruhe Tritium Neutrino Experiment (KATRIN). Tritium is the heaviest hydrogen isotopologue, consisting of a proton and two neutrons in the nucleus and an electron in the shell. Due to the neutron excess it decays via beta-decay, where one of the neutrons is converted to a proton by emitting an electron and an electron anti-neutrino. The relatively low half-life time of tritium of 12.3 a [LU00] yields a high specific activity. Combined with the low endpoint energy, this is the ideal candidate for the direct neutrino mass measurement[Bor08], as it is done with the KATRIN experiment, which will be explained in section 2.3.

Caused by the highest nuclear fusion reaction cross section at lower temperatures, a mix of tritium (T_2) and deuterium (D_2) is the first choice as fuel for fusion power plants, see section 2.2. Crucial aspect of the success of fusion for energy is the continuous recycling of tritium. For designing and improving such systems extensive simulations are needed, but input data like equation of state and transport coefficients for tritiated molecules are scarce. For better tritium inventory management, higher accuracy in fluid simulations is mandatory, as this is needed for the optimization of tritium handling components, as well as gas dynamics research. For improved fluid simulations, the viscosity of tritium is crucial.

Current existing values are either extrapolated from the viscosity of the lighter hydrogen isotopologues, or are ab initio calculations but only by classical approaches, neglecting quantum mechanical effects, which become increasingly important with decreasing temperatures. These values are given with accuracies in a range of 2 % to 10 % for ab initio and extrapolated values, respectively [Son16; Kuc16]. To improve the accuracy of these values and test the validity of the calculations and the uncertainty estimation, this work focuses on the measurement of the tritium viscosity in a temperature range of 100 K to 300 K in the zero-density limit with the Cryogenic Viscosity Measurement Apparatus (Cryo-ViMA). As the accuracy for calculations of the current values is 2 % to 10 %, the measurement shall improve the knowledge on the tritium viscosity to 2 % accuracy.

The KATRIN tritium loop system has temperatures from 673 K at the permeators down to 80 K in the tritium source, and pressures between a few 100 Pa and ultra-high vacuum, hence the temperature is chosen close to these values with a focus on the low temperature range, to get closer to the tritium source working conditions. By going up to 300 K, the ab initio calculations can still be compared with the measurement. For such measurements, a unique facility is needed, which is capable to handle a significant amount of tritium, to measure its properties. The Tritium Laboratory Karlsruhe (TLK) is the only such facility in Europe, with a license to handle 40 g of tritium [KIT23]. It hosts a whole infrastructure for tritium storage, handling, exhaust processing, isotope separation and tritium analytics.

The Cryo-ViMA setup is coupled to the Tritium Hydrogen Deuterium experiment (TriHyDe), which is a facility to accurately produce and analyze gas-mixtures of all hydrogen isotopologues and helium [Nie21]. For the measurement a setup based on a spinning rotor gauge is developed, which is not only tritium compatible, but also able to operate at temperatures down to 77 K [Wyd22]. With this setup, accuracies of around 2 % are achievable, meeting the requirements of the planned measurements.

Chapter 2 is focused on the question, what the viscosity of tritium is needed for, thereby giving overviews of fusion science and the KATRIN experiment. In chapter 3 a brief introduction to fluid dynamics and the transport properties is given, before viscometry is explained, leading to the choice of the spinning rotor gauge (SRG) for the measurement of the viscosity of tritium, which is based on tritium compatibility, cryogenic compatibility and the adequate pressure range of the measurement. The design constraints of a tritium handling experiment, which are compatibility to ultra-high vacuum, explosion protection and radiolytic resistance, are given in chapter 4 and the final setup is shown together with the measurement and analysis procedure. Chapter 5 is focused on the accuracy of the measurements conducted with the Cryo-ViMA setup, which is limited by the isotopic purity of T_2, the thermal gradient inside the SRG, the dimensions of the rotor, the pressure measurement and the calibration accuracy. The measurement of the viscosity of hydrogen and deuterium for testing the uncertainty budget and calibration, as well as the final tritium measurement campaign are depicted in chapter 6. Finally the selected data is used to build a data driven model for the viscosity of tritium in the zero-density limit for a temperature range from 100 K to 300 K, as shown in section 6.4. The impact of these measurement results on the previously listed research topics is given in chapter 7, before in chapter 8 this work is summarized together with an outlook of future research planned with the Cryo-ViMA setup.

2. Necessity of the knowledge on tritium viscosity

The viscosity of tritium is a crucial property to design tritium processing systems, like cryogenic distillation, vacuum and roughing pumping systems, gas chromatography systems, getter and molecular sieving systems, and, in special cases like KATRIN, the windowless gaseous tritium source. It has not been measured to date and the currently available, complex ab-initio calculations possess high uncertainties of 5 % to 10 % [Kuc18]. While the calculation of thermodynamic properties has reached high accuracy in the ab initio modeling, transport properties like viscosity that cannot be derived by the partition-function alone but need structural information and interaction models are way more complex and therefore have higher uncertainties. In this chapter a short summary of the research topics in need for the tritium viscosity is given.

2.1. The viscosity of gases in vacuum science and technology

Vacuum science and technology is a specialized sector of general fluid dynamics. Figure 2.1 shows a rough sketch of different sub-categories of fluid dynamics. For gaseous media, one can divide the field into above atmospheric pressure (pneumatics) [Gro06] and below atmospheric pressure (vacuum) [Jou18; Unr13]. In both cases, the gas flow is important for the efficiency of the setup or calculation under investigation and is always dependent on the gas species and therefore on the viscosity, which describes the momentum transport within the medium. Whenever the fluid dynamics have to be calculated, the viscosity is needed. Prior to the manufacturing of a prototype, simulations are conducted to estimate the performance and refine geometries or workflows. These simulations need the viscosity as an input parameter. Latest works concerning such developments can be found for example in [TD21].

2.2. Tritium in Fusion

To achieve the climate goals and to have affordable and clean energy for humanity an intelligent mix of energy sources is needed. Fusion energy is CO_2 neutral, which is mandatory for new energy sources during times of climate crises [Sch01; Gi20]. Therefore fusion is a valuable candidate to deliver reliable base load electric and thermal power to the grid to back up other renewable energy sources [Sch01; Cla23; ITE; Fam24]. Over the last few years it gained a lot of publicity through the increasing amount of reached milestones

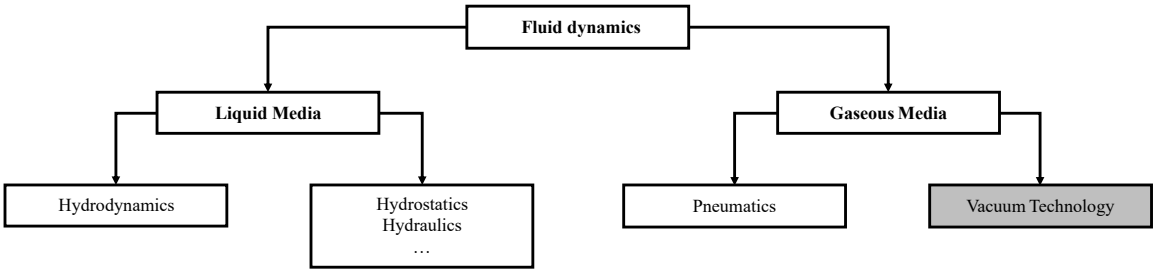

Figure 2.1.: **Overview of Fluiddynamics topics.** Similar diagrams can be found for example in [Bsc18].

(see e.g. [Zyl21; Atz22; Cle]), and many new startup companies like Commonwealth Fusion Systems, Tokamak Energy, Proxima Fusion, and Gauss Fusion, to name only a few. In this section the fusion reaction and a brief explanation of the fusion fuel cycle is given. The crux of fusion reactions is that the mass of the products is smaller than the mass of the educts, leading to an energy release through Einstein's formula $E = mc^2$ [Cla23; Sta12]. The nuclear fusion reaction with the highest fusion cross-section at low thermal energies of a few 10 keV, corresponding to ≈100 000 000 K [SH11; Sta12] is

$$\mathrm{T} + \mathrm{D} \rightarrow {}^{4}\mathrm{He} + \mathrm{n} + 17.6\,\mathrm{MeV}\ [\mathrm{SH11; MRS79}], \tag{2.1}$$

where the released energy is distributed with a fraction of 1 : 4 between the helium-4 atom and the neutron as kinetic energy [Sch01]. Most fusion projects, no matter if scientific or commercial, using magnetic (Tokamak or Stellarator) or inertial (Laser Fusion) confinement, use this reaction as a fuel [BB01]. The alpha particle stays in the plasma where its energy is used for self sustained plasma heating and the neutron is used for energy extraction [Max] and tritium breeding [Cri20; Cis20] in the blankets at once. Besides the nuclear reaction producing ^{4}He that pollutes the plasma over time, tritium decays to ^{3}He and wall interactions produce further plasma contamination like methane. In addition buffer gases are needed and injected for disruption mitigation and control of the heat load on first walls. All this pollution will mitigate the fusion reaction. In the end only about 0.3 % to 3 % of the fuel injected to the reactor will be burned [IDV] before it has to be extracted again. Due to its scarcity, price and radioactivity the tritium needs to be recycled continuously in a closed loop. A closed fuel cycle is mandatory, where tritium and deuterium are injected into the plasma chamber and evacuated for cleaning and enrichment [DG13]. Such a closed tritium cycle has been developed and tested at the Tritium Laboratory Karlsruhe (TLK) [Glu00] and is also used in the Karlsruhe Tritium Neutrino Experiment (KATRIN) as described in section 2.3.

Tritium viscosity in fusion and material science The closed fuel cycle of the fusion power plants is composed of several different systems, such as pumping stages for gas transport between the systems, exhaust processing, tritium recovery, isotope separation, detritiation stages, storage and finally the fueling. All the parts underlie permanent development to improve their characteristics, concerning tritium transport, separation

and storage. For crucial components, like the huge variety of pumps intended to be used, pretests and longterm studies have been conducted, as for example described in [Hil24]. Others are still being developed, as described in [Bul93; Ili93; TD21]. For efficient development, simulations are often needed, as tritium is not available everywhere and for every facility. To be able to simulate the behaviour of such pumps, the transport properties of tritium are needed, especially the viscosity [TD21]. The tritium fuel cycle is not only in need of optimized pumping systems, but also of cryogenic distillation columns. These hold a high amount of the total tritium inventory and have to be optimized [Cri06] through simulation where again transport properties like the viscosity of tritium are needed. As the viscosity of tritium is not trivial to calculate, experimental values are needed, to reduce the uncertainty on the viscosity value and the thereby arising uncertainty on the simulation results. For such an experiment, a facility like the TLK is needed, where tritium is available in a significant amount.

2.3. The tritium viscosity in the KATRIN experiment

The Karlsruhe Tritium Neutrino Experiment (KATRIN) is designed to measure the mass of the electron anti neutrino with unprecedented sensitivity of 0.2 eV at 90 % confidence level [Ake21b]. In the latest publication a new upper limit on the anti electron neutrino mass of 0.8 eV has been reached [Ake22a]. A new paper is currently under review claiming an even better upper limit of 0.45 eV. The basic principle of the experiment is to use the tritium beta decay and measure the energy spectrum of the decay electrons. From the difference of the measured spectrum to the calculated spectrum with an estimated neutrino mass of zero, the actual neutrino mass is calculated. Detailed information on the experiment and its latest results can be found in [Ake21b; Ake21a; Ake22b; Ake22a] and [Ake24]. To reach KATRIN's design goals, many challenges were to overcome and some issues are still open, like the missing value for the viscosity of tritium, which is an input parameter for the column density profile simulation. After a brief introduction to the KATRIN setup, this question will be addressed.

2.3.1. KATRIN Working principle

Tritium is fed from the supply systems ("Loops") to the 10 m long windowless gaseous tritium source where it decays providing electrons. These electrons are adiabatically guided by the transport section through the spectrometer to the focal plane detector. The transport section consists of the differential pumping section (DPS) and the cryogenic pumping section (CPS).

DPS: The beam tube inside the DPS forms a chicane, so that the charged electrons are guided through by magnetic fields along the beam tube, but the neutral tritium molecules collide with the beam tube walls and can be pumped out with turbo molecular pumps. By this a gas flow reduction factor of approximately 9×10^7 is achieved [Mar21].

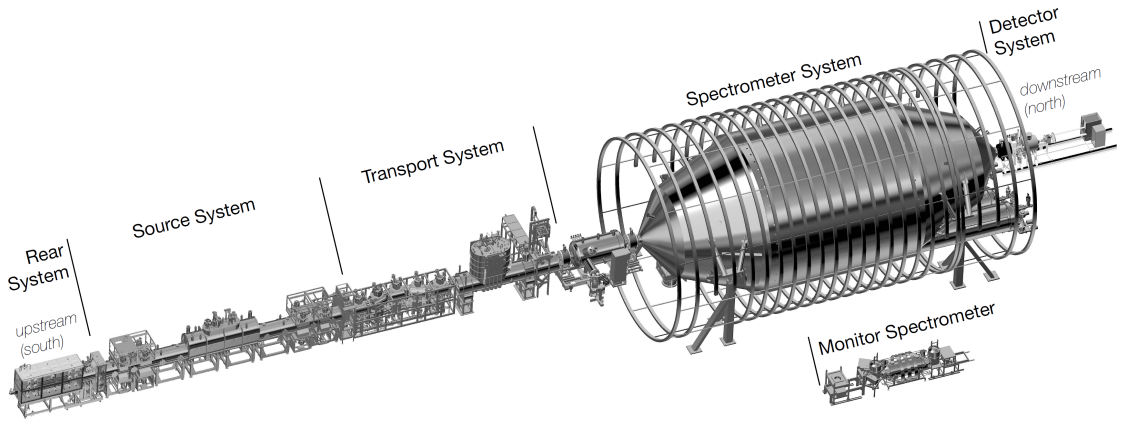

Figure 2.2.: **The KATRIN experiment.** The complete beamline is about 70 m long and includes the rear section with the electron gun, the windowless gaseous tritium source denoted as "Source System", the transport section with the differential pumping section and the cryogenic pumping section, the spectrometer system and the focal plane detector, where the β-electrons are detected. [Ake21b][CC BY 4.0]

CPS: The CPS utilises a similar beam tube geometry as the DPS, but tritium molecules are not mechanically pumped but adsorbed on an argon frost layer with a high pumping capacity, reducing the gas flow by more than seven orders of magnitude [Röt23]. The CPS marks the end of the tritium confinement.

Spectrometer : The spectrometer is designed as a high pass filter on the basis of a magnetic adiabtic collimator and electrostatic filter (MAC-E Filter). The electrons entering the MAC-E Filter have a transverse and a longitudinal momentum, where the energy is distributed in likewise proportions, broadening the energy spectrum, as the filtering of the electrons is only sensitive to the longitudinal energy. The magnetic field is applied such, that the transverse momentum is turned to be longitudinal to the flight direction, thereby converting the transverse proportion of the energy to the longitudinal one. The center-plane of the spectrometer spans an electrostatic field, where only electrons with a surplus energy can pass. To get the full spectrum, the MAC-E-filter is set to different electrostatic field energies.

Detector: At the focal plane detector (FPD) the electrons which pass the MAC-E Filter are counted, to get the integral spectrum of the decay electrons.

To enable a stitching of single spectra taken at different energy filtering settings - amongst other important aspects - the source has to be stable over time since fluctuations in intensity, temperature and density would spoil the neutrino analysis. This is directly linked to

the WGTS, the gas dynamics inside and ultimately, the viscosity of tritium. The WGTS working principle and the influence of the viscosity will be explained in the following.

2.3.2. The windowless gaseous tritium source

The windowless gaseous tritium source (WGTS) is the source of all beta-decay electrons measured with KATRIN. It is supplied with tritium by a complex loop system, shown in Figure 2.3 in a simplified way. In the top part of this picture, the source and transport section of the KATRIN experiment is depicted with the gas density of tritium indicated with the transparency of the red bulk below all sections. The Loops-System is divided into the Outer Loop System (OL) which includes all parts apart from the ones supplying the WGTS, which is the Inner Loop System (IL). The WGTS consists of a 10 m long stainless steel tube with an inner diameter of 90 mm which is surrounded by a cryostat. Tritium is fed into the middle of the beam line of the WGTS and evacuated at both ends. To achieve a stable density profile

- the pressure in the buffer vessel has to be stabilized,
- the gas flow along the injection line and the WGTS has to be stable and therefore
- the temperature along the injection line and the WGTS has to be stable and
- the gas inside the source has to be continuously pumped to keep a constant gas composition at high tritium proportion to reach a constant electron rate.

The form of this profile is mainly influenced by the temperature along the beam tube and the inlet and outlet pressure. For the pressure stabilization there is a pressure and temperature controlled buffer vessel which is fed by an additional buffer vessel. The temperature along the beam tube is stabilized by a two phase cooling system utilizing neon or argon to cool down to 30 K, 80 K and 100 K. Temperature sensors are distributed along the beam tube and an analysis by [Mar21] shows the exceptional temperature stability for such a large cryostat, meeting technical design report requirements [Ang05]. Pressure stabilisation of the inlet gas is facilitated with a complex gas handling system with various pressure and flow sensors at all critical points. Tritium purity is permanently monitored inline with a Laser-Raman-system. The gas density inside the WGTS, called column density (CD), is one of the main contributions of uncertainties to the data analysis of the KATRIN experiment [Ake22a] and directly linked with the viscosity of tritium [**block_determination_2022**; Kuc16].

2.3.3. The influence of the tritium viscosity on the column density

Depending on the CD the scattering probability of the electrons changes, which has a direct impact on the electron energies and hence the energy spectrum. This is accounted for during the analysis but the CD can only be measured in an integral way over the whole length of the WGTS, since any measurement device inside the gas volume of the source would disturb the free path of the electrons and destroy the measurements. What is also needed is the so called response function, which includes properties of the spectrometer and the scattering probability of the decay electrons and hence the CD. For the response function the CD profile is needed, not only the integral value. In addition, the CD profile

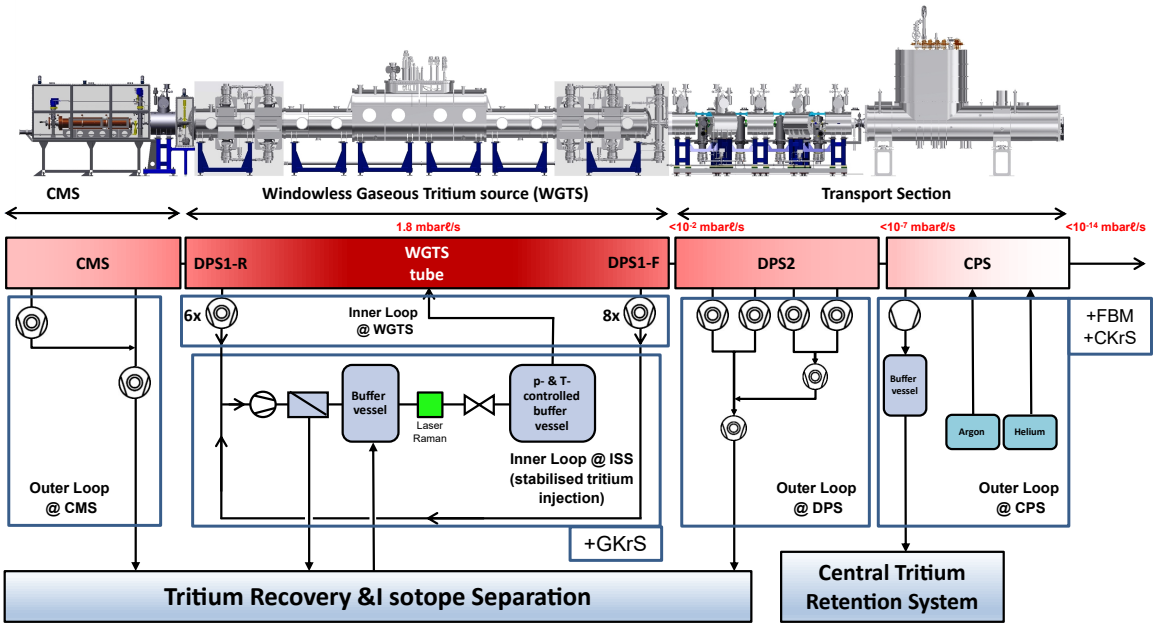

Figure 2.3.: **The KATRIN Loops.** The Loop system of the KATRIN experiment is shown with buffer vessels, permeater, Laser-Raman-Cell to track the gas composition and the pumping system. The column density inside the beam tube is indicated as red color profile. (Adapted from [Ake21b] under [CC BY 4.0])

is needed as an input parameter for the simulation of the magnetic fields of the WGTS. These magnetic fields influence the flux tube which guides the electrons to the FPD. From the flux tube, information about the path of the electrons is extracted, only by registering on which of the pixels of the FPD the electrons impinged [**block_determination_2022**]. To get a handle on the CD profile L. Kuckert conducted simulations of the gas dynamics in her doctoral thesis [Kuc16]. As already stated in section 2.1, for such a simulation the viscosity of tritium is needed. Since the viscosity of tritium was not accessible in literature at the time of conducting the gas dynamics simulations, values extrapolated by the mass ratio from deuterium were used. The extrapolation of these values is further described in section 3.4. Their uncertainty of approximately 7 % [Kuc18] translates into an uncertainty on the CD profile of ±0.5 %, as shown in figure 2.4. The CD profile is shown in terms of pressure normalized to the injection pressure against the position along the WGTS beamtube. To demonstrate the influence of the estimated uncertainty of 7 %, the calculated viscosity is increased and decreased by this factor for the upper (orange line) and lower boundary (blue line), respectively. The difference of these newly created profiles to the expected one is shown in the lower graph of figure 2.4. This influences the scattering probability of the decay electrons in dependence of where they are produced inside the source and therefore on the response function used for the neutrino analysis [Sei19]. The overall impact of the gas dynamics systematic of the WGTS on the neutrino mass reaches 3.3 % [Sei19]. This includes the CD, the inelastic scattering cross-section, the product

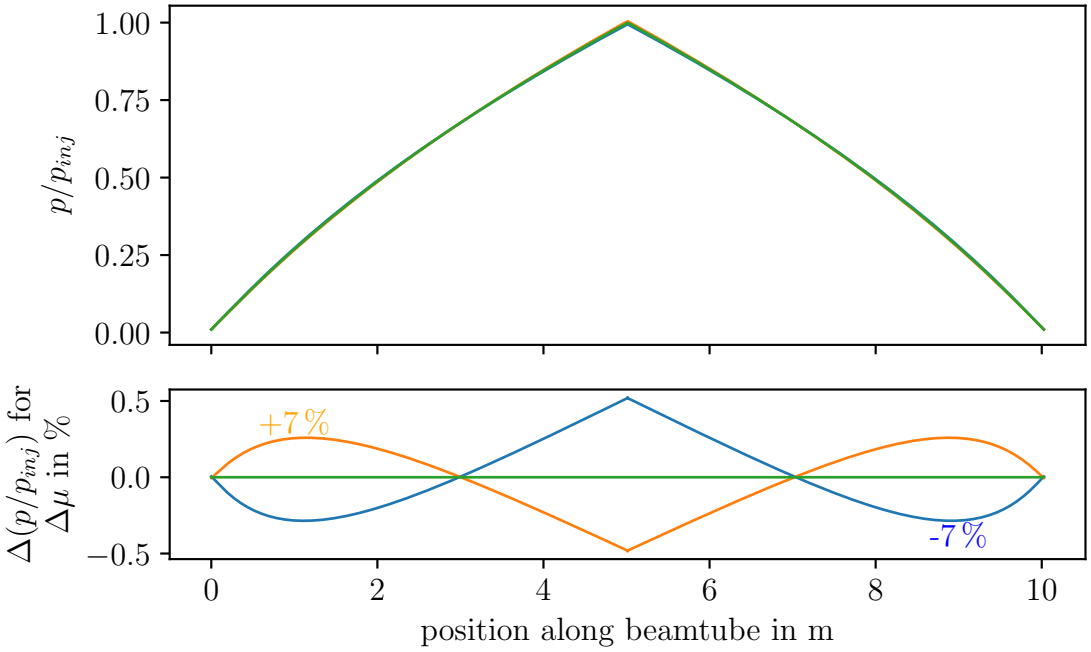

Figure 2.4.: **The Column Density Profile of the WGTS.** The CD profile is plotted in terms of the pressure along the beam tube normalized to the injection pressure. In the lower graph the difference in the density profile is shown once for the estimated tritium viscosity in green and the viscosity with ±7 % difference.

of these two as well as the gas-dynamical model of the source plasma. The viscosity of tritium is in this case mostly affecting the last part of this list, as for the CD, the integral column density is meant, which is measured separately.

2.4. Tritium viscosity - the missing parameter

As explained in the previous sections, the viscosity of tritium is a crucial value needed in a diversity of fields in physics, concerning particle physics experiments on the way to find new physics beyond the standard model [**block_determination_2022**; Kuc16; Sei19; Hei19], as well as in fusion science and technology [TD21]. In addition, transport coefficients in gases are currently challenging to model. The six hydrogen isotopologues and the three isomers therefore are a valuable testbed to benchmark and improve on ab initio modeling. Mixing these different molecules further adds to the parameter space and therefore the value of this test bed that should be exploited. The existing values are all afflicted with high uncertainties of 7 % to 30 % [Kuc18; Yan24], depending on the estimated temperature, pressure and state of tritium and are only calculated values. [Kuc18] does a very basic approach by extrapolating the viscosity of tritium with the mass ratios from hydrogen and deuterium up to tritium and including a factor, gathered from die extrapolation from hydrogen to deuterium, given with an uncertainty of "up to" 7 %.

Table 2.1.: Properties of tritium

molar mass in u	3.0160497	[Fie92]
half life time in years	12.32	[LU00]
beta decay energy in keV	18.54	[Fie92]
specific activity in 1×10^{14} Bq g^{-1}	3.56	[Fie92]
zero-point energy in kJ mol^{-1}	15.10	[Fie92]
dissociation energy in kJ mol^{-1}	444.98	[Fie92]
heat capacity	?	
thermal conductivity	?	
viscosity in µPa s	?	

[Son16] calculated the viscosity of tritium ab initio, but only on a classical approach with an expanded uncertainty of 0.7 % and a confidence level of 95 %. Nevertheless, they are only valid for temperatures of 300 K and higher. Since the KATRIN experiment uses a tritium source in a temperature range of 30 K to 100 K, and also fusion needs values for the tritium viscosity below 300 K, the calculations of [Son16] have to be taken with caution. Newer calculations of transport coefficients for tritium by [Yan24] show uncertainties in the percent range for the viscosity of tritium, but only in the liquid phase for temperatures from 20 K to 35 K. Caused by the lack of values for the tritium viscosity, [Yan24] use extrapolated viscosity values, as done by [Sou86], to validate their simulation results, showing the need for experimental values for the viscosity of tritium. In table 2.1 a few properties known for tritium are listed. In [Fie92] and [Sou86], there are a lot more to be found, but most of them are marked as estimated or extrapolated, so they are not listed here. Basic properties like the heat capacity, thermal conductivity, and the viscosity are still not found in literature. The reason for the missing information on material properties of tritium is, that there are only very few infrastructures allowed, able and willing to deal with tritium. The Tritium Laboratory Karlsruhe (TLK) is Europe's most capable facility, having the license to handle up to 40 g of tritium on site and many years of experience in tritium handling [KIT23].

3. Viscosity of hydrogen isotopologues

This chapter is focused on the theoretical background in fluid dynamics needed to understand the importance of the viscosity of gases in general. Starting with an overview of basic theory, different types of viscometers are explained and the method for the measurement of the tritium viscosity is selected with respect to compatibility to tritium and cryogenic temperatures. Following this, an overview of current research is given, concluding with the guiding questions to be answered in this thesis.

3.1. Fluid dynamics in vacuum technology

In section 2.2 and section 2.3, examples of vacuum systems with gas flows containing tritium have been explained. In fusion technology for example, the gas flow through pumps has to be simulated to improve their design. The KATRIN experiment uses a gaseous tritium source, where tritium is circulated through a closed loop system. High technical effort is taken to achieve a dynamic but constant source profile by precision pressure and temperature control of the injection line and source tube itself and finally constantly pumping on both ends with several turbomolecular pumps. However, to describe the gas source profile viscosity is the main parameter in the simulation. In both cases, the viscosity is crucial for correct simulations. To be able to fully understand the importance of the viscosity of gases, it is necessary to explain basics of fluid dynamics in vacuum technology. This section gives an overview of the different flow regimes in fluid dynamics and the transport properties thermal conductivity and viscosity.

3.1.1. Parameters for the classification of a fluid system

Fluid systems are commonly characterized by their flow regime, e.g. the prevalent interaction of gas particles within it. The flow regime is commonly classified from high to low gas density as: the continuum flow, the transition or Knudsen flow, and the molecular flow [Jou18; Unr18]. In addition, the slip flow in between the Knudsen and the continuum regime is defined [Cer00]. The mean free path λ of a gas particle in a fluid system is used as a key parameter to differentiate between these flow regimes. For a simplified model of gas particles as hard spheres, λ is defined as

$$\lambda = \frac{k_\mathrm{B} T}{\sqrt{2}\pi d^2 p}, \tag{3.1}$$

in dependence of the pressure p and the temperature T (as found in chapter 2.5 in [Jou18]), with the Boltzman constant k_B. The only gas specific parameter is the diameter d of the

gas particle. As real gas particles are not hard spheres, a potential like the Lennard-Jones potential has to be used. Thereby, πd^2 can be substituted by the interaction cross-section σ. Another way to calculate the mean free path is shown for example in chapter 2 of [McC90] by solving the Bolzmann equation for a hard sphere, resulting in

$$\lambda = \frac{4\mu\overline{v}}{5p}, \tag{3.2}$$

where μ is the viscosity of the gas and $\overline{v}$ is the average thermal speed of the gas particles in equilibrium. This directly shows the connection between the mean free path and the viscosity. To differentiate between the different flow regimes, the mean free path is correlated with the characteristic length of the gas flow. For a long tube, its radius r is used. The quotient K_n of the mean free path and the characteristic length of the gas flow

$$K_n = \frac{\lambda}{r} \tag{3.3}$$

is called Knudsen number [Sha16]. The discrimination between the flow regimes is done as follows:

- **molecular flow ($K_n \gg 1$)**:
  The gas flow is dominated by the interactions between the gas particles with the walls of the system

- **Knudsen flow ($K_n \approx 1$)**:
  Neither intermolecular interactions nor interactions with the walls of the system can be neglected

- **continuum flow ($K_n \ll 1$)**: The gas flow is dominated by interactions between the gas particles and can be treated as a continuum

The boundaries between these different flow regimes are not standardized. For the Knudsen regime there are Knudsen numbers of $0.01 < K_n < 2$ [Unr18] found as well as $0.01 < K_n < 0.5$([Jou07]). In addition, the characteristic length of a system is not always trivial to define. For a long straight tube, the radius is quite easy to use as the characteristic length, but if there are systems like pumps with moving parts, the characteristic length is not obvious. What is even more is that these numbers only hold for fixed or slow moving walls. Otherwise, additional effects on the surface occur, which change the gas flows behavior. The slip flow regime is located between the continuum and the Knudsen regime. Since the discrimination between these different flow regimes is not strictly given by the Knudsen number, the relevant ranges have to be determined for every experiment individually, which will become important later in the analysis of the measurements conducted within this work.
With these main parameters to classify fluid flows, section 3.1.2 defines the two transport coefficients frequently needed in gas dynamics.

3.1.2. Transport coefficients for gases in the transition regime

While working with gas flows there are always two questions one has to answer:

- How much material is moving through the setup or parts of it and
- How high is the thermal load on the system or the heat transfer through the gas?

To answer these questions, the thermal conductivity, the diffusion constant of the gas and its viscosity are needed. As this work is focused on the measurement of the viscosity of tritium, only this transport property is of importance, however, to understand the simulations on the temperature correction as shown in section 5.2, also the thermal conductivity has to be understood, which is why it will also be explained in this section. How these quantities are defined and what information can be extracted from them is explained in this section.

Thermal conductivity λ_Q is a property where information on how much heat is transferred through the medium without convection, in dependence of the heat flux and the temperature gradient is stored. It is defined as the proportionality factor between the heat flux density $\dot{Q}$ and the temperature gradient $\frac{\Delta T}{dx}$ (to be found for example in [RHC98; Sha16])

$$\dot{Q} = -\lambda_Q \cdot \frac{\Delta T}{dx} \tag{3.4}$$

but can also be derived from the Prandtl-number Pr [Jou18; RHC98], which is defined as the quotient of momentum transport and heat transport. It reads

$$\mathrm{Pr} = \frac{\mu}{\lambda_Q} c_V \,, \tag{3.5}$$

where μ is the viscosity and c_V is the heat capacity of the gas.

Viscosity can be understood as the inner friction of a medium, however, for dilute gases it is common to use the momentum transfer, as the gas molecules are not tightly bound to each other as it is the case in liquids. Similar to the thermal conductivity, the viscosity μ is a proportionality factor, defined as

$$p = \mu \cdot \frac{\Delta v}{dx} \,, \tag{3.6}$$

where p is the pressure and $\frac{\Delta v}{dx}$ is the bulk velocity of the gas. For gases the viscosity can be derived through kinetic gas theory [HCB64]

$$\mu = \frac{5 \cdot \sqrt{\pi \cdot m_g \cdot k_\mathrm{B} \cdot T}}{16 \cdot \pi \cdot \sigma^2 \cdot \Omega^{(2,2)^*}} \,, \tag{3.7}$$

where m_g is the mass of the sample gas, k_B is the Boltzmann constant, T is the temperature of the gas, σ is the cross section of the gas molecule and $\Omega^{(2,2)^*}$ is the collision integral. This term describes the viscosity in the zero-density limit and corresponds to the first term

of the expansion of the total viscosity received through an empirical approach, as shown in [Bel20]. The original definition reads

$$\mu = \mu_{\rho N \to 0}(T) + \mu_{init}(T, \rho) + \mu_r(T, \rho) + \mu_{crit}(T, \rho)\,, \tag{3.8}$$

where the first coefficient is defined as equation (3.7) for the viscosity in the zero-density limit, the second coefficient is the initial density contribution, the third coefficient is the residual contribution, both important for higher pressure or zero temperature, and the last one considers boundary effects for the critical point of the gas [Bel20]. The interaction cross-section as well as the collision integral in equation (3.7) are not trivial to calculate. The interaction cross section is mainly defined by the potential energy of the interacting particles [Son16]. There are plenty of approximated potentials, the first and very basic one being the Lennard-Jones-Potential [LSH24; FW23]. As those are often empirical approximations, the accuracy of viscosity calculations only reaches values in the percent region. For molecules, where quantum mechanical effects play an increasing role, the calculations become more and more complex leading to higher uncertainties through approximations ([CDL19], e.g. Born-Oppenheimer approximation [Bor26]). As the collision integral is calculated by integrating the interaction cross-sections over the collision energy, this is a second source of uncertainty. In addition, the geometry of the collision is of interest for poly-atomic gases, as by external electric or magnetic forces a specific orientation of the molecules and the collisions is preferred, introducing an anisotropic viscosity as described in chapter 7 of [McC99].
The interaction cross section as well as the collision integral are the main factors that make the viscosity of tritium difficult to calculate. For a full description of interactions between diatomic molecules, a six dimensional interaction potential is needed. For hydrogen and deuterium, these potentials can give good estimations on the viscosity values, but for tritium, things will look different, as in tritium gas also other components are present, like decay products ^{3}He and electrons. But also other substances created through radiochemical reactions with the walls of the containment add complexity to the calculations. So even with a fully described potential for tritium, the issue is not solved. Approaching from an experimental point of view, there are also ways to measure the viscosity of gases, which yield results in very good agreement with literature, depending on the pressure and temperature range. A few of these will be explained in the subsequent sections.

3.2. The viscometry of gases

As mentioned in subsection 3.1.2, the viscosity of gases is of major importance for any gas dynamics outside the ultra high vacuum regime. There are different techniques to measure the viscosity of gases, of which the most widely known ones will be explained in the following paragraphs. The measurement precision, pressure range and tritium compatibility of these methods is summarized in table 3.1. Finally, the reason why the spinning rotor gauge method was chosen as the only practicable way for measurements with tritium gas will be laid out.

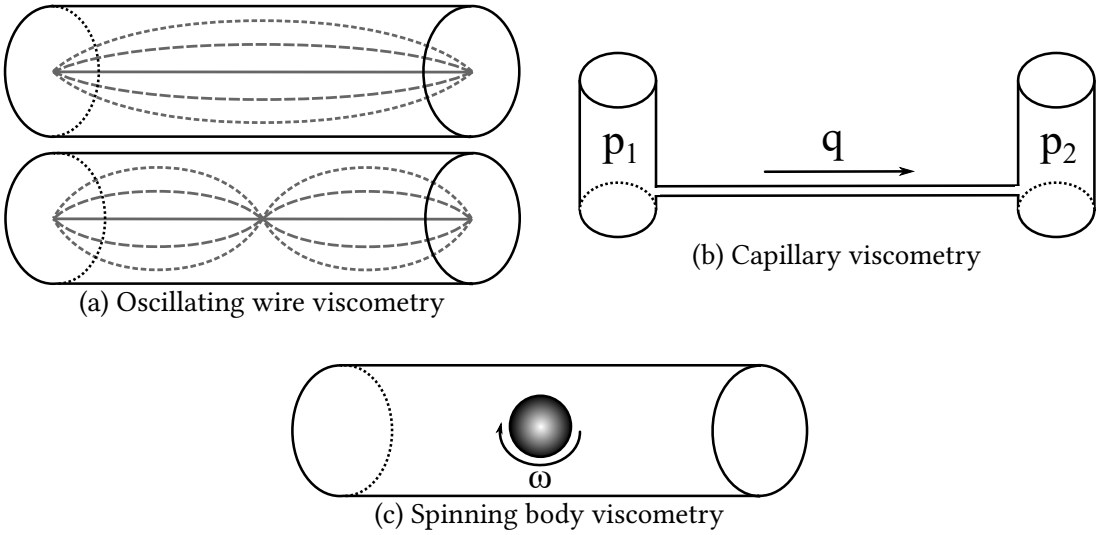

(a) Oscillating wire viscometry

(b) Capillary viscometry

(c) Spinning body viscometry

Figure 3.1.: **Different types of viscometry.** Figure 3.1a shows the basic principle of an oscillating wire viscometer, where the damping rate and the resonance of the wire are dependent of the surrounding sample gas. Figure 3.1b shows the capillary viscometer, where the flow rate through a long capillary connecting two vessels is dependent on the pressure difference in the vessels and the viscosity of the sample gas. Figure 3.1c shows the spinning body viscometer, where the deceleration of the rotating body is dependent on the pressure and the viscosity of the surrounding sample gas.

Oszillating wire viscometry Deeper information on this method can for example be found in [Ass14]. Figure 3.1a shows a simplified sketch of the measurement principle. A thin wire is placed inside a cylinder and excited using electromagnets, also used for signal pick-up. The resonance frequencies of the wire as well as the damping rate of the oscillation depend not only on the wire but also on the surrounding gas. A precision of the viscosity in the sub-percent region is achieved with an accuracy of approximately 2 % [Pád96]. This measurement method is normally used either for high pressure fluids or low temperatures in the mK region to study superfluid helium [Ass14]. This method is preferred whenever possible, since it is a direct measurement of the viscosity of a fluid, without the need to calibrate the setup against another medium. The mechanics of an oscillating wire is well known. Amongst others, Pádua explains in [Ass14] p. 97, that it is paramount for this method to work, that the compressibility of the fluid is negligible. The problem for the case considered within this work is that the compressibility of a gas is never negligible, so this method to measure the viscosity will not work.

Capillary viscometry Figure 3.1b shows a simplified sketch of the capillary viscometer setup. Two vessels at different starting pressures p_1 and p_2 are connected by a long capillary. If $p_1 > p_2$ a gas flow q will result. The throughput of gas is dependent on the pressure difference between the inlet and the outlet of the capillary, the length and width of the

capillary, the temperature of the gas and its viscosity. The viscosity can be extracted from the gas flow rate $\dot{n}$ [Ass14]

$$\dot{n} = \frac{\pi r^4 (p_1^2 - p_2^2)}{16 L R T \mu_{0,T}^g} C^g(T, p_1, p_2) \tag{3.9}$$

with the universal gas constant R, the viscosity $\mu_{0,T}^g$ of gas g at temperature T in the zero density limit, the flow rate $\dot{n}$, length L and inner radius r of the capillary and the up- and downstream pressures p_1 and p_2 respectively. $C^g(T, p_1, p_2)$ is a correction term for a variety of flow effects. The capillary viscometer has to be calibrated against a reference gas, leading to a relative viscosity measurement. Nevertheless, these measurements reach a high accuracy of better than 1 % [MBM07]. The pressure range of this method fits the requirements for the measurement of the tritium viscosity. The capillary viscometer has also been often used inside cryogenic setups. As the capillary itself is made of glass or steel it is by definition tritium compatible in terms of material selection only. The problem in this case is given by the combined requirement of compatibility to cryogenic temperatures parallel to tritium compatibility. For glass capillaries, there is the non-acceptable risk of breaking while stainless steel ones usually have an at least 100 times higher surface roughness compared to glass leading to unknown errors. The surface roughness RA of stainless steel is given with a range of $0.1\,\mu m < RA < 12\,\mu m$ [Ros16], that of glass with $5\,nm < RA < 100\,nm$ [RWW10]. For temperature cycling of the setup to have a high resolution of the temperature dependency of the viscosity this method is not practicable with high accuracy. Usually, the capillary is too long to be thermally stabilized without a thermal bath, which posses additional challenges under glove box conditions.

Spinning body viscometry The measurement principle of spinning body viscometry is based on the deceleration with a rotating body caused by collisions of the surrounding gas particles. The first viscometers of this type used a disc shaped rotor fixed through a thin rod to a motor causing the rotation. From the deceleration of the disc the dynamic viscosity in the zero density limit can be calculated. The problem with these devices was, that there were very high frictional losses already without gas inside the device [Jou18]. This problem was solved by magnetically levitating the disc in new devices, while the basic principle stayed the same. In figure 3.1c a simplified sketch of a spinning body viscometer is depicted with a spherical rotor as used in the spinning rotor gauge (SRG). The sphere is held in suspension and the rotational axis is perpendicular to the cylinder axis. The mechanics of such a rotating body inside a cylinder are not analytically solved yet, so each device has to be calibrated against a reference gas of known viscosity, preferably helium, making every measurement not an absolute but a relative one to the calibration standard. The accuracy of these measurements is hard to find in literature. [BTL97] only gives the deviation to previous values with a range from 0.5 % to 2.6 %, depending on the size of the sphere and the tilt angle of the cylinder. Nevertheless, this range is acceptable for the planned viscosity measurements.

Table 3.1 gives a short summary of the above described types of viscometers and the

Table 3.1.: Summary of the basic features of the different viscometers. The capillary viscometry seems to be the best choice, but only as long as no cryogenic temperatures in combination with tritium compatibility are needed.

viscometer	observables	pressure range	compatibility			accuracy
			cryo	tritium	comb.	
oscillating wire	ω & ω_{res}	incompressible fluids	yes	yes	yes	2.0 %
capillary	Δp & $\dot{n}$	slip regime	yes	yes	no	< 1 %
spinning body	$\dot{\omega}$ & p	slip regime	yes	yes	yes	2.0 %

environment for which they are applicable. Going only by the overview table, the capillary viscometer would be preferred, as it is compatible to tritium, cryogenic temperatures, and has the highest accuracy. But, as the compatibility both for tritium and cryogenic temperatures is needed, a capillary setup would be very challenging to build with yet unknown sources of error.

3.3. Previous measurements on the viscosity of non-tritiated hydrogen isotopologues

The viscosity of non tritiated hydrogen isotopologues has already been measured many times with different techniques, aiming at different pressures and temperatures. A. van Itterbeek measured the viscosity of pure protium and deuterium at room temperature and between 14 K to 300 K with an oscillating disc [VC38; VV40] already back in 1938 and 1940. In 1957 A. O. Rietveld and A. van Itterbeek measured the viscosity of non tritiated hydrogen isotopologue mixtures with the same apparatus [RV57]. An oscillation disc was used by J. Kestin et al in 1964, [KN64], and an improved version in 1972, [KRW72]. All these measurements are given with an accuracy in the single-digit percentage range. In 1952 E. W. Becker and O. Stehl measured the difference in viscosity for ortho- and para-protium with a setup using four capillaries in a temperature range between 15 K to 90 K [BS52]. In 1955 E. W. Becker and R. Misenta measured the viscosity of HD and He^3 in comparison to H_2 and D_2 for temperatures between 14 K to 20 K [BM55]. In 1958 Coremans et al. measured the viscosity of helium, neon, H_2 and D_2 from 20 K to 80 K again with an oscillating disc [Cor58]. But only from 1996 on, after Loyalka explained a way to measure the viscosity of gases in the zero-density limit with a spinning rotor gauge, a new type of measurement has been conducted [Loy96]. With this new device, normally used as a vacuum pressure gauge, measurements with noble gases [Tek96] as well as methane [BTL97] were done. In table 3.2 the measurements for helium, hydrogen, deuterium and hydrogen deuteride are listed. The value for helium measured by Tekasakul et al. is the averaged value of their setup with the same rotor size as used within this thesis. The measured viscosity deviates about 1 % from the averaged value of all measurements for H_2, while for D_2 the deviation increases to nearly 2 %. For HD the deviation reaches 3 %. These values will act as a first benchmark for the targeted accuracy of the measurement

Table 3.2.: Previous measured values of the viscosity μ of helium, hydrogen, deuterium and hydrogen-deuteride at room temperature with the given uncertainties $\Delta\mu$ as given by the respective papers. The value with a * is only the standard deviation of the given measured values. For this measurement, the SRG has been used, while for the other measurements an oscillating disc has been used. The uncertainties written in bold type are the values given in the respective papers, the others are calculated from these for better comparability. The comparably high uncertainty on the HD-value by [RV57] is mostly caused by the uncertainty of the purity of HD.

Gas	μ in µPa s	$\Delta\mu$		source
		in %	in µPa s	
He	19.55	-	-	[VV40]
	19.73	0.9	**0.17***	[Tek96]
H_2	8.827	-	-	[VC38]
	8.89	-	-	[VV40]
	8.669	-	-	[RV57]
	8.828	**0.1**	0.009	[KN64]
	8.91	0.1	**0.013**	[KRW72]
D_2	12.31	-	-	[VC38]
	12.780	**0.6**	0.077	[KN64]
	12.67	0.1	**0.018**	[KRW72]
HD	10.526	**+4 to -8**	0.42 to -0.84	[RV57]
	11.152	**0.5**	0.056	[KN64]
	10.95	0.1	**0.015**	[KRW72]

of the tritium viscosity. As it is not trivial to measure the viscosity of tritium, the only values available in literature are theoretical values calculated through different approaches. These approaches will be explained in the following section.

3.4. Current values for the viscosity of tritium from theoretical calculations

There are mainly two approaches to calculate the viscosity of tritium. The first is a more empirical one, where the tritium viscosity is extrapolated from the values of hydrogen and deuterium by the mass ratio. This approach has been conducted by [Kuc16], to get the viscosity of tritium as an input parameter for the gas dynamics simulation of the KATRIN source plasma. The second approach uses equation (3.7) and requires calculation of the collision integral and the interaction cross-section. This has been done by [Son16] in 2016, but only using a classical approach, neglecting quantum mechanical effects.

Viscosity extrapolation by mass ratios The first approach claims that the collision integral as well as the interaction cross-section are the same for all isotopologues of one

element. In this case, the only variable to distinguish between the isotopologues is their mass. Equation (3.7) then changes to

$$\mu_{H_2} = \sqrt{m_{H_2}} \cdot A \tag{3.10}$$

with A being a factor containing all other constants of the former equation. The viscosity ratio of hydrogen to deuterium can then be written as

$$\frac{\mu_{H_2}}{\mu_{D_2}} = \sqrt{\frac{m_{H_2}}{m_{D_2}}} \tag{3.11}$$

eliminating A, as it is assumed to be the same for both isotopologues. Therefore, the viscosity of deuterium can be written in dependence of the viscosity of hydrogen as

$$\mu_{D_2} = \sqrt{\frac{m_{D_2}}{m_{H_2}}} \cdot \mu_{H_2}\,, \tag{3.12}$$

leading to a value which is higher than the experimentally determined one by approximately 7 % [Kuc16]. The same can be done for the viscosity of tritium, using deuterium as the base value. The thought behind the use of deuterium is, that the mass deviation to tritium is smaller. But, if the potentials between the isotopologues differ stronger, it might also be that the extrapolation with hydrogen as base would be more appropriate, since tritium and hydrogen are both fermionic molecules, while deuterium is bosonic. Nevertheless, these extrapolations show deviations of 5 % to 7 %, depending on the chosen basis molecule and are only to be rated as a first estimate, as long as no experimental value for tritium is available to compare the results to.

Viscosity from classical kinetic gas theory The calculations of the viscosity of tritium from the classical kinetic gas theory are summarized in this paragraph. The detailed equations can be found in [Son16]. The potential interaction energy of the participating molecules is calculated to extract the deflection angle Θ of the collision. For each type of collision the interaction cross-section σ is calculated giving the first missing variable for calculating the viscosity. The interaction cross-section is then integrated over the potential collision energy to get the collision integral $\Omega^{(2,2)^*}$, the second missing variable. The problem with this calculation is that the quantum mechanical effects are completely neglected. For temperatures > 300 K up to a few thousand Kelvin this causes no significant deviation. [Son16] already states that the deviation of these calculations to measured values of helium and hydrogen does not exceed 2 %. For lower temperatures, quantum mechanical effects do affect the transport properties. This is caused by the quantization of the rotational eigenstates of the hydrogen isotopologues. Hydrogen isotopologues can have two possible configurations, depending on the spin-orientation of the protons of the coupled atoms. For parallel spins, the quantum number J for the rotational ground state is 1 (ortho-hydrogen). For anti-parallel spins, the quantum number J is 0 (para-hydrogen). As stated already for example in [Sou86] and [Grö15] for low temperatures the transition between ortho- and para-hydrogen is not allowed. This is one of the many effects causing deviations from the classical approach concerning the accuracy of the calculated viscosity.

As no experimental or other calculations concerning tritium are currently to be found in literature, it is hard to prove this deviation also for tritium.
There are additional approaches to calculate the viscosity of tritium with simulation tools including machine learning [Yan24], where only hydrogen isotopologues in the liquid phase are addressed, making a comparison impossible.

3.5. Goals of this work

As shown in the previous sections, the viscosity of tritium is not only an important parameter for particle physics beyond the standard model, but also for fusion science. There is a lack of information on the transport coefficients of tritium in general. The viscosity of tritium is still only known from calculations with an estimated uncertainty of up to 7 % [Kuc16]. By providing experimental values for the viscosity of tritium, this is the first ever possibility to compare the theoretical results with. Models for transport properties including the viscosity are still lacking high accuracy. By measurements with an uncertainty around 2 %, validation of the theoretical models of simple molecules can be improved. Tritium is one of the simplest molecules to be calculated, but the influence of its decay and the decay products on the viscosity and other quantities still needs clarification. For astroparticle physics experiments like the KATRIN experiment, the viscosity of tritium is needed for gas dynamics simulations of the tritium source plasma [Kuc18; Mar21]. The source is currently operated between 80 K and 100 K at low pressures as described in section 2.3.2. For this reason, the zero-density viscosity of tritium is measured down to 100 K with an opportunity to go to lower temperatures by small manipulations of the setup. To improve the knowledge of the temperature dependence of the tritium viscosity as an example for other more complex radioactive elements, the viscosity is measured across the whole temperature range from 100 K to 300 K, with fine temperature steps. As current theoretical models reach an accuracy of 2 % to 10 %, the uncertainty of the measurements shall reach 2 % (see chapter 5) to be able to compare the measured results to theoretical models. To reach these goals a tritium compatible setup based on the spinning rotor gauge (SRG) is developed, which has to be operable in a temperature range from 100 K to 300 K, see chapter 4. To validate the trueness of the results and show a proof of principle, section 6.1 shows the measurements with nontritiated hydrogen isotopologues protium and deuterium, before the results of the measurement of the viscosity of tritium are shown in section 6.2. The finely resolved temperature curve of the viscosity enables the development of an empirical equation, see section 6.4, with which the viscosity of tritium can be calculated also for temperatures to slightly higher and lower values of about 20 K, including temperatures from 80 K to 320 K.

4. Design of Cryo-ViMA - the Cryogenic VIscosity Measurement Apparatus

The development of the Cryogenic Viscosity Measurement Apparatus (Cryo-ViMA) needs to follow guidelines for tritium compatibility, explosion protection, pressure safety, kryogenics safety and electric safety. Those are put together in the "technical terms of delivery and acceptance" (TLA) [Wel15]. Apart from compatibility to the aimed temperature range, material selection is of major importance to guarantee tritium compatibility, along with different quality tests concerning pressure resistance, leak tightness, and proof of principle measurements with H_2 and D_2 as done in [Wyd22] and [Wyd23]. The experiment follows these guidelines and is able to measure the viscosity of hazardous gases like tritium. The scientific and technical parameters of measuring the viscosity of tritium are explained in section section 4.1. In section 4.2 the spinning rotor gauge, the measurement and analysis concept behind it and the technical description is given. Section 4.3 is focused on the viscosity measurement setup with the different subsystems and their tasks. The different measurement procedures are presented in section 4.4.

4.1. Design parameters for measuring the viscosity of tritium

Tritium being an isotopologue of the smallest existing molecule, namely hydrogen, it can permeate through metals, requiring ongoing research into methods to prevent tritium permeation by passivation of surfaces (see for example [Hu15]). As it is radioactive, tritium decays with a half life time of 12.3 a [Fie92; LU00] triggering radio-chemical reactions and the synthesis and decomposition of molecules [Glu88] as well as isotopic exchange reactions [She92]. These reactions take place in the gas phase itself as well as through interactions with the walls of the containment or its bulk material (see for example [Mor77; Kra23]). As a result of these effects, there will never be pure tritium inside an experiment. What this means for the measurement of the tritium viscosity will be explained in the following two sections.

4.1.1. Scientific design parameters

As mentioned in section 3.5, the temperature and pressure range for the measurement of the tritium viscosity is chosen close to the KATRIN settings shown in figure 4.1, to

improve the accuracy of the column density simulations. The measurement setup has to be able to measure the viscosity of tritium at approximately 100 K in the zero density limit. In an ideal experiment, one would take 100 % pure tritium and perform the measurement, without further investigation of the gas sample. As explained above, tritium will never be pure tritium inside an experiment and every gas mixture containing tritium will change its composition with time. At TLK we are able to purify tritium to of approximately 99 % [Hil24]. As tritium decays during the measurements, the gas composition will change through the previously described effects, into a mixture of tritium with helium-3 as the decay product, HT, and tritiated hydrocarbons [Mor77; Gil80; GME83; Mal13; Ake20]. These effects are amplified if the inducing particle is not the decay electron of tritium, but the tritium ion itself [Mat76; HD86]. Most of these effects are not possible to get rid of by design of the experiment, so they have to be evaluated through systematic studies, as they are changing the overall gas composition and its viscosity. According to the approximated equation by [Wil50], the viscosity of a gas mixture μ_{mix}

$$\mu_{mix} = \sum_{i=1}^{n} \frac{\mu_i}{1 + \frac{1}{x_i} \sum\limits_{\substack{j=1 \\ j \neq i}}^{n} x_j \Phi_{ij}}, \tag{4.1}$$

is only dependent on the viscosities μ_i of the individual components, their molar fractions x_i and weighting factors Φ_{ij}, which are dominated by the molar masses M_i of the components:

$$\Phi_{ij} = \frac{\left[1 + (\mu_i/\mu_j)^{\frac{1}{2}} (M_j/M_i)^{\frac{1}{2}}\right]^2}{\left(4/\sqrt{2}\right) \left[1 + (M_i/M_j)\right]^{\frac{1}{2}}}. \tag{4.2}$$

This approximation of μ yields values in accordance with literature within an uncertainty of 1.9 %[Wil50]. Since the goal of this work is the measurement of the tritium viscosity with an accuracy of 2 %, equation (4.1) is suitable for this study and can be used to derive a maximum allowance for impurities like helium-3, methane and so on within one gas sample.

4.1.2. Technical design parameters

Tritium is radioactive and at room temperature in gaseous phase, requiring special treatment, to guarantee the safety of experimenters. In [Wel15] the administrative and technical framework of the TLK is explained, main aspects being explosion protection, as needed for all experiments handling hydrogen isotopologues, hazard and operability studies (HAZOP) and choice of material. As explained in section 2.4 the decay electrons of tritium have very low energy, so the radiation field is very easily blocked but it must be prevented to incorporate tritium. One of the main safety measures is the arrangement of the whole laboratory in three containments, with a successive negative pressure gradient to the inner containments. In case of any leakage, the gas flow will be directed to the innermost containment, so no tritium will be released to the environment. The outermost contain-

ment is the laboratory building itself, with 30 Pa lower pressure than the environmental pressure. The second containment corresponds to the gloveboxes within which all tritium containing experiments are set up. The first containment is the so called primary system, including all parts in direct contact to tritium like tubes, vessels, connectors, pumps etc. To prevent radio-chemical reactions, all so called "wetted" materials, meaning everything in direct contact with tritium, have to be made out of metal, glass or ceramics. In our case the setup is mainly build of stainless steel.
Experiments which have to be operated inside a glove box are limited in space. Still, all parts have to be within the reach of the gloves in such a way that operation is possible. Apart from this, all sensors, controlled from outside the glovebox need electric feedthroughts. In addition, media like coolants need to be fed through ports inside the glove box, without opening the box for refilling. Moreover, the setup has to be designed in a way that maintenance is possible without opening the glovebox. With tritium being a hydrogen isotope, all guidelines regarding explosion protection have to be followed, too.

4.1.3. Temperature range

In the zero-density limit, the viscosity is dependent on the temperature. To be able to validate theoretical calculations, it is convenient to not only measure the viscosity at one single temperature set-point, but to measure its temperature dependence. To be of use for example for the KATRIN experiment, the temperature shall reach approximately 100 K, which is the highest temperature at which KATRIN is operated [Ake21b]. At the time of writing this thesis, an upgrade of the Cryo-ViMA setup is in preparation, to measure the viscosity of tritium at 77 K. Going further down will need a fully new system but is considered at TLK, since KATRIN is able to measure at 30 K [Ake21b]. Temperatures down to 10 K to 20 K where the saturation vapor pressure becomes limiting, are desirable, but were not targeted in this setup due to the associated increase in system complexity of going below liquid nitrogen temperatures. On the high temperature end it is only needed to measure up to room temperature, from where ab initio calculations [Son16] are available to compare the measured values to. Goal of this work is a complete temperature dependent viscosity measurement of tritium between 100 K to 300 K to reach the upper end of the operation temperature of KATRIN. To achieve this, a setup is needed which is able to not only measure at some dedicated temperature setpoint, but over the whole temperature range with fine steps.

4.1.4. Pressure range

The knowledge on the trueness of the pressure is the second important value influencing the accuracy of the measured viscosity. Again, the main motivation for measuring the viscosity of tritium was its need as a modeling input for the tritium source plasma of the KATRIN experiment [Kuc18; Mar21]. The pressure inside the source and transport section ranges from 1×10^{-8} Pa to 3×10^{-1} Pa, where the viscosity influences the shape of the pressure profile in the higher pressure levels from approximately 1×10^{-3} Pa to 3×10^{-1} Pa [Kuc16]. The viscosity measurement using an SRG is only valid in the slip regime, which has been described in subsection 3.1.1. For the Cryo-ViMA experiment, this

corresponds to pressures in the range from 20 Pa to 2000 Pa, where the lower pressures are needed for lower temperatures and higher pressures for higher temperatures. Apart from the measurement boundaries there is also a maximum design pressure given for safety reasons, which is at 90 kPa in accordance with the tritium safety requirements described in section 4.1.2.

4.2. The spinning rotor gauge (SRG)

As described in section 3.2 the best way to measure the viscosity of gases like tritium is spinning body viscometry. The SRG is a commercially available device and is off the shelf tritium compatible, as it is completely made out of stainless steel. As described in section 3.2, the spinning rotor gauge consists of a rotor inside the sample gas volume. The working principle and data analysis concept are described in section 4.2.1. In section 4.2.2 the technical description of the SRG used in this experiment is given.

4.2.1. Measurement and analysis concept

In 1964, Brenner and Sonshine derived a calculation for spinning body viscometers, where the rotational axis and the cylinder axis are parallel and the cylinder is assumed infinite in length [BS64]. Loyalka et al. showed with their calculations that this theory can be also used for viscosity measurements with spinning rotor gauges, where the cylinder of these gauges is neither infinitely long nor parallel to the rotational axis of the sphere [Loy96]. Tekasakul, Bentz and Loyalka already showed first measurements of the viscosity, the velocity slip coefficient and the tangential momentum accommodation coefficient of different gases with such a spinning rotor gauge [Tek96; BTL97]. In [Wyd22] first measurements of viscosities with a SRG inside a liquid nitrogen bath are shown. The aim here was to demonstrate that the SRG is also able to work under cryogenic temperatures, since the manufacturer only specifies the SRG to operate down to 0 °C. The observable in these kind of measurements is the normalized deceleration rate (DCR) as described in section 3.2. The basic analysis concept for viscosity measurements with a SRG is derived in [Loy96]. The DCR of a rotating sphere inside a cylinder is mainly dependent on the pressure and the temperature of the surrounding gas. The underlying effect is the residual drag caused by the colliding gas particles with the rotor. The momentum of the gas particles is transferred to the rotor decelerating it. In [Loy96] the viscosity μ is derived from the y-axis interception of

$$\frac{1}{D/\Omega} = \frac{1}{8\pi a_1^3 C_0 \mu} + \frac{1}{p} \cdot \sqrt{\frac{2k_B T}{m}} \left(\frac{c_m}{8\pi a_1^3 C_0} \left(\frac{3}{a_1} + \frac{1}{a_2} \right) \right), \tag{4.3}$$

where D is the torque[1], Ω is the rotational frequency of the sphere, a_1 is its radius, a_2 is the cylinder radius, p is the pressure of the sample gas inside the cylinder, k_B is the Boltzmann constant, T is the temperature of the sample gas and c_m is the velocity slip

[1] In the original paper this is T, but since this is easy to confuse with the temperature, here this is called D, as in German it is the "Drehmoment" of the sphere.

coefficient, from which the momentum accommodation factor can be calculated for the gas-surface interactions [Tek96; BTL97]. C_0 is a setup specific calibration constant. This factor originally describes the movement of the rotating sphere inside the evacuated cylinder, where the rotational axis is parallel to the cylinder axis. As explained in [Tek96], for a sphere rotating perpendicular to the cylinder axis, C_0 has to be extracted from calibration measurements. Using a calibration gas of well-known viscosity like helium ([HM00; Ass18]), C_0 can be determined from the y-axis intercept. Since the SRG is not measuring the quotient of the torque and the rotational frequency of the sphere but the normalized deceleration rate (DCR), equation (4.3) has to be modified, to show the dependencies between the observables. The torque D of a sphere normalized to its rotational frequency Ω can be written as

$$\frac{D}{\Omega} = \frac{8\pi}{15} \cdot \rho \cdot r^5 \cdot \frac{{}^{\mathrm{d}\Omega}/_{\mathrm{d}t}}{\Omega}, \tag{4.4}$$

where ρ is the density of the sphere and r is its radius, in the case of the SRG this corresponds to a_1[Tek96]. The moment of inertia I is the proportionality factor between the torque and the angular acceleration and equation (4.4) can be written as

$$\frac{D}{\Omega} = I \cdot \frac{{}^{\mathrm{d}\Omega}/_{\mathrm{d}t}}{\Omega}, \tag{4.5}$$

and implemented in equation (4.3) leads to

$$\frac{1}{{}^{\frac{\mathrm{d}\Omega}{\mathrm{d}t}}/_{\Omega}} = \frac{I}{8\pi a_1^3 C_0 \mu} + \frac{I}{p} \cdot \sqrt{\frac{2k_B T}{m}} \left(\frac{c_m}{8\pi a_1^3 C_0} \left(\frac{3}{a_1} + \frac{1}{a_2} \right) \right). \tag{4.6}$$

This equation holds only true for measurements within the slip regime of fluid flows. As described in section 3.1.1, in this regime the mean free path of the gas particles is in the order of the characteristic size of the container, in case of the SRG the diameter of the cylinder. Here, neither the interactions between the gas-particles nor the interactions between the particles and the cylinder wall or the rotating sphere can be neglected. To define the different flow regimes, the Knudsen number is used, as described in section 3.1.1. For the viscosity measurements with the SRG the slip regime corresponds to Knudsen numbers from 0.02 to 0.5. To get the viscosity, the DCR has to be measured in dependence of the pressure of the sample gas. The pressure has to be measured by a gas species independent pressure gauge. By inverting both quantities and plotting the inverted DCR against the inverted pressure, a linear fit can be conducted. From this fit the interception with the y-axis contains the information about the kinetic viscosity in the zero density limit. The intercept reads

$$\mu = \frac{I}{8\pi a_1^3 C_0 y_0}, \tag{4.7}$$

where y_0 is the offset of the linear fit performed with equation (4.6). As only a linear fit is performed, a three pressure level measurement would be sufficient. However it has to be assured to stay within the slip regime. In figure 4.2 an example of the measurement of the viscosity at one single temperature is shown. For the high and low pressure region, the

Table 4.1.: Technical data of the MKS instruments SRG3[MKS09]. *no modification allowed.

entity	value
wetted material	stainless steel 1.4034
density	7.70 g cm^{-1}
Sphere diameter	4.5 mm
rotational frequency	420 Hz to 850 Hz
connecting cable length*	2 m

values start to bend away from the fit, indicating the end of the Knudsen number range of the slip regime.

4.2.2. Technical description

The device used in this experiment is the SRG3 by MKS instruments and is off the shelf tritium compatible, as all parts in contact to tritium are made of stainless steel. A short overview of the main technical data are listed in table 4.1. The cylinder is welded to a ConFlat® flange which is directly connected to the tubing for the gas transfer. The SRG is normally used as a pressure gauge for ultra high vacuum (UHV). It uses the effect of deceleration of a rotating sphere by residual drag of the sample gas. Therefore the rotor has to be decoupled from any other effects decelerating the sphere, which is why the sphere is held in suspension by a magnet system. Figure 4.3 shows a sketch of the cylinder of the SRG with the permanent magnets on top and bottom of the cylinder, which introduce a homogeneous magnetic field building the basic condition to be able to levitate the rotor. The horizontal and vertical stabilization coils hold the sphere in place, whereas the four surrounding drive coils accelerate the sphere's rotation. The pickup coils then measure the deceleration of the sphere by the induced current caused by inhomogeneities in the magnetic field of the sphere itself. The sphere is accelerated to 440 Hz, then the acceleration is stopped and the measurement of the deceleration starts until a rotational frequency of 420 Hz is reached [MKS09]. This acceleration-deceleration cycle is automatically repeated by the control system, to which there are four cables for the control of the magnet coils. The control of the position and rotational speed of the sphere is done by an oscillating circuit of fixed frequency. This circuit includes the cabling between the control unit and the motor head, so the cabling cannot be extended. Therefore, the manufacturer demands to have a direct coupling of the plugs to the control unit, which is why this has to be installed inside the glove box. More details on the working principle of the SRG can be found in [Jou18] in Chapter 24.3 . The SRG is normally used as a pressure gauge at UHV. In contrary to this the viscosity measurements are conducted in the slip regime, where the rotating sphere has to be re-accelerated every few seconds. The effect of these accelerations is discussed in more detail in section 5.1.5.

4.3. The Cryo-ViMA setup

In this section, the setup of the Cryogenic Viscosity Measurement Apparatus (Cryo-ViMA) experiment is explained. As it is typical for experiments in the Tritium Laboratory Karlsruhe, also the Cryo-ViMA experiment is divided into a primary system, section 4.3.1, and the functionalities, meaning the cooling system, section 4.3.2, and the measurement readouts, section 4.3.4 and section 4.3.3. In figure 4.4, the flow diagram of the Cryo-ViMA experiment is shown with the primary system in red. In addition all temperature and pressure sensors are indicated at their respective position. The cooling system, which will be explained in section 4.3.2, is shown in the right part of the flow diagram.

4.3.1. The primary system

Components of the primary system are depicted in red in figure 4.4. The primary system of the Cryo-ViMA experiment is fully made out of stainless steel to guarantee tritium compatibility. In principle it only consists of a long tube which ends with the spinning rotor gauge (SRG). On the way to the SRG there are two paths to be selected, one with an orifice to be able to adjust the pressure inside the SRG precisely. The other one bypasses the orifice for a better pumping efficiency while evacuating the system. Between the SRG and the orifice, there is a gas species independent capacitance diaphragm gauge[2] installed, to measure the pressure in the sample gas volume. The sensor is still outside of the cryostat and is not cooled down. The impact of this arrangement is discussed in subsection 5.1.4. Inside the primary system is a platinum 100 Ω temperature sensor (Pt100), which measures the temperature of the sample gas as close as possible to the SRG. The measurements of this sensor are intended for the final mapping of the measured viscosity of tritium to the temperature it is measured at. As temperature impacts measurement accuracy most, a detailed description of the temperature measurement is given in section 4.3.3, while its impact on the accuracy is elucidated in section 5.1.

4.3.2. The cooling system

The cooling system is operated with a cold gas system[3], fabricated by KGW Isotherm. It includes a 200 L dewar[4] with evaporator and filled with liquid nitrogen as seen in figure 4.4. From there, a 5 m transfer line is feeding the cold gas via a Johnston coupling inside the second containment (glovebox) and to the in-box cryostat (standard dewar from Cryotherm) with a customized lid-flange. The pipe for the cold gas is insulated through vacuum, which can be renewed by a scroll-pump. The dewar containing the SRG is a standard dewar from Cryotherm with a customized flange as a lid. The cold-gas is fed into the dewar through a pipe, of which the outlet is directly pointing towards the cross-fitting on which the Pt100 temperature sensor and the SRG are mounted, close to point ⑤ in figure 4.5. Also shown in this picture is the diffusion plate, so that the cold-gas entering the dewar below this plate is accumulated around the SRG, before it leaves through the

[2] MKS AA02A, 20 torr full scale with an accuracy of 0.10 % Reading
[3] KGW-Isotherm TG-LKF H)
[4] Cryotherm Apollo 200L nitrogen tank

open lid to the glovebox.
As the dewar might have to be opened from time to time for maintenance and the SRG has to be decoupled from vibrations of pumps inside the glovebox, a special mounting is needed, damping vibrations from TriHyDe and fixing the lid of the dewar separately from the dewar-vessel. For better operation and easier maintenance, the cryostat is mounted with brackets on the top flange to the mounting construction with damping buffers in between. This way, the dewar can be opened without moving any parts of the measurement section, by simply lowering the vessel.
The cold gas system is equipped with a control unit, where it is possible to either set the target temperature inside the cryostat or the jet in terms of percent from its maximum output stream caused by higher heating power at the evaporator.
As tests of the cooling system concerning the temperature stability showed, the system is thermally too massive to be controlled via the temperature. The sensor for the feedback control is inside the cryostat, but not close to the SRG. When this sensor reaches the target temperature, the SRG is still warmer, causing the temperature to increase again over time. Until the temperature at the sensor is changed, so that the feedback control is again cooling down, the SRG already warmed up even more. Even after 24 hour, the thermal fluctuation is in the range of $5\,\mathrm{K\,h^{-1}}$.
To have stable measurements, it is more convenient to only set the jet power to cool down and wait for the system to warm up again for a thermal cycle.
With this operation mode it is possible to cool down to approximately 98 K and heat up to 375 K, whereas the SRG only works up to 318 K according to the manufacturer. An example of such a thermal cycle is shown in figure 4.6. A detailed look into the different temperature curves and their effect on the measurement is presented in section 5.1.5.

4.3.3. Temperature instrumentation

As mentioned before, the temperature impacts the accuracy of the tritium viscosity measurement most. All temperature sensors are calibrated against liquid nitrogen and the freezing point of water. This way, all offsets and slopes can be corrected for. For the temperature of the sample gas, a Pt100 temperature sensor is installed at the cross-fitting of the primary system. As this is approximately 0.15 m away from the rotor of the SRG, it will be not the exact temperature of the gas surrounding the rotor, but still is the best technically feasible solution. To account for any temperature gradient caused by the rotor being re-accelerated every few seconds, a simulation is performed. The results for the different gases and pressure settings are described in section 5.2. The cooling of the sample gas and SRG is done with cold gas, inducing a thermal gradient inside the cryostat. For thermally perfectly stable measurements of the viscosity, a thermal bath would have given better results, but to measure the viscosity in dependence of the temperature with this high resolution throughout the whole temperature range, the setup would have become too complicated for reliable operation inside a glove box. With the cold gas system, this is possible, if the thermal cycles are slow enough for the system to have only a small temperature gradient. The fourth thermocouple sensor is mounted to the end of the evacuated cylinder of the SRG. The sensors are distributed in this way, so that the temperature along the primary system is known, and the thermal stability along the pipe of the primary

system to the SRG is monitored. For the analysis, it is important that the temperature difference between the Pt100 sensor and the lowest two thermocouple sensors does not exceed 3 K, which corresponds to a gradient of $0.2\,\mathrm{K\,cm^{-1}}$. The uncertainties arising from the temperature measurements are explained in section 5.1.5.

4.3.4. Pressure instrumentation

As precise knowledge of the pressure is necessary, a dedicated, gas independent capacitance gauge[5] is employed to measure the gas pressure at ambient temperature. Due to thermal creep flow, there will be a temperature dependent pressure gradient along the tube, causing an overestimation of the pressure. How this is accounted for is explained in section 5.1.4. Apart from the pressure sensor for the primary system, there are two more pressure sensors mounted to the cryostat and the insulation vacuum of the cold gas tubing. A Wika WU-20 high purity transducer is mounted on the lid of the cryostat, to monitor the pressure inside the cryostat. Here the pressure is measured relative to ambient pressure. A Pfeiffer TPR 280 Pirani pressure sensor is used to monitor the vacuum pressure of the insulation vacuum of the cold gas tubes.

[5] MKS AA02A, 20 torr full scale with an accuracy of 0.10 % Reading

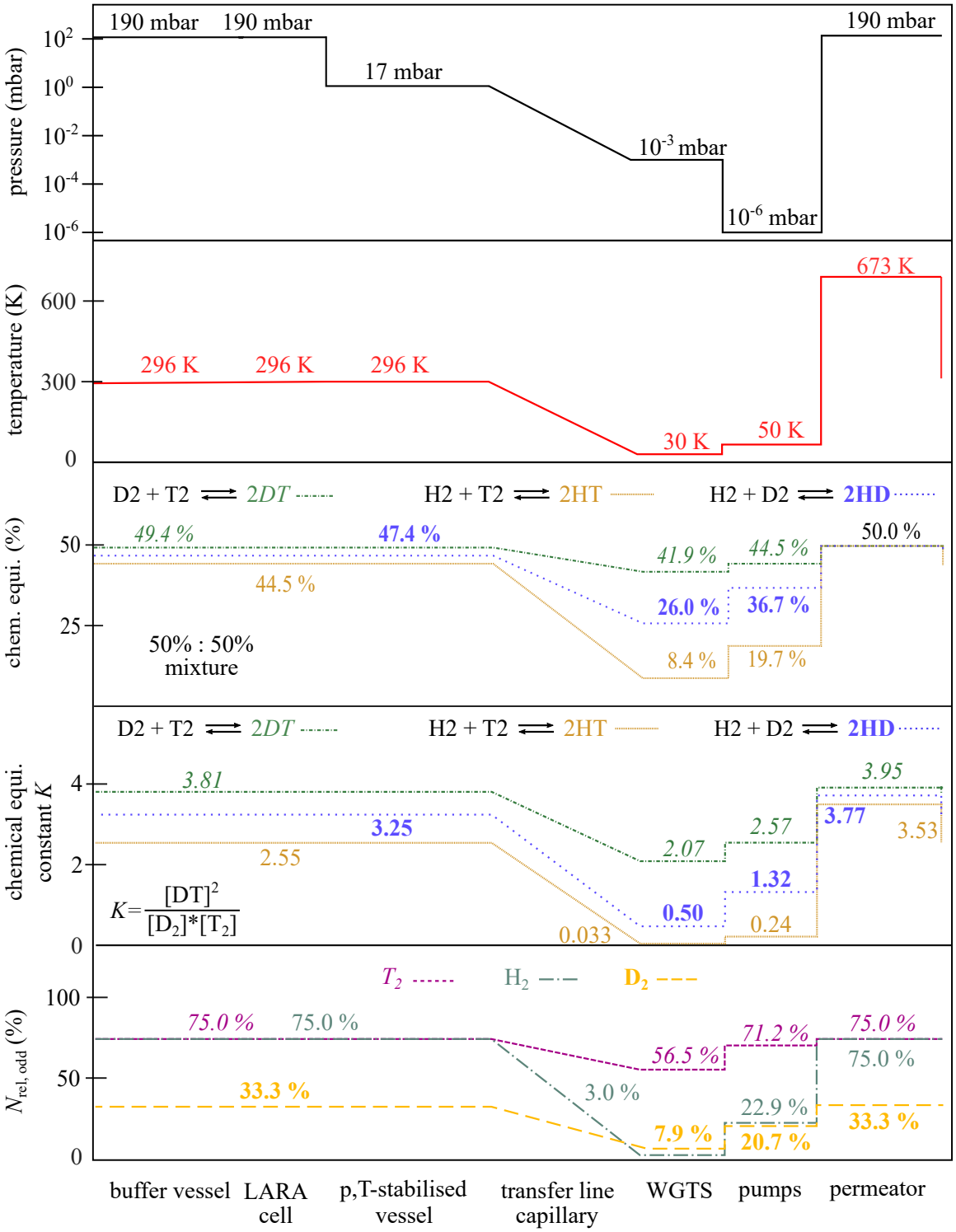

Figure 4.1.: **KATRIN Loops parameters.** On the x-axis the different parts of the KATRIN Loops system are listed. The left and right end are closed, so after reaching the permeator, the gas is stored in the buffer vessel again. On the y-axis different quantities are listed. On the topmost plot the pressure is shown in mbar, below that the temperature in K is plotted. The next two plots show the chemical equilibrium in % and for constant equilibrium constant K, the last plot shows the equilibrium of ortho- and para-hydrogen isotopologues. (Graphic form [Kra23], CC-BY 4.0)

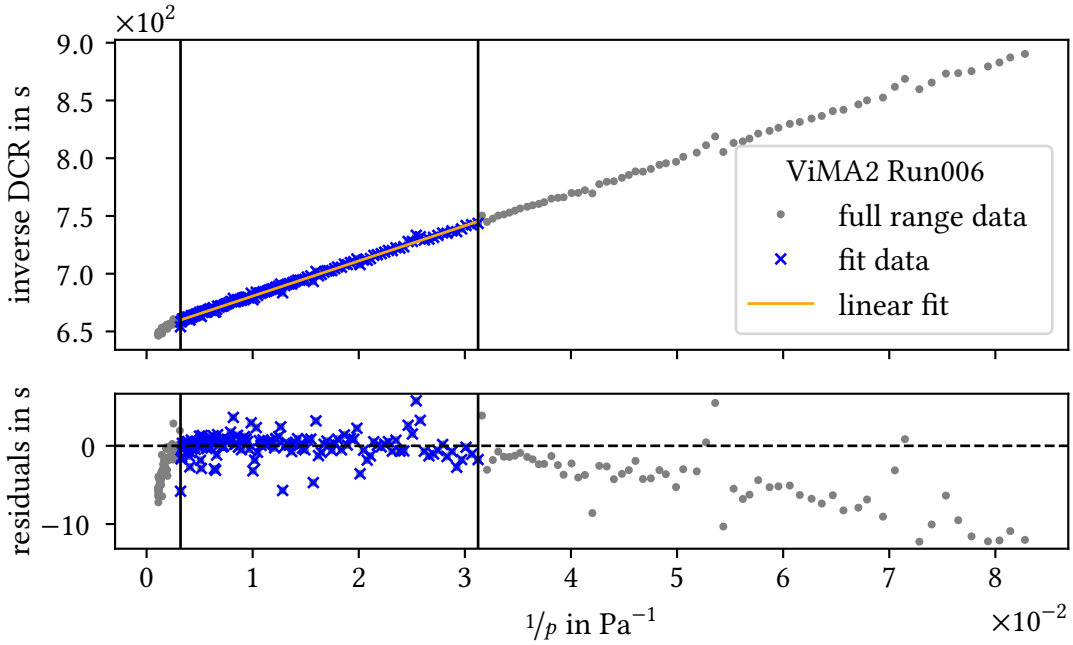

Figure 4.2.: **Knudsen boarders for SRG-viscosity measurements.** This is a picture of a fit to measured data, to show where the Knudsen number exceeds the boarders of the relevant range. The error on the normalized deceleration rate is in the range of 0.2 % and therefore not shown in the diagrams. In the high pressure end (left) as well as in the low pressure end (right) the values start to deviate from the fit.

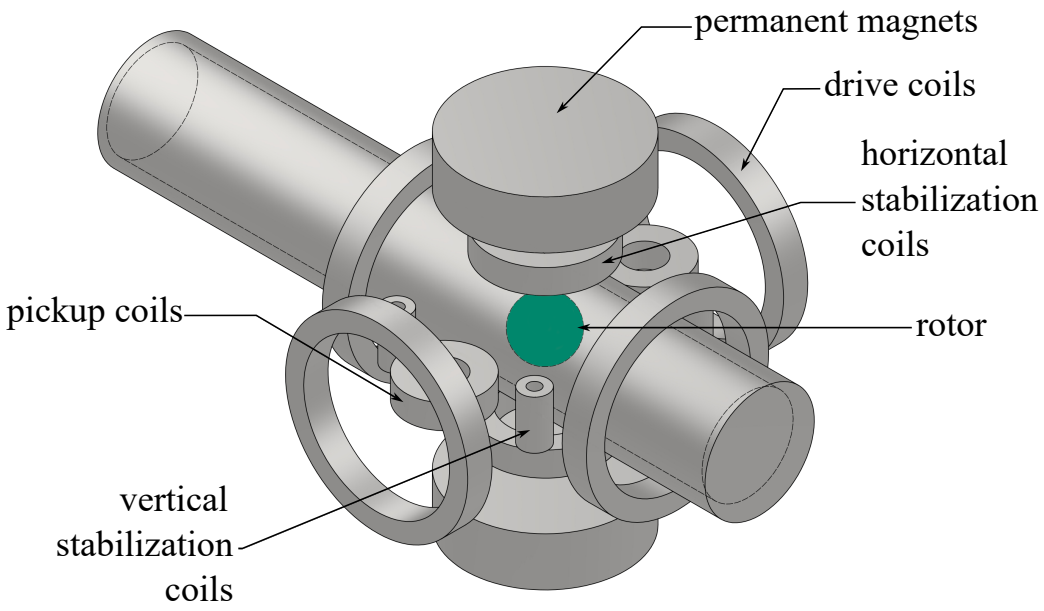

Figure 4.3.: **The SRG magnet system.** The evacuated cylinder is shown with the rotor (green) inside and the different magnet coils for suspension, stabilization, acceleration, and measurement. The sketch is based on [Fre85].

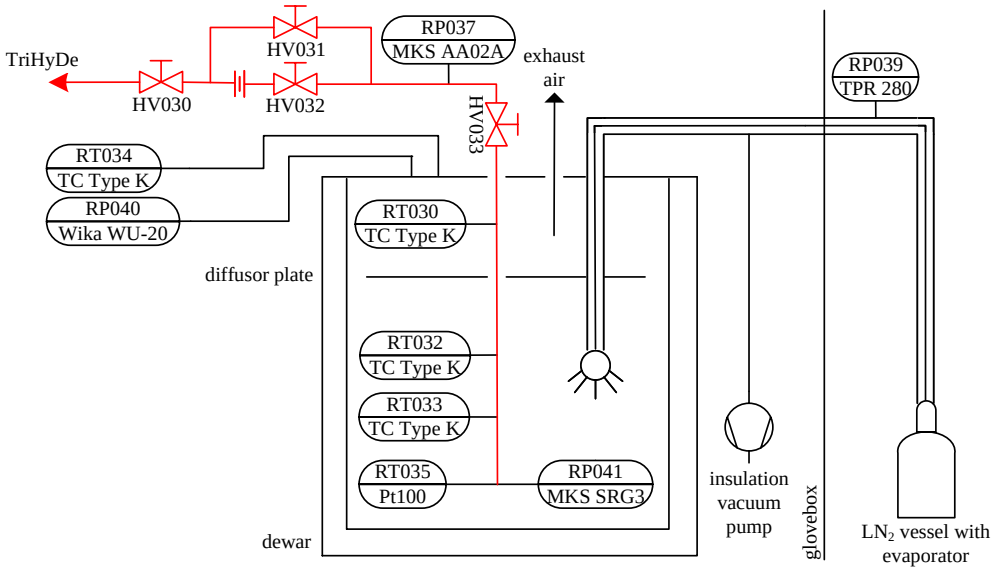

Figure 4.4.: **Flow diagram of the Cryo-ViMA setup.** The primary system is depicted in red. The cryostat together with the coldgas system belong to the cooling system. The vertical line between the LN_2-vessel and the insulation vacuum pump indicates the window of the glovebox. All parts left of this line are inside the glovebox, all parts on the right side of this line are outside of the glovebox.

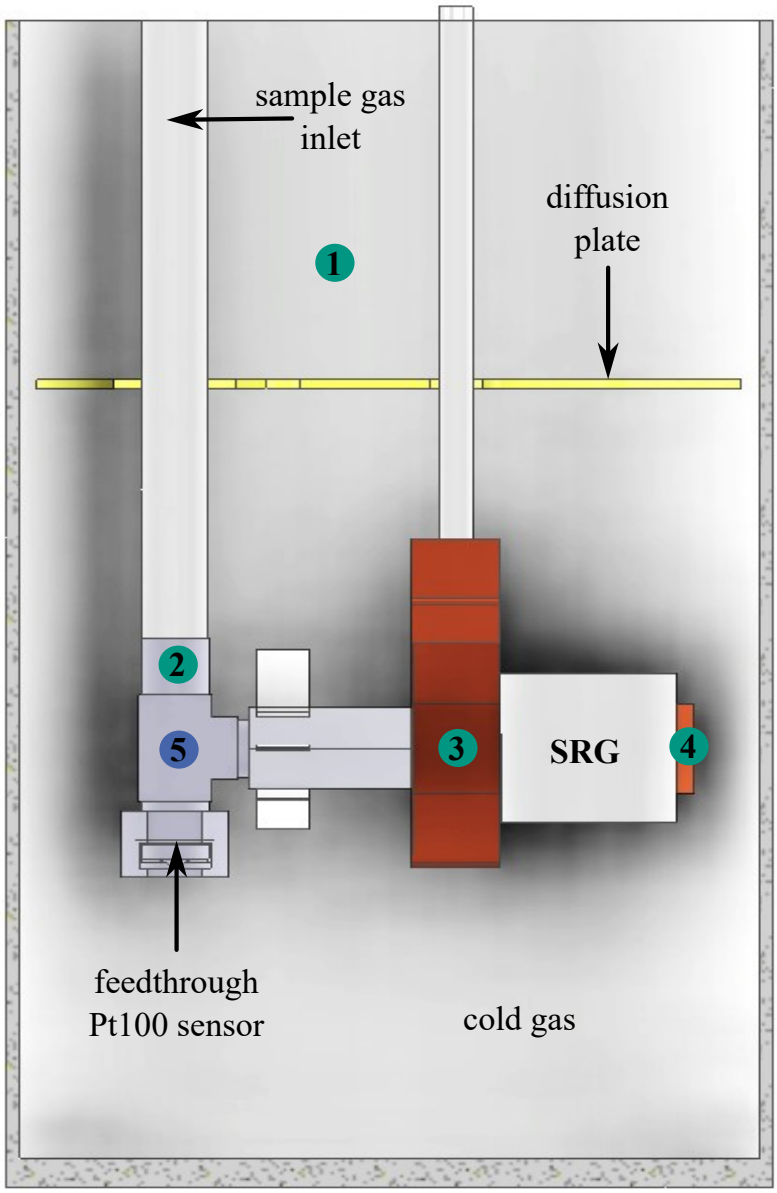

Figure 4.5.: **CAD cut of the Cryo-ViMA setup.** The green dots mark the places of the thermocouple sensors inside the cryostat. ①: temperature sensor for control of the cryostat for measurements at constant temperature. The sensors on positions ②, ③ and ④ are at the connection of the T-shaped tube, the copper clamp and the screw with contact to the evacuated finger, respectively, the blue dot with number ⑤ marks the place of the Pt100 sensor inside the sample gas volume of the primary system.

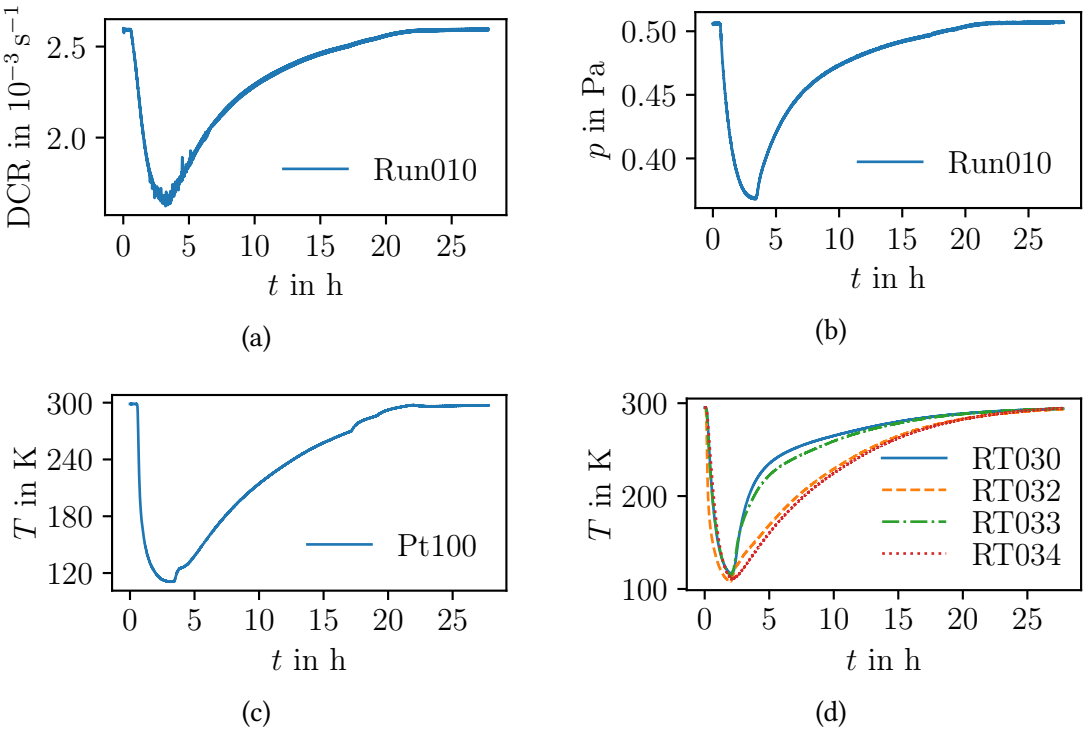

Figure 4.6.: **Thermal cycle of Cryo-ViMA.** On the x-axis of all graphs, the time is shown in hous. On the y-axis the measured deceleration rate (figure 4.6a), the pressure (figure 4.6b), the temperature of the Pt100 (figure 4.6c), and the temperature of the different sensors inside the cryostat (figure 4.6d) is plotted. The positions of the thermocouple sensors are shown in the flow diagram in figure 4.4.

4.3.5. Sample preparation with TriHyDe

As the aim of this work is the measurement of the tritium viscosity, the purity of the gas is guaranteed by the highly selective processing of tritium from the isotope separation system (ISS) [Doe02], clean storage in the tritium transfer system (TTS), and monitoring by the Tritium Hydrogen Deuterium experiment (TriHyDe) [NB24]. Before the gas is transferred to Cryo-ViMA, every gas sample composition is verified at TriHyDe, enabling a precise study of the systematic uncertainty on the viscosity of the gas sample.
TriHyDe is a facility to prepare and measure accurate gas mixtures of hydrogen isotopologues, detailed information can be found in [Nie21]. The facility consists of two loops, the processing loop (P-Loop) and the analyzing loop (A-Loop). The A-Loop comprises two vessels with calibrated volumes, which can be individually filled at precise pressures with different gas types, provided by storage vessels from the P-Loop. For the analysis of the gas composition, the A-Loop contains multiple methods and devices, namely a LArge-RAman system (LARA) system [Sch13; PBG24], a binary gas analyzer (BGA), a system using beta-induced X-ray spectrometry (BIXS) (such as described in [Mat03] and a quadrupole mass spectrometer (RGA). While most of these methods are capable of in-line measurements, the RGA needs to be differentially pumped offline due to the lower maximum operating pressure. For the preparation of a gas sample, the mixing vessels are filled to a precise pressure. By calculating of the molar fractions from the pressure, the volume and the temperature inside the system, the gas composition can be derived with subpercent uncertainty. Gas mixtures of the homogeneous hydrogen isotopologues H_2, D_2 and T_2 always perform equilibrium reactions in the form:

$$H_2 + T_2 \rightleftharpoons 2HT\,, \tag{4.8}$$

not changing the atomic fractions of the constituents, but the fractions of the molecules [Sou86]. The duration of these reactions until an equilibrium of the gas composition is reached varies depending on the involved species. To accelerate the equilibration process, a catalyst is integrated inside the A-Loop, which can be used in the case of non-tritiated mixtures. The Cryo-ViMA experiment is connected to one of the three sampling ports at TriHyDe. This way, the periphery for filling and evacuating gas to and from Cryo-ViMA is completely provided by TriHyDe.

4.4. Measurement procedure

For the data analysis only three quantities are important, the pressure, the temperature and the normalized deceleration rate. The pressure and the temperature of the primary system are read out with the control unit of the SRG. The temperatures and pressures for the monitoring of the cryostat are measured with a separate program. All three primary quantities are measured in intervals of 2 s. To measure the viscosity there are two different measurement procedures. One is done by pressure cycling (figure 4.7b), the other by temperature cycling (figure 4.7a). The general procedure for both modes is the same. At the start of each measurement the rotating sphere is accelerated to 440 Hz. When the

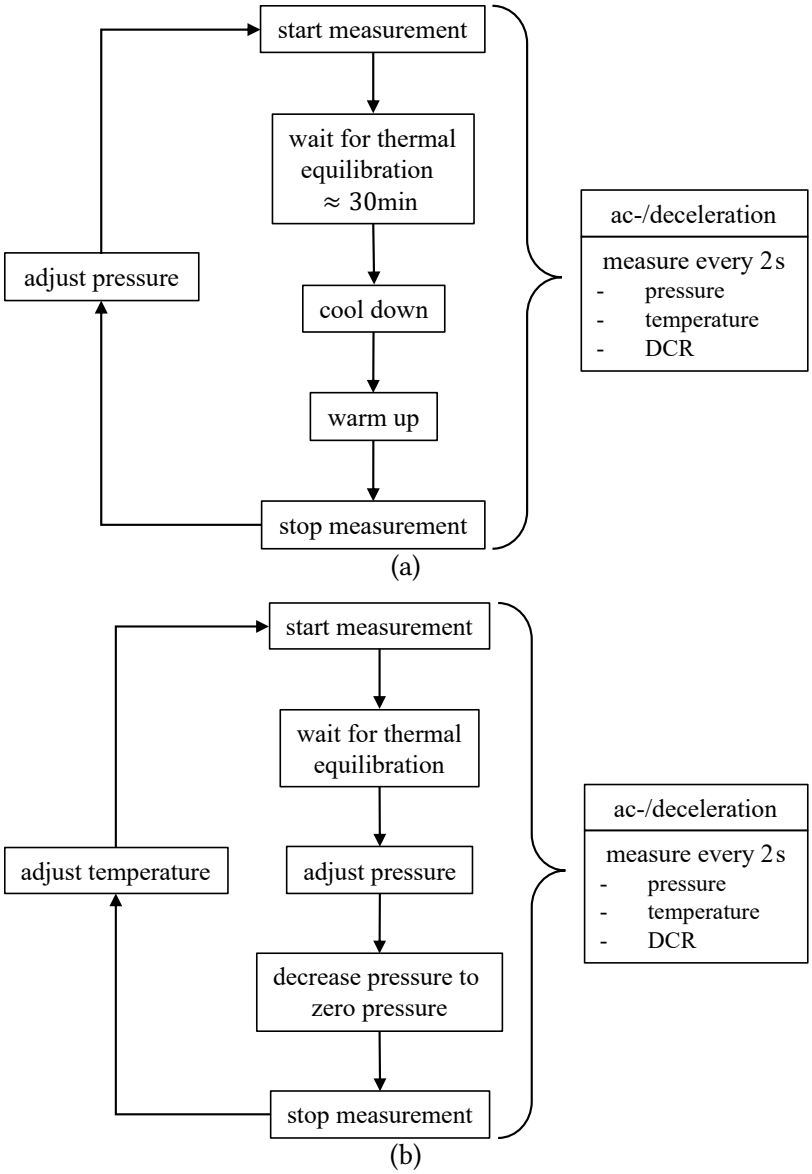

Figure 4.7.: **Block diagrams for pressure and temperature cycling measurements.** figure 4.7a shows the measurement procedure for the pressure cycling mode, figure 4.7b shows the measurement procedure for the temperature cycling mode as described in section 4.4.1 and section 4.4.2, respectively.

acceleration is stopped, the rotation of the sphere is slowly decelerated down to 420 Hz through the residual gas inside the evacuated cylinder. During this phase, the normalized deceleration rate, the pressure and the temperature are read out and logged every two seconds. In addition, the rotational frequency of the rotor is included in the readout process, to be able to account for frequency dependent effects. One measurement cycle is defined as the time between the re-accelerations of the rotor. When 420 Hz are reached, the rotor is automatically re-accelerated to 440 Hz. A graph of such measurement cycles is shown in figure 4.8. This continuous re-acceleration of the rotor has an impact on

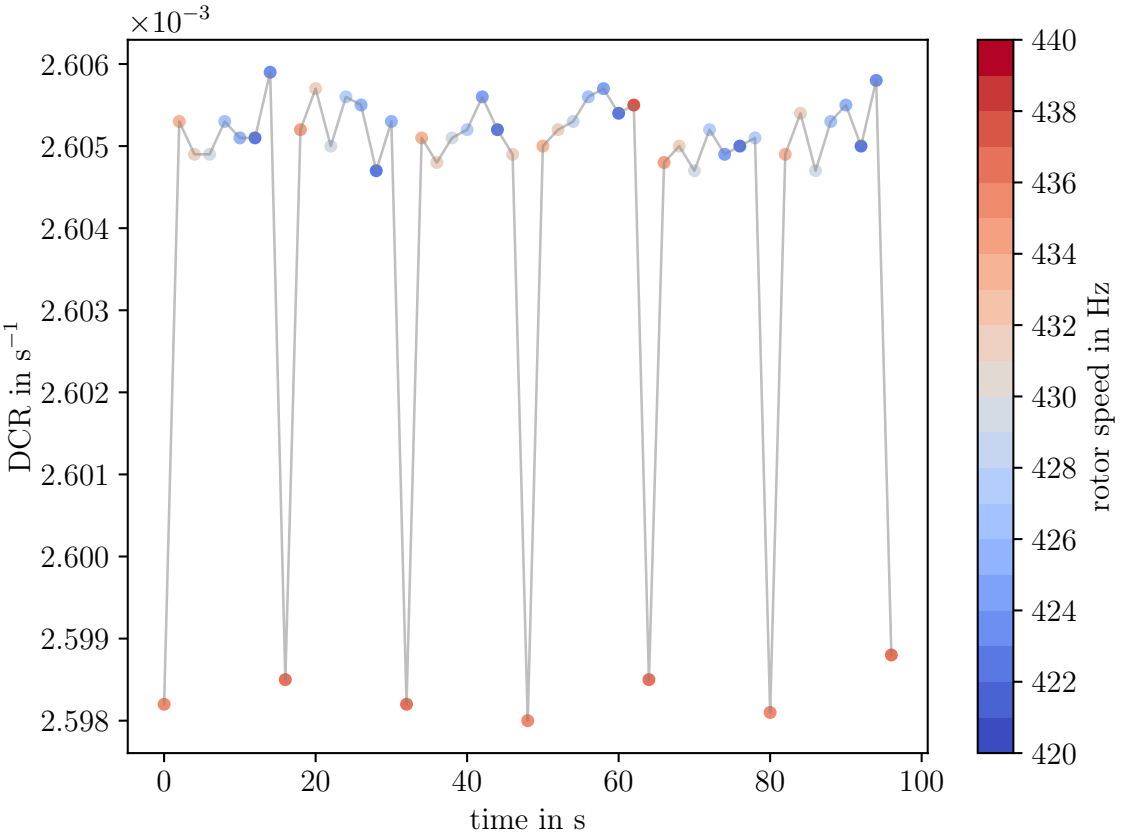

Figure 4.8.: **Measurement cycle of the SRG.** On the y-axis the measured normalized deceleration rate is plotted against the time in seconds on the x-axis. The colored dots represent the measured values, the light grey line is only for eye guidance. The color of the dots indicates the rotational frequency at which the normalized deceleration rate is measured. The downward spikes are the measured values right after the rotor has been re-accelerated to 440 Hz.

the thermal distribution inside the sample gas, which is described in detail in section 5.2. In the following sections the two measurement procedures, with their advantages and disadvantages, are explained in detail.

4.4.1. Pressure cycling

In this mode the pressure is not constant. During a measurement, the temperature is stabilized and the pressure is cycled from 20 Pa up to 2000 Pa and back again. The stabilization of the temperature takes between one hour and one day, depending on the target temperature. The lower the target temperature, the longer the system will need to be stabilized within $2\,\mathrm{K\,h^{-1}}$. This value was found to be the maximum acceptable deviation for high precision results of the viscosity. Otherwise, the temperature gradient inside the SRG is too high and would lead to two problems.

- First, the temperature would be too far away from the measured temperature at the Pt100 sensor, leading to a shift during the viscosity mapping.
- Second, the fit would not be linear anymore, as the temperature rises faster than the pressure can by cycled.

As the viscosity is calculated from the y-intercept, it is not possible to account for temperature changes there. With the temperature stabilized, there are two ways to scan the pressure range. The pressure inside the sample gas volume is set to a specific value, then the measurement is started and after equilibration, which takes about half an hour, data is taken for some minutes to have enough statistics (described in [Wyd22]). This is repeated for different pressure setpoints, leading to an overall measurement time of up to three days. The result of such a measurement is shown in figure 4.9a. For faster results for the viscosity at one single temperature, the measurement of the SRG is started and after equilibration, the pressure in the sample gas is slowly increased, such that after 30 min the whole valid pressure range has been covered as shown in figure 4.9b. In both cases the viscosity can be measured within about two hours up to three days at maximum, depending on the temperature setpoint. This procedure needs to be repeated for every temperature step, which results in a very time consuming measurement campaign. For a highly resolved temperature dependence of the viscosity, this procedure is not very efficient.

4.4.2. Temperature cycling

The previously described method is good to search for the boundary pressures, between which equation (4.3) is valid. As for the viscosity itself the linear fit does not profit from finely stepping through the entire pressure range. To accurately measure the temperature dependence of the viscosity, temperature instead of pressure needs to be measured with a small step width, as it is conducted in [Wyd23]. Still for the data analysis the pressure has to be varied. At the beginning of every new measurement, gas is filled inside the SRG to some dedicated pressure setpoint before the system is closed off. With the system staying closed, the temperature is ramped down and up again, which takes approximately one to two days, depending on the cool-down speed. This temperature cycling is repeated for different pressure setpoints. To have enough data for one linear fit, this measurement mode takes at least one week. The particle number inside the primary systems volume is kept constant over the time of one thermal cycle. According to the ideal gas law, at constant particle density, cooling down will decrease the pressure in the system while heating up will increase the pressure. As the pressure inside the sample gas volume is measured along with all other important quantities, this is no problem. In order to perform a non-trivial linear fit according to 4.2.1, at least three measurements at different pressures are required. This is the preferred mode for measuring the viscosity of tritium over the temperature range from 100 K to 300 K, since it enables a highly efficient way to finely scan through the entire temperature range. In this case, the pressure inside the sample volume is adjusted to one setpoint. Afterwards, the data logging is started before the SRG is started. When the system is in thermal equilibrium, the temperature inside the cryostat is slowly reduced down to 100 K. When this temperature is reached, the cold gas jet is turned off, so the system is passively warmed up again. This thermal cycling takes approximately two

days. Afterwards the pressure can be changed for the next thermal cycle of the system. The advantage of this procedure is the reduced need in temperature stability. The change in temperature only has to be slow enough to allow the system to only form a small thermal gradient, which is monitored with the thermocouple temperature sensors inside the cryostat.

Within this chapter the different challenges of working with tritium in general as well as measuring its viscosity have been explained. The spinning rotor gauge has been described as the perfect measurement device for measuring the viscosity of gases in the zero density limit, as it is needed for the KATRIN experiment. In section 4.3 the measurement setup for measuring the viscosity of tritium over the temperature range from 100 K to 300 K has been shown and the measurement procedure was explained in section 4.4. It has been explained that there are two possible measurement modes, temperature and pressure cycling, which are both practicable, depending on the intended result. Pretests in different development stages described in [Wyd22; Wyd23] showed that the experiment is capable of measuring the viscosity of gases in a temperature range from 77 K to 300 K. In the following section the resulting accuracy of the Cryo-ViMA setup will be pointed out.

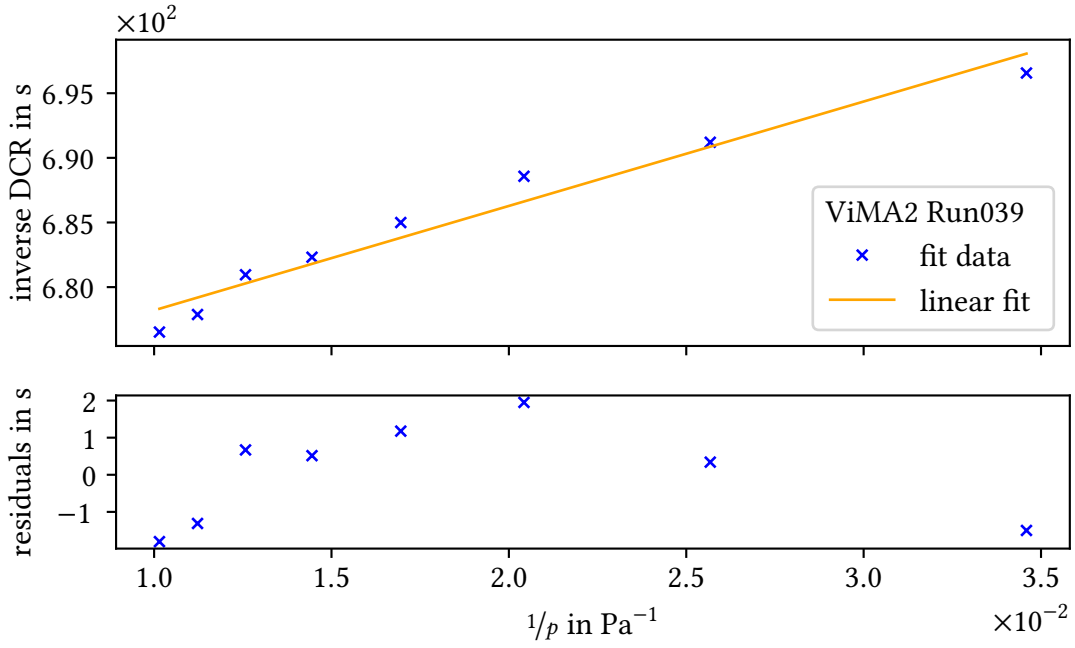

(a)

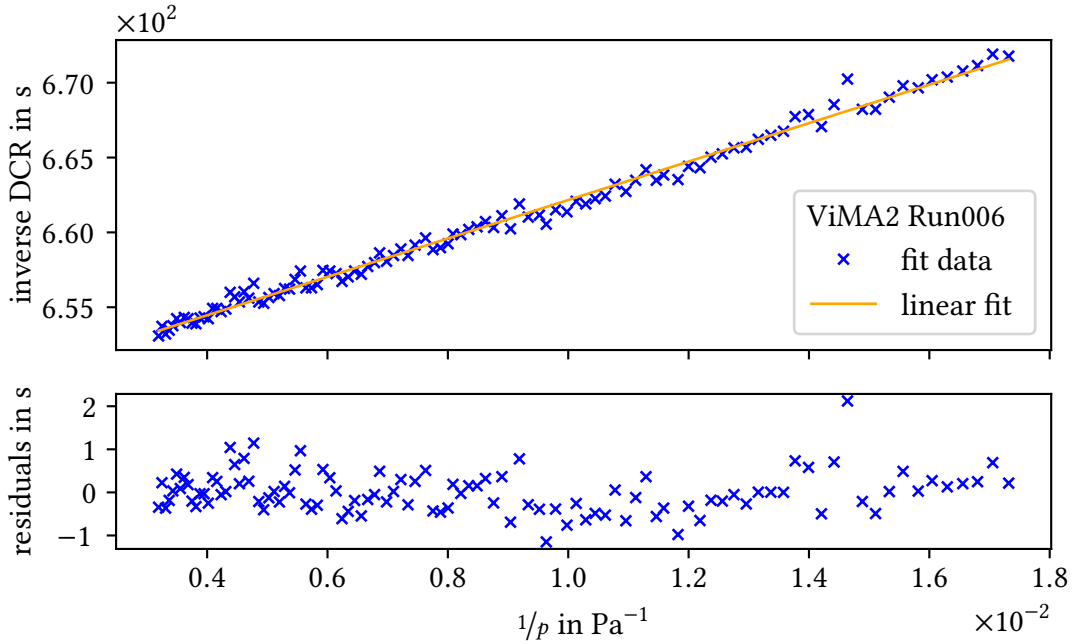

(b)

Figure 4.9.: **Pressure cycling with the SRG.** On the y-axis the inverse normalized deceleration rate is plotted against the inverse pressure in Pa^{-1} on the x-axis. The uncertainty on the normalized deceleration rate is in the range of 0.2 % and therefore not shown in the diagrams. Figure 4.9a shows a measurement for H_2 at 80 K with the discrete pressure cycling method while figure 4.9b shows a measurement for a continuous pressure change under the same conditions. In both plots, the residuals are calculated as the measured inverse normalized deceleration rate (DCR) minus the linear fit.

5. Accuracy of the viscosity measurements with Cryo-ViMA

In the previous chapter the Cryogenic Viscosity Measurement Apparatus (Cryo-ViMA) has been presented as a fully tritium compatible measurement setup. In this section, the achievable accuracy is explained. In section 5.1 the different influences of

- isotopic purity (section 5.1.1),
- dimensions of the SRG (section 5.1.2),
- normalized deceleration rate (DCR) (section 5.1.3),
- pressure (section 5.1.4),
- temperature (section 5.1.5) and
- calibration factor (section 5.1.6)

on the accuracy of the Cryo-ViMA setup are listed and explained. In section 5.2 thermal simulations to account for the temperature gradient inside the sample gas are presented. In section 5.3 results from the calibration measurement with helium are shown. A summary of the contributing uncertainties and their impact on the viscosity measurement is shown in table 5.1.

5.1. Quantities influencing the accuracy of the Cryo-ViMA setup

In this section it is explained how the aforementioned quantities enter the data analysis and their impact on the final measurement is quantified. A short summary of these values and their impact on the viscosity measurement is shown in table 5.1.

Table 5.1.: Uncertainties of the Cryo-ViMA setup and their contribution to the viscosity measurement. The values marked with * can be reduced by additional measurements or are in general negligibly small.

quantity	value	uncertainty on μ in %
Isotopic purity	99 %	0.2*
rotor radius	2.25 mm	2.0
cylinder radius	3.5 mm	0.07
DCR	$<0.01\,\mathrm{s}^{-1}$	0.08
pressure	20 Pa to 2000 Pa	0.2
temperature	100 K to 300 K	0.2
calibration factor	1.24 to 1.26	0.08

5.1.1. Isotopic purity

The first bias on the viscosity measurement is given by the purity of the gas sample. For hydrogen and deuterium, this is not an issue as these samples are pure to the permill level and transferred through clean pipes to Cryo-ViMA. For tritium this looks a bit different. At TLK, tritium can be enriched to over 99 % [Hil24], so the starting purity is already less than for H_2 (99.9999 %) and D_2 (99.8 %). Nevertheless, the impurities of this tritium are only small amounts of hydrogen and deuterium (1 %), as all ^{3}He from the decay of tritium and other impurities like methane are filtered through the isotope separation system (ISS) before the tritium is transferred to TriHyDe via the TTS [Doe02; Nie21]. As explained in section 4.3.5 the samples containing tritium are provided by the TriHyDe facility. Effects from the first contact of the system with tritium, where tritium reacts with surface impurities as mentioned in section 4.1.1, are reduced through a dedicated commissioning phase. For this purpose tritium is filled into the whole Cryo-ViMA system at slightly higher pressure than for the viscosity measurements, and kept there for nearly two weeks. The gas composition is measured at TriHyDe after the two-week commissioning phase. In addition the measurement with the SRG is started to monitor the deceleration rate during this time. In this measurement, it can be seen that the normalized deceleration rate (DCR) first increases, which is normal and caused by the heat produced while starting the rotation of the sphere. But afterwards the DCR slowly decreases again. This behavior might be caused by the buildup of impurities, discussed in section 4.1.1. The proper measurement of the viscosity of tritium is then conducted with tritium directly transferred through TriHyDe from the tritium transfer system (TTS), where the purity of the sample is measured to be 99 %. From equation (4.1) the viscosity of a gas mixture can be calculated. As impurities can be interpreted as a gas mixture, their influence on the viscosity measurement can be determined with this equation. If the sample gas has a composition of 99 % of tritium and 1 % of H_2, equation (4.1) gives a viscosity of the mixture of 15.26 µPa s, calculated with extrapolated values for tritium at room temperature of 15.296 µPa s. If H_2 is replaced by D_2, the viscosity of the mixture is 15.274 µPa s. The deviation to the viscosity of pure tritium is 0.145 % for D_2 and 0.234 % for H_2 as impurity. Depending on the other uncertainties and the total uncertainty budget of about 2 %, it is possible to analyze the gas mixture after the measurement, to double check the gas composition and include this in the analysis.

5.1.2. Dimensions of the sphere and evacuated cylinder

A second source of uncertainty are the dimensions of the sphere and evacuated cylinder. Equation (4.7) can be written in terms of rotor radius and density by including the knowledge of equation (4.4)

$$\mu = \frac{a_1^2 \cdot \rho}{15 \cdot C_0 \cdot y_0}, \tag{5.1}$$

with a_1 being the radius of the rotating sphere, ρ its density, C_0 a calibration constant and y_0 the intercept with the y-axis of the linear fit. The radius of the cylinder a_2 only enters through C_0 in this equation, so it only influences the uncertainty of the viscosity indirectly. Apart from its influence through C_0 it only appears in the slope of the linear fit, which has no influence on the viscosity. As C_0 is not analytically solved but measured

through calibration with helium as explained later in section 5.3, the influence of a_2 on the viscosity is covered by the uncertainty considerations on C_0. For the radius of the sphere a_1 this is different. The rotor radius also enters through C_0, but as this is determined by calibration, this has no direct influence on the viscosity. Nevertheless, equation (5.1) has a dependency on the radius of the sphere squared, resulting in a high impact of the rotor radius on the viscosity. In addition, the setup is thermally cycled between 100 K and 300 K, which causes the radii to change slightly with temperature. For C_0 this is not an issue, as again, the system will be calibrated for the whole temperature range. But for a_1 this is neglected. The material of the rotor is stainless steel of type EN 1.4034, which has an thermal expansion coefficient of $10.5\,\mu m\,m^{-1}\,K^{-1}$ [Ede04], leading to a total expansion of 0.2 %, which is negligible in a first order approximation as the radius is only known to 1 %. The uncertainty of the viscosity caused by the uncertainty of the rotor radius a_1 is ≈2 %, so the original uncertainty goal of 2 % cannot be achieved, while the influence of the cylinder radius is below 0.1 %.

5.1.3. Angular deceleration rate

The angular deceleration rate is the main measurement parameter over which the fit is performed. As shown in figure 4.8, the DCR is not constant over time and pressure, but varies with some spikes depending on the pressure inside the SRG and the temperature of the gas. The maximum spread of the DCR at any temperature between 150 K to 300 K is approximately 0.2 %. The uncertainty on the DCR is 0.1 % according to the manufacturer. From previous investigations by V. Skrobocz[1], it is known that the spikes in the DCR as shown in figure 4.8, are values which are taken right after the re-acceleration of the rotor. In figure 5.1, the rotor-speed of the SRG rotor is plotted over time together with the temperature measured at the Pt100 sensor. The orange values are the outliers of the measured deceleration rate, the aforementioned spikes. At temperatures from 150 K to 300 K, it is easy to filter these points, leaving a maximum deviation of the DCR of 0.08 %. At temperatures below 150 K, the DCR shows more noise, which makes any filtering worthless. Still, the effect on the measured viscosity is in the order of 0.08 % and therefore negligible compared to the other uncertainties.

5.1.4. Pressure

The pressure is measured with a capacitance diaphragm manometer from MKS Instruments[2] with an accuracy of 0.10 % of reading. What has to be accounted for, is that the pressure is measured at an ambient temperature of approximately 295 K, depending on the temperature inside the glove box. The SRG is thermally cycled down to 100 K leading to a temperature gradient inside the setup. This temperature difference along the piping of the setup produces a pressure gradient inside the gas, which is called thermomolecular pressure difference [Sha96]. This effect increases in importance with decreasing pressures and

[1] Bachelor Thesis: "Systematische Untersuchung der temperaturabhängigen Viskosität von Protium und Deuterium aus dem Cryo-ViMA-Experiment" Vincent Skrobocz (04.2024)

[2] MKS AA02A, 20 torr full scale

higher temperature gradients. The actual pressure of the sample gas within the cryostat can be calculated with equation (1) of [Sha96]

$$p_c = p_h \cdot \left(\frac{T_c}{T_h}\right)^{\gamma}, \tag{5.2}$$

where p_c is the pressure of the cold sample gas, p_h is the actually measured pressure and γ is a coefficient depending on different gas and tube specific factors. For the current setup, with a total tube length of 1 m, and pressures from 20 Pa to 2000 Pa, this effect only needs to be regarded from 100 Pa downwards to lower pressures. As the higher pressures are closer to the y-axis intercept, the effect of pressure gradient along the tube on the viscosity is only a second order uncertainty. Nevertheless this correction is implemented in the analysis, meaning the measured pressure is corrected for the gradient depending on the temperature inside the cryostat and pressure measured in the warm part of the system.

5.1.5. Temperature

The temperature is the most critical parameter during the measurements, since it has the highest impact on the trueness of the result. There are two different temperature criteria, one concerning the stability, the other concerning the temperature gradient inside the sample gas volume. The latter one directly influences the trueness of the temperature measurement and therefore the accuracy of the measured viscosity and the trueness of the mapping between temperature and measured viscosity. Also the temperature gradient inside the sample gas volume must not exceed $1\,\mathrm{K\,mm^{-1}}$, otherwise it needs to be corrected for in the analysis.

In addition the different types of temperature sensors have to be calibrated, which is done with a liquid nitrogen bath and ice-water, to get two fixed temperatures. With this calibration the deviations of the temperature sensors from the standard temperature curves is accounted for. The results of this calibration is listed in table 5.2.

The temperature stability of the system is important, if the viscosity has to be measured at one single temperature setpoint, in the pressure cycling method as described in section 4.4.1. The DCR is not only dependent on the pressure, but also on the temperature. A change in temperature during the pressure cycling would cause an additional change in the normalized deceleration rate. This will change the slope of the linear fit and also influence the y-axis intercept from which the viscosity is calculated.

As already has been shown in [Wyd24], there is a temperature gradient inside the sample gas volume built up through the continuous re-acceleration of the rotating sphere. With every acceleration, heat is produced inside the rotor through eddy currents and energy loss, causing the temperature of the rotor to increase. This heat is then slowly transferred through the sample gas to the outer side of the evacuated cylinder, where the system is cooled with cold nitrogen gas. The temperature of the gas cannot be measured close enough to the sphere to measure the increase of the temperature. To still get a handle on the temperature gradient inside the sample gas, two different types of simulations have been performed. The results of these simulations for the measurements with hydrogen and deuterium are found in [Wyd24] and are summarized with the simulations for T_2 in

Table 5.2.: Calibration results of the temperature sensors used in the Cryo-ViMA setup.

Sensor	T_{LN_2} in K	T_{H_2O} in K	corrected slope	corrected intercept in K
Pt100	79.02	275.40	0.999	−1.927
RT030	79.9	273.2	1.014	−4.006
RT032	80.1	272.1	1.022	−4.831
RT033	78.0	272.0	1.011	−1.864
RT034	79.4	272.6	1.015	−3.612

table 5.3. The main results from the investigation by [Wyd24] are shown in figure 5.2. How these kind of simulations are conducted and the results for the simulation for tritium is described in the following sections.

A third uncertainty on the trueness of the temperature measurement is caused by the position of the temperature sensors. The Pt100 sensor, which is read out through the control unit of the SRG, is approximately 10 cm away from the rotor, where the cold gas enters the cryostat. In addition, the thermocouple sensors are mounted on different parts of the primary system, but only outside the sample gas volume, to monitor the temperature gradient inside the cryostat. The temperature curves are shown in figure 4.6c and figure 4.6d. It can be seen that the temperature is not homogeneous throughout the whole cryostat, but there are differences in the reached lowest temperature and the slope during the warm-up period of the system. The difference of the measured temperatures in the relevant region around the SRG reaches about 5 K. It is expected that the Pt100 sensor inside the sample gas volume and the thermocouple sensor named RT034, which is installed at the end of the evacuated cylinder, are the ones closest to the true temperature of the sample gas. RT034 tends to temperatures of about 5 K higher than the Pt100 sensor at the lowest temperatures. As the Pt100 sensor is located inside the sample gas volume but directly behind the outlet of the cold gas, its measured temperature is likely slightly lower than the true temperature around the SRG. RT034 is closer to the rotor of the SRG and outside the sample gas volume. The sensor is coupled to the end of the evacuated finger with a copper screw for better thermal contact. The whole motor head of the SRG is also surrounded by a copper clamp and a block around the KF50 flange, so the temperature distribution in this area is very flat due to the high thermal conductivity of copper. It is expected that this sensor measures slightly higher temperatures than the true temperature of the sample gas, leading to the true temperature being between the values measured by RT034 and Pt100. This has no direct influence on the measured value of the viscosity, but on the temperature mapping leading to an uncertainty on the x-axis of the temperature dependence plot of the viscosity. As the mapping is done with the Pt100 sensor, the mapped temperature is likly to be approximately 2 K lower than the true temperature, but only in a temperature range of 100 K to 150 K.

5.1.6. Calibration factor C_0

The calibration factor C_0 is calculated from the helium measurement utilizing the ab initio calculated viscosity values for helium from [HM00]. These are known with an uncertainty on the sub-percent level, so the uncertainty on these values is negligible compared to the previously discussed uncertainties. As these measurements are all conducted in the same manner, with the same temperature curves and pressure setpoints, it is possible to not only use helium as a calibration gas, but conduct the measurement with neon for example, where there are also good ab initio values for the viscosity known. The calibration could then be conducted with neon and validated with viscosity values of helium. This was not possible to do within the scope of this thesis, but will be done in the future. With such a validation, all deviations from the expected behavior can be explained by the different behavior of diatomic molecules compared to noble gases when it comes to hydrogen and deuterium or even the radioactive nature of tritium. Without this, the uncertainty on the calibration factor C_0 is still on the order of 1 % to 2 %, depending on the temperature setpoint. With the test first setup without thermal stabilization at room temperature, there were many measurements in the pressure cycling mode done. The variation of C_0 calculated with these measurements was approximately 1 %. This is used as the statistical uncertainty for the calibration measurement with the Cryo-ViMA setup, even though the statistical uncertainty should be much lower with the thermal stabilization of the final setup. The result of the calibration measurement is shown in section 5.3.

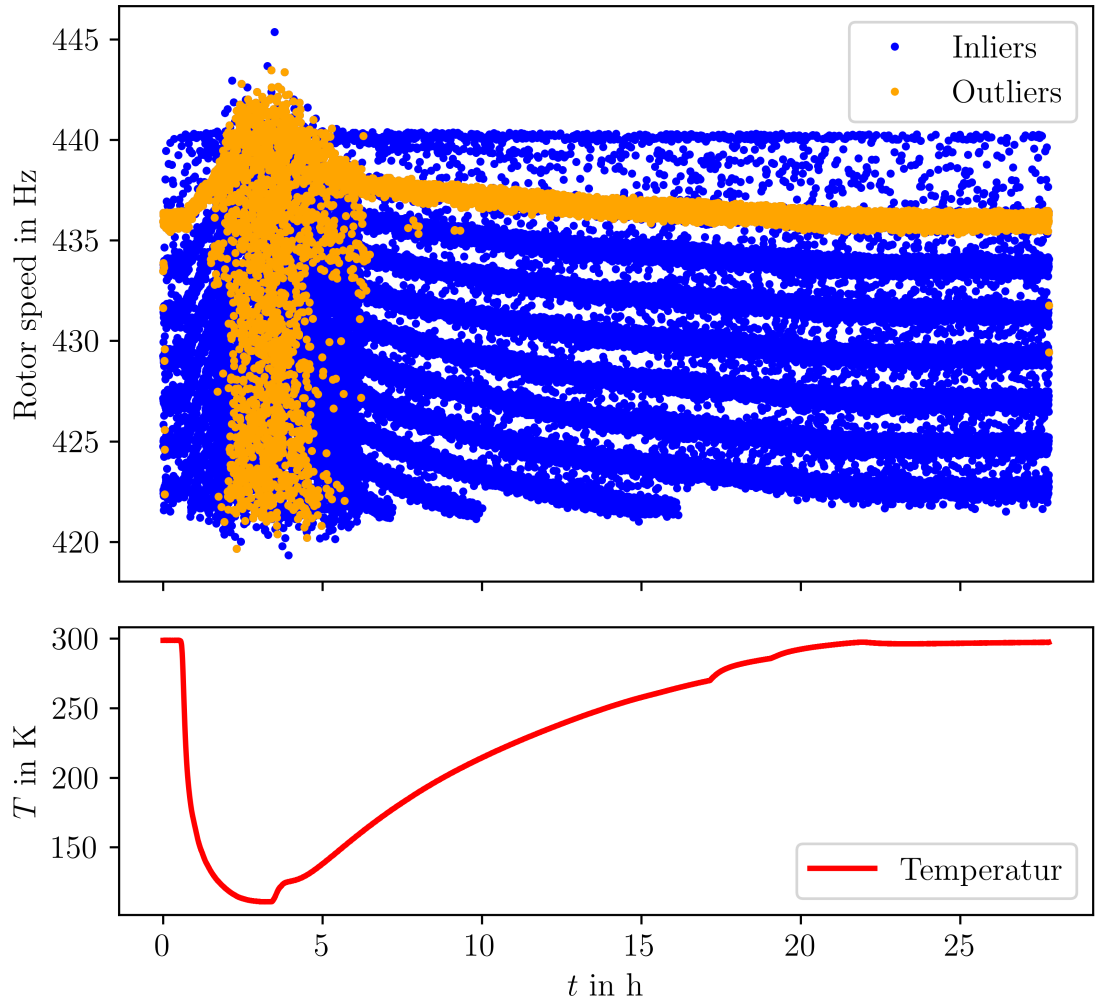

Figure 5.1.: **Rotor speed of the SRG rotor during one thermal cycle.** The rotor speed is plotted as blue points against the measurement time. The orange points correspond to the measurements for which the DCR deviates more than the average. On a second axis the temperature of the measurement is plotted over the measurement time, showing that the frequency bands of the rotor speed vanish below 150 K.

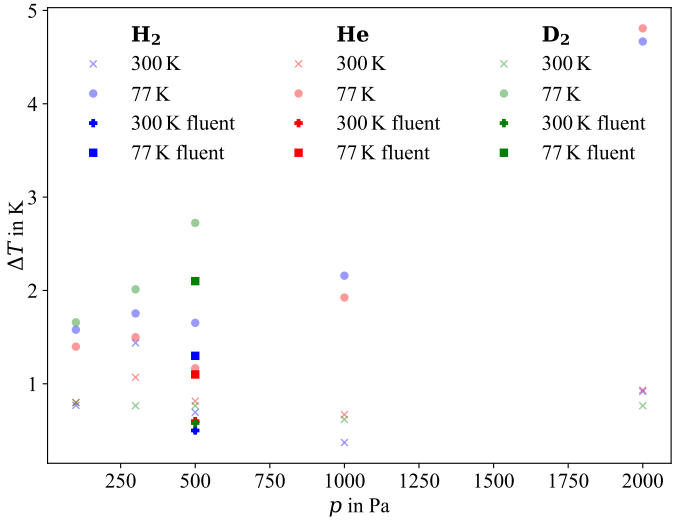

Figure 5.2.: **Simulated temperature difference for He, H_2 and D_2.** The temperature difference is shown in dependence of the pressure setpoint. As can be seen, the temperature difference is smaller for measurements at 300 K than for measurements at 77 K. Also the simulations conducted with Ansys® Workbench Fluent show smaller temperature differences. This plot is found in [Wyd24] under CC-BY 4.0.

5.2. Thermal simulations of the Cryo-ViMA primary system

To be able to understand the results of the simulations done to improve the knowledge of the temperature gradient inside the SRG, it is crucial to first understand the basic principle of the finite elements method (FEM). More information can be found in standard books like [Öch23] and [Dem24]. A more practical book, which also explains the usage of Ansys® Workbench, an FEM multiphysics program, is for example [Geb18]. In figure 5.3, the basic principle of FEM is depicted by taking the example of a long tube which is bent by an external force F. In this easy example, the bending radius could also be calculated by hand. This changes if the geometry under estimation is not simple anymore, but has a complex shape. To keep things easy, the tube example shall suffice to explain the working principle of the FEM. If the depicted tube is fixed at one end, and on the other end an external force F is applied, the tube will be bent. The bending radius can in first approximation be calculated from the angle β between the relaxed tube and the stressed tube. To get closer to the real bending radius, the tube can be sliced into two parts. In this way the uncertainty will become smaller, as the tube is sliced into smaller and smaller elements. This method can be used for many different types of problems. Within the Ansys® Workbench, it is possible to simulate mechanical stress, vibrations within workpieces, and thermal stress. Different types of simulations can be performed as stand-alone solutions or even coupled with one another. The thermal simulations are of interest for this thesis. There are two different ones provided by Ansys® Workbench, which will be explained separately. The basic principle is the same, so the general procedure is explained here. At the beginning of every simulation, the needed material properties have to be defined. Ansys® Workbench offers a huge material library, but special material like deuterium and tritium are not included. The second part is the geometry generation and model building. Often geometries are given, but still, there are many possibilities to reduce them to simpler models exploiting symmetries, to reduce the computing time. The so called mesh, the slicing of the geometry, has to be applied and adjusted. As a rough guide, regions where high stress, thermal load, or gradient thereof is expected, the mesh has to by finer than in other regions. Afterwards the physical boundary conditions, such as thermal heat loads or mechanical forces, have to be applied. Depending on the type of simulation chosen, there are different solver types to choose from. For mechanical and normal thermal simulations, the solver itself stays the same, but the underlying equations can be adjusted. For fluid simulations the solver has to be chosen depending on the Reynolds-number, density of the fluid and flow rate. After the simulation is finished, there are multiple tools to analyse the results during the post processing, depending on whether a thermal gradient along a trace, across a plane or through a volume is needed. Also integral heat loads can be calculated from the loads on each cell of the mesh. How the thermal simulations on the SRG are conducted is explained in the following section 5.2.1. In addition, a fluid simulation has been conducted, which is explained in section 5.2.2.

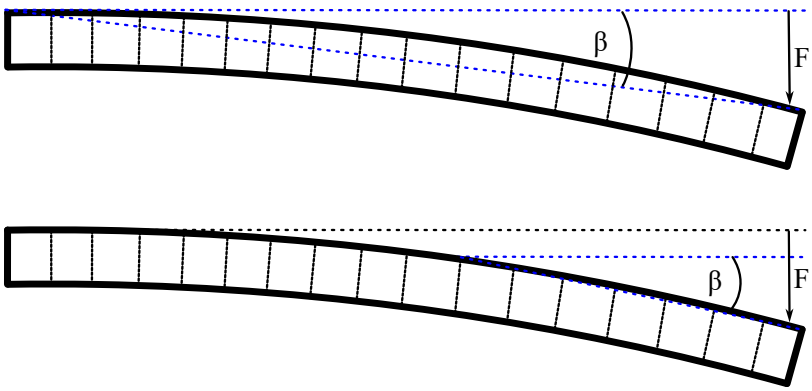

Figure 5.3.: **Basic FEM problem.** The bending radius of a tube which is bent by some external force F can be calculated with FEM, by slicing the tube into small segments. For each segment the forces and the positions of the corners, the so called nodes, are calculated by approximated equations.

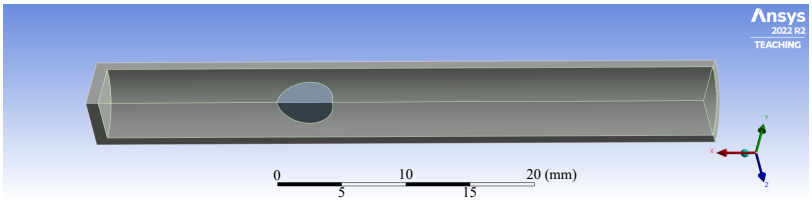

Figure 5.4.: **Geometry used for the thermal simulation of the SRG.** As can be seen, for the simulation only a quarter of the cylinder together with the rotor and the sample gas volume are used.

5.2.1. Thermal simulation of the SRG with ANSYS®

The basic principle of FEM simulation has been explained in the previous section. In this section, the geometry used for the simulation will be shown with its special boundary conditions and the calculations used for the heat generated inside the rotor of the SRG. The simulation is done with Ansys® WorkbenchR2 Mechanical, which includes a transient thermal analysis. There is also a static thermal analysis, but as the heat load is periodically applied, the transient analysis is the more appropriate choice. The theory used for the calculations can be found in [Jou18], chapter 24.3. A brief description of how the simulation is conducted together with the results has been explained in [Wyd24]. As described in section 5.1.5, it is expected that the rotating sphere is heated up by the continuous reacceleration. The effect on the surrounding sample gas is not measurable, as the total gradient is only a few millimeters away from the rotor, where it is not possible to place a temperature sensor. For the simulation, the heat load on the rotor is needed. From this, its temperature can be calculated and with this and the known thermal conductivity of the rotor and the gas, the temperature of the gas can be simulated. As a start, the thermal heat is defined as

$$Q = c \cdot m \cdot \Delta T\,, \tag{5.3}$$

with c being the specific heat of the rotating sphere, m being its mass and ΔT being its temperature difference between the start and the end of the acceleration. From the manufacturer of the SRG the radius and the density of the rotor is given, replacing the mass of the rotor in equation (5.3). Based on the Pirouette-effect, which couples the rotational frequency of the sphere with its expansion, [Jou18] stated that the normalized deceleration rate $\frac{\mathrm{d}\Omega}{\mathrm{d}t}/\Omega$ is coupled to the temperature through

$$\frac{\mathrm{d}\Omega}{\mathrm{d}t}/\Omega = 2\alpha \cdot \frac{\mathrm{d}T_{rotor}}{dt} \tag{5.4}$$

with the thermal expansion coefficient α of the rotor. Assuming a small time-step $\frac{\mathrm{d}T_{rotor}}{dt}$ can be transformed to ΔT. With this, equation (5.3) can be written as

$$Q = c \cdot \rho \cdot V \cdot \frac{\Delta(\frac{\mathrm{d}\Omega}{\mathrm{d}t}/\Omega)}{2\alpha}, \tag{5.5}$$

where $\Delta(\frac{\mathrm{d}\Omega}{\mathrm{d}t}/\Omega)$ is the difference between the highest and the lowest normalized deceleration rate within one acceleration cycle of the sphere. ρ is the density and V the volume of the rotor. The values for $\Delta(\frac{\mathrm{d}\Omega}{\mathrm{d}t}/\Omega)$ differ between the measurements, depending on the measured gas, its pressure, and its temperature, which is why the simulations can only be conducted after the measurements. In figure 5.4 the geometry as used for the thermal simulation is shown. For the simulation, only the evacuated cylinder with the rotating sphere is simulated, including the gas volume. To keep the simulation time efficient, the geometry is cut two times along the cylinder axis, so only a quarter of the SRG is simulated. The heat Q calculated from equation (5.5) is applied to the rotor as an internal heat generation, which resembles best the heating of the sphere by eddy currents, as it happens within the SRG. The thermal contact between the sphere and the sample gas is interpreted as perfect. In contrast to the fluid simulation, the gas flow and the resulting smoother temperature gradient is completely ignored. The pressure of the gas inside the cylinder is defined by the particle density during the material specification according to the pressure range of the measurement. Concerning the thermal boundary conditions, the outer surface of the cylinder is set to ambient temperature, meaning 300 K for all gases and 77 K for helium, hydrogen and deuterium and 110 K for tritium, depending on the targeted temperature of the measurement. The measurements at 77 K have been conducted with a previous test-setup, where the SRG was installed inside a liquid nitrogen bath. This setup is not the final one installed inside the glovebox and therefore a measurement with tritium was not possible here. As the tritium measurements have not been conducted yet with liquid nitrogen, the lowest measured temperature here is 110 K. These given temperatures are also the initial temperature of the complete simulated system, so the simulation is started from thermal equilibrium. To mimic the heat production from the acceleration cycles, the heat load is activated for 2 s before the system has time to cool down again for 6 s to 17 s, depending on the values found during the measurements. The parameter set and the simulated maximum difference in temperature ΔT for each simulation is listed in table 5.3. The values for helium have been taken from [HM00], the ones for hydrogen and deuterium have been taken from [NIS22]. In section 2.4, it is explained that the viscosity

is not the only material property of tritium which is missing, but also experimental values for the thermal conductivity and the heat capacity are unknown to the best knowledge of the writer of this thesis. Still, the thermal conductivity of tritium is essential for the thermal simulation of the temperature distribution inside the sample gas. Therefore, is has to be approximated by a calculation as explicitely described in [MS66]. It can also be extracted from the results of the Boltzmann equations for the viscosity and the thermal conductivity as shown in [McC90]. Here the viscosity μ is defined as

$$\mu = \frac{5k_{\mathrm{B}}T}{4\overline{v}_r\sigma_{tot}} \tag{5.6}$$

with the relative speed of the gas particles $\overline{v}_r$ and the total cross-section σ_{tot}. The thermal conductivity is defined as

$$\lambda_Q = \frac{75k_{\mathrm{B}}^2T}{16m_g\overline{v}_r\sigma_{tot}} \tag{5.7}$$

with the mass of the gas particles m_g. It can easily be seen that the thermal conductivity can be written in terms of viscosity as

$$\lambda_Q = \frac{15k_{\mathrm{B}}}{4m_g}\mu\,. \tag{5.8}$$

From the results of the temperature difference within the sample gas, it can be seen that the temperature difference does not change linearly with the heat load as seen in table 5.3. It can even happen, as it does for deuterium, that for decreasing heat load the temperature gradient increases. Nevertheless, the temperature difference at 300 K is always smaller than at 77 K (see Fig. 4 in [Wyd24]). This is caused by different time conditions. For deuterium the time of cool down within one deceleration cycle is longer than for hydrogen or helium. Tritium seems to have higher temperature differences than the other gases, which will be crosschecked with the fluid simulation in the following section.

5.2.2. Fluid simulation of the SRG with ANSYS®

The transient thermal simulation of the previous section does not include any gas particle motion, which leads to lower heat transfer through the gas. To see the effect of this, a fluid simulation is performed, which includes the gas motion caused by the rotation of the sphere. The fluid simulation of the same setup is done with Ansys® Workbench2022 R2 Fluent. The results for helium, hydrogen and deuterium have been published in [Wyd24]. In this section, the results for the measurements with tritium are shown. The geometry remains the same as for the transient thermal simulation with the exception, that the full cylinder and rotor are simulated, to account for the gas flow around the rotor. In this case it is expected, that the maximum temperature difference is slightly lower, as the heat produced by the rotor is more efficiently, and therefore much faster, transported away from the rotor to the outside of the cylinder, where the system is cooled. This is shown in [Wyd24]. As the simulation does not include any heat from the decay of tritium but only the standard gas parameters, it is also expected that the fluid simulation gives smaller

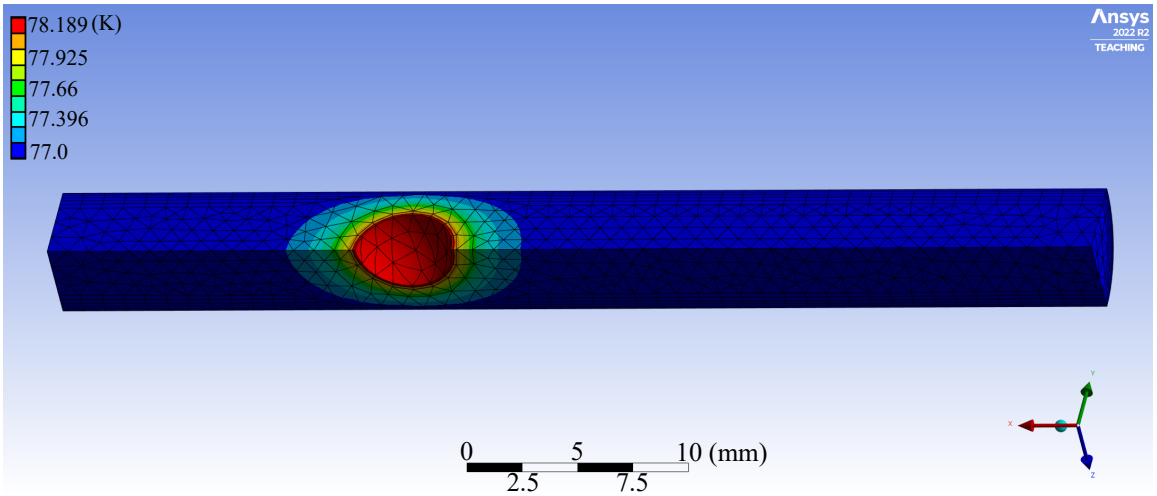

Figure 5.5.: **Thermal simulation of the SRG.** The thermal gradient, generated with this simulation of the heat inside the SRG at 300 K and 2000 Pa is ≈ 1 K over a distance of 3 mm.
Example for the thermal gradient inside the sample gas volume. The Cylinder and the rotor are included in the simulation, but excluded on the graph for optical reasons. This picture shows the simulation result for helium at 300 K and 2000 Pa.

temperature differences than the transient thermal simulation for tritium. In section 3.1, it is explained that the slip regime is a small region below the continuum flow in terms of particle density. Nevertheless, the densities are high enough to be able to simulate the gas flow in terms of continuous flow, as for the study the exact flow is not of interest, only the maximum transported heat. For this simulation again, the heat is produced inside the rotor as internal heat production, which replicates the heat caused by eddy currents inside the rotor. A second boundary condition to the rotor is given by its rotation, which is implemented as moving wall. This means that the gaseous zone is coupled to the wall of the rotor, which causes the gas particles to move around the rotor, according to their implemented material properties. The geometry itself is not rotated, only the wall or contact region is rotating. The result of the particle motion can be seen in figure 5.6. Each line on this figure is to be understood as a particle track. This shows that the flow inside the SRG can be interpreted as two main turbulences around the sphere and next to it. To be able to resolve this motion, the time steps for each iteration have to be smaller than the ones for the transient thermal simulation by a factor of 100, increasing the computing time from a few minutes to hours for one complete simulation. In [Wyd24] it is shown that the resulting temperature difference of these kind of simulations are slightly lower than the ones calculated by the transient thermal simulations. As seen in the transient thermal simulation, the values for the temperature difference for tritium are higher by nearly a factor of two, compared to the other gases, which is caused by different effects: First, the thermal conductivity is only a calculated value as described with equation (5.8), where it is stated in [MS66] that these values are normally slightly underestimated, leading to a lower heat transport and higher temperature gradient. Second, the heat capacity in the

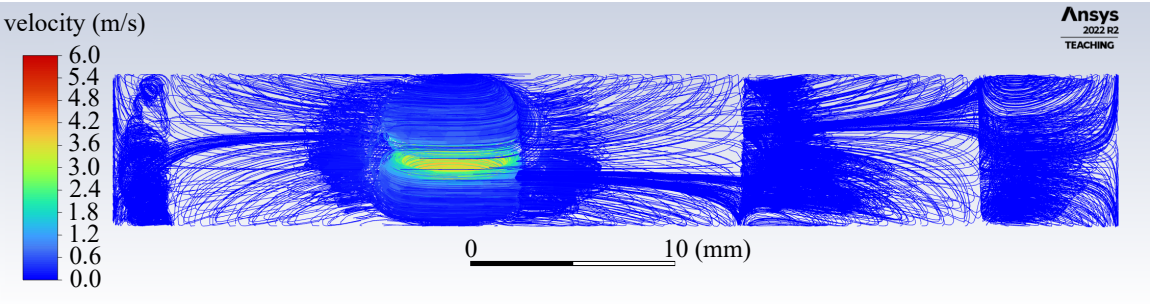

Figure 5.6.: **Gas flow around the rotating sphere.** The lines correspond to the simulated particle tracks, the color indicates the velocity. It can be seen, that there is a higher velocity where the rotating sphere is located. The other particle tracks are indicated with nearly zero velocity, still some turbulences seem to form.

needed temperature and pressure range is unknown in literature and only extrapolated from hydrogen and deuterium. Third, the time for acceleration and deceleration is not as clearly distinguishable as for the measurements of the other gases. This is caused by the fact that for tritium, there are no measurements conducted at constant temperature, so the intervals from which the time can be extracted are much smaller than for the other gases, where these values are extracted from the measurements with the former test setups. The last point on this list is caused by the same circumstance as the time of the acceleration cycles. While the temperature is slowly changing with time, the deceleration also changes, leading to higher differences in the deceleration rate, than for a measurement at constant temperature. This leads to higher heat loads on the rotor, increasing the temperature difference inside the sample gas. In general, it can be said that the temperature difference for tritium is overestimated. A second simulation with a thermal conductivity 5 % higher than the calculated one, and a heat capacity 3 % higher than the extrapolated one, and 20 % lower heat load results in a temperature difference of 1.9 K, which fits the results of the other gases. By only changing the difference in the deceleration rate by 10 %, which is not much for the measurements under consideration, the temperature difference reaches values of 2.2 K. This shows how important it is to get the input parameters of the simulations right.

As shown in table 5.3, the differences of the results of the two types of simulation are negligible compared to the accuracy of these simulations. During the analysis process, the temperature mapping is only dependent on the average temperature of the Pt100 and the thermocouple sensor with a small offset function, to account for the results of the simulation.

5.2.3. Influence of the temperature gradient on the viscosity

The previous two sections show results for the thermal simulations conducted for the viscosity measurements with a SRG. As the transient thermal simulation is much faster concerning computing time, it is conducted for many different pressure and temperature settings. The computing time of the fluid simulation is larger by a factor of 10 to 100,

Table 5.3.: Parameters and resulting temperature difference within the sample gas of each simulation. ρ_g is calculated from the given pressure and temperature. For helium, λ_Q is taken from [HM00], for tritium it is calculated from [MS66], for the other gases it is taken from [NIS22]. The heat capacity for all gases is taken from [NIS22]. The heat load Q is calculated with equation (5.5) from the difference in the DCR for each measurement. The pressure corresponds to the measured pressure at room temperature from which the gas-density ρ_g needed for the simulation is calculated. TTS corresponds to the result from the transient thermal simulation, FS are the results from the fluid simulation. The values containing a * are taken from [Wyd24].

Gas	helium		hydrogen		deuterium		tritium	
T in K	300	77	300	77	300	77	300	110
p in Pa	2000	500	2000	500	2000	500	2000	500
ρ_g in $10^{-3}\,\mathrm{kg\,m^{-3}}$	3.21	3.126	1.616	1.574	3.231	3.147	4.837	3.298
λ_Q in $\mathrm{W\,m^{-1}\,K^{-1}}$	0.156	0.065	0.186	0.054	0.132	0.381	0.076	0.035
c in $\mathrm{J\,K^{-1}}$	5193.6	5193.2	14307	10632	7246.1	7326.6	4632	4632
$\Delta(\frac{\mathrm{d}\Omega}{\mathrm{d}t}/\Omega)$ in $10^{-6}\,\mathrm{s^{-1}}$	2.8	3.4	3.78	6.33	2.6	2.3	7.8	6.0
Q in $10^{-2}\,\mathrm{W\,m^{-2}}$	2.25	2.74	2.04	5.09	2.09	1.85	6.28	4.83
ΔT TTS in K	0.61	1.19	0.71	1.52	0.66	0.89	2.6	4.0
ΔT FS in K	0.52	1.1*	0.5*	1.3*	0.6*	2.1*	2.6	3.9

depending on the settings and the time until the system reaches equilibrium. As the fluid simulation shows results which are compatible to the ones from the transient thermal simulation, the fluid simulations are only conducted at the higher relevant pressures for two different temperatures as there the highest temperature differences are seen. As shown in the thermal simulation, the maximum temperature difference is the higher the lower the temperature setpoint is. This shows that a correction of the measured temperature to the actual one is not a simple offset, but has to be adjusted to the temperature setpoint and the pressure. The difference between maximum and minimum temperature is distributed over a distance of 3 mm, which corresponds to a gradient of $0.5\,\mathrm{K\,mm^{-1}}$, which is half as much as the maximum allowed temperature gradient, stated in section 5.1.5 for hydrogen. For tritium the gradient is $1.3\,\mathrm{K\,mm^{-1}}$, which is above the accepted maximum temperature gradient. Concerning the pressure dependence of the temperature gradient, as seen in [Wyd24], the temperature difference can be assumed to be constant within the slip regime and increasing to higher pressures except for the measurements at 2000 Pa, where the temperature difference is again rather small, compared to the uncertainties of the simulation. This means that for decreasing temperature setpoints, an increasing temperature offset has to be added to the measured values, but can be assumed to be constant over pressure, as long as the values used for the analysis are within the slip regime. Seeing that the parameters of the simulations conducted within this thesis are at the border of the slip regime, the true thermal gradient inside the sample gas volume for the relevant measurements will be smaller than the simulation suggests. The viscosity is temperature dependent, but the temperature is only used for the mapping of the calculated

results, not for the analysis directly, since from equation (4.7) it is known that the y-axis intercept is not dependent on the temperature.

5.3. Characterization and calibration of Cryo-ViMA with helium

In section 3.2, it has been explained that the viscosity measurement with a spinning body viscometer is a relative measurement, since the apparatus has to be calibrated against another gas. In the case of Cryo-ViMA, the calibration is conducted with helium, where the viscosity is known from ab initio calculations with an uncertainty of 0.1 % [HM00]. To make sure that no temperature dependent effects of the calibration factor affect the analysis of the viscosity of other gases, the calibration is also conducted over the full temperature range. The measurement mode used is the temperature cycling mode, described in section 4.4.2. The results of this calibration measurement is shown in figure 5.7a. Only the pressure cycles which are included in the analysis are shown, as many are excluded by the Knudsen-criteria for the slip regime. For every temperature, the corresponding pressure setpoints are selected and a linear fit of equation (4.6) is conducted. From this linear fit, the y-axis intercept is used to calculate the calibration factor C_0, of which the results are shown in figure 5.7b. There are different artifacts in the temperature dependent results of C_0.

- From 125 K to lower temperatures, the values of the deceleration rate start to scatter more than above that value, which causes the measurement to abort at temperatures around 100 K. The drift towards higher values is also amplified by the mapping of the temperature. As seen in figure 4.6c, the temperature measured with the Pt100 sensor rises first very fast when the cool-down is stopped. This is not directly the temperature of the sample gas around the rotating sphere but ≈10 cm away from the sphere.
- Between 175 K to 200 K C_0 decreases slightly before it increases again. This might be caused by some resonance effect of the SRG readout, as the same was seen in the second calibration run, but this still needs to be proved. Nevertheless, this has an impact on the viscosity results, as will be seen in section 6.1 and section 6.2.
- From 275 K to 300 K there are again a few steps to be seen in the data. These are simply caused by the fact that for the calibration measurements, the thermal cycle routine included additional heating steps in this temperature range, which will also affect the resulting viscosities.

The uncertainty on the calibration factor is in the order of 4 %, but translates into an uncertainty of the later calculated viscosity in the sub-percent level. As the uncertainty on C_0 is high compared to the drift and the artifacts, it is useful to not directly use the measured values of C_0, but to assume the true C_0 to be a smooth function and fit the values with a linear function. It is also possible to fit a higher order polynomial, but the effect on the results of the viscosity is negligible. The result of this fit is shown in figure 5.7b. Using the C_0 values from the fit and not from the measured data prevents any influence of the previously listed effects on the temperature distribution of the viscosity $\mu(T)$.

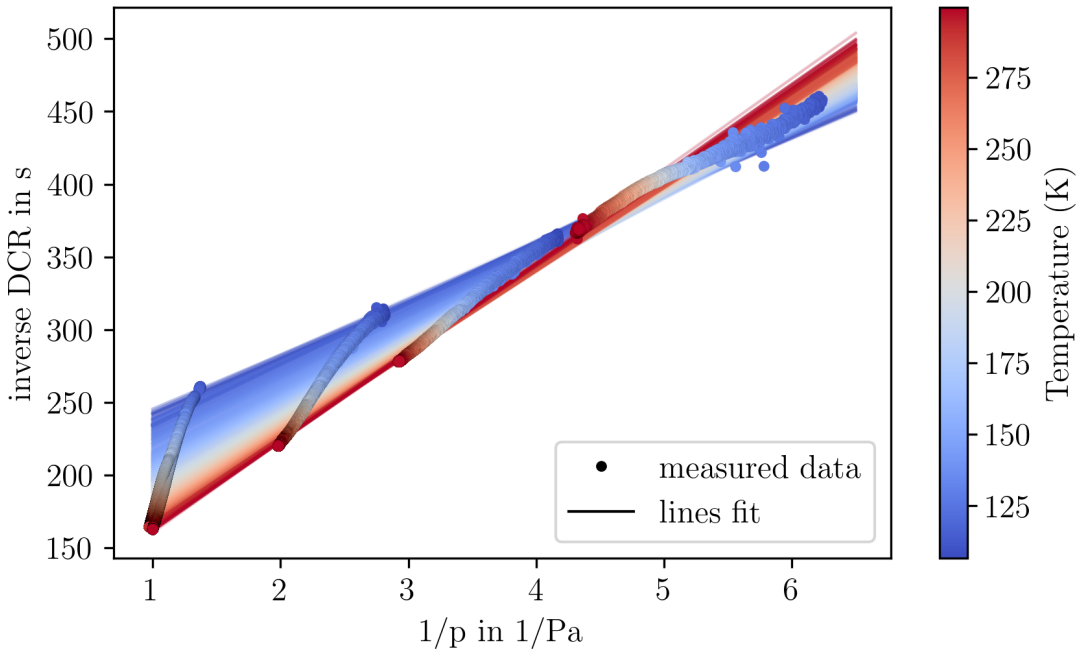

(a) Calibration procedure

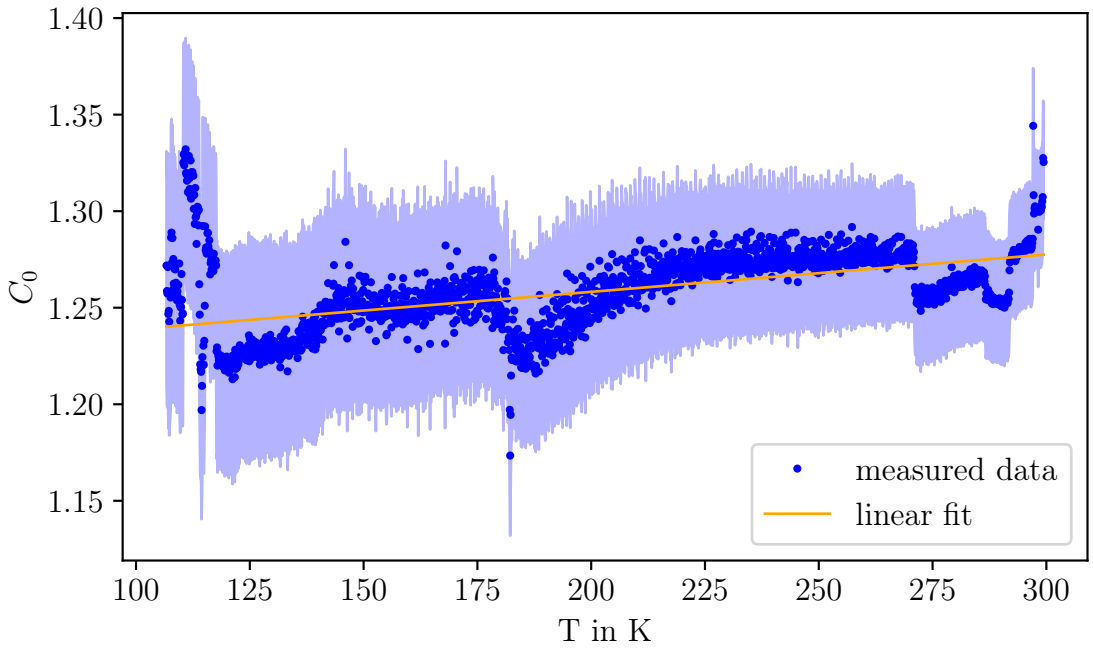

(b) Calibration factor in dependence of the temperature

Figure 5.7.: In figure 5.7a the measurement points for each pressure cycle are shown together with the linear fits, conducted separately for each temperature, indicated by the color of the points and lines. In figure 5.7b the calibration factor C_0 is plotted against the temperature. The blue dots are the results for C_0 of the calculation from the linear fit, whereas the light blue lines indicate the uncertainty for each value. The different sections between the jumps are explained in the text. The orange line is a linear fit over all values.

Within this chapter the different quantities isotopic purity, dimensions of the SRG, normalized deceleration rate, pressure, temperature, and calibration factor C_0 are discussed with respect to their respective impact on the accuracy of the measurement of the tritium viscosity. It has been shown that the radius of the rotor of the SRG has the highest impact on the uncertainty with approximately 2 %, while the temperature has the highest impact on the trueness of the measurement, shifting the results up to 2 K to lower temperatures. The last section of this chapter is focused on the calibration of the Cryo-ViMA experiment, showing that the calibration factor is slightly temperature dependent. In the following chapter, the viscosity measurements for H_2, D_2 and T_2 are shown.

6. Experimental driven model development for the viscosity of T_2

In the previous sections, the Cryogenic Viscosity Measurement Apparatus (Cryo-ViMA) experiment has been explained, fully characterized, and calibrated. To show the accuracy of the results gained with this apparatus, first measurements with non-tritiated hydrogen isotopologues are conducted and compared to current ab initio calculated viscosity values. For all shown results, the measurements are conducted in the same way as for the calibration with helium, with the only difference that the additional heating during the warmup phase has only been done for helium and protium. In section 6.1, reference measurements with H_2 and D_2 are discussed, to guarantee the validity of the measurements and improve the measurement procedure. In section 6.2 the results of the measurements with T_2 are shown and compared to theoretically calculated viscosity values, before a model to describe the thermal behavior of the T_2 viscosity is developed.

6.1. Reference measurements with H_2 and D_2

The viscosity of H_2 and D_2 are measured, enabling a better understanding of the accuracy of the measurement setup. These reference measurements provide a basis for interpreting the results of subsequent measurements with T_2. By comparing these results to established literature data, the reference measurements enable a more informed evaluation of whether any observed discrepancies arise from experimental errors or limitations in the theoretical ab initio calculations.

6.1.1. Protium

As explained in section 5.3, it is possible to calculate the viscosity with the directly measured C_0-values or with a linear fit to these values. A comparison of these methods is shown in figure 6.1. In figure 6.1a the same artifacts as in the calibration can be seen, with the difference that the direction of the steps is mirrored. The increase of the calibration values causes a decrease of the viscosity values and vice versa. The results calculated with the fitted C_0-values can compensate for these short drifts to a certain extent, as seen in figure 6.1b. Still there are two parts with higher deviation left in this plot. The first is the one at temperatures below 125 K. This shift is relevant for every measurement and is most likely some systematic issue, caused by the cooling system. Still, from the residuals it can be seen that the effect is decreased by ≈25 %. As the drift is caused by the temperature mapping with the Pt100 sensor, which is repeated for every single measurement, the calibration fit cannot fully account for this. The second part is a spike at ≈275 K, which is

nearly unchanged between the two evaluation methods. As mentioned before, during the measurements with helium and protium, the coldgas system was not only used for cooling the cryostat, but also for a faster warm-up in three steps form 275 K onward until 300 K have been reached. As there are three upwards edges, it is expected that this additional heating is also the reason for the spike. Otherwise, this effect would still be visible in other measurements. Regarding the residuals between the measured values and the ab initio ones, there seems to be a slope. To find out if this is only an effect of the type of measurement or if this is a true effect from the sample gas, a second measurement is conducted with deuterium. Nevertheless, both plots show that the ab initio values calculated by [MHH10] fit within the error bars of the measurement, except for the named effects at both ends of the temperature scale.

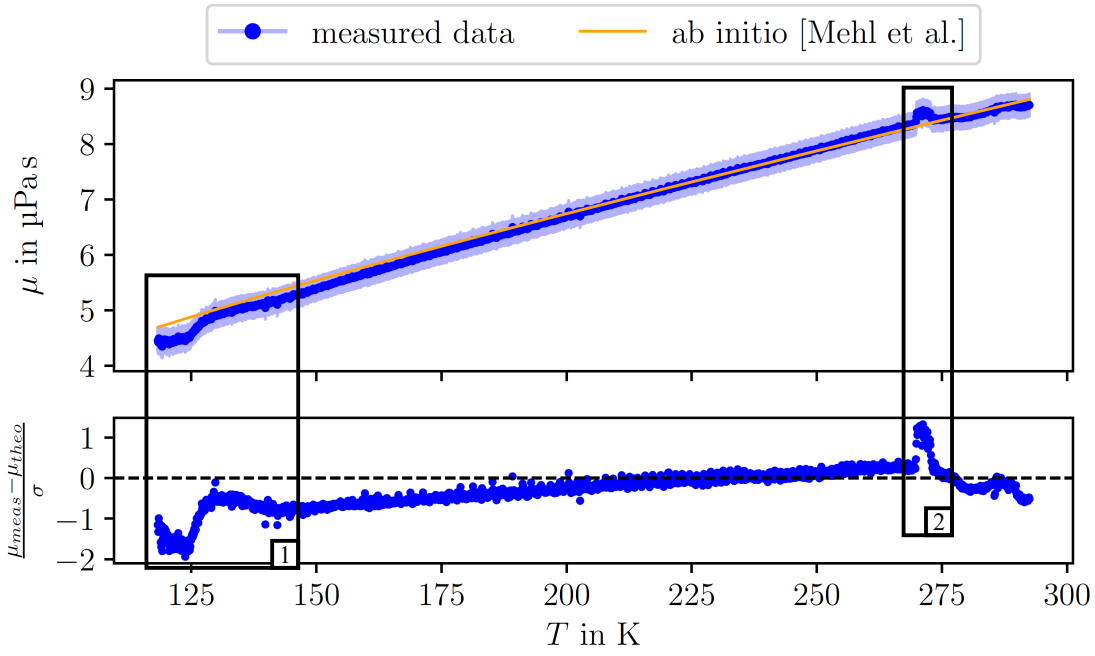

(a)

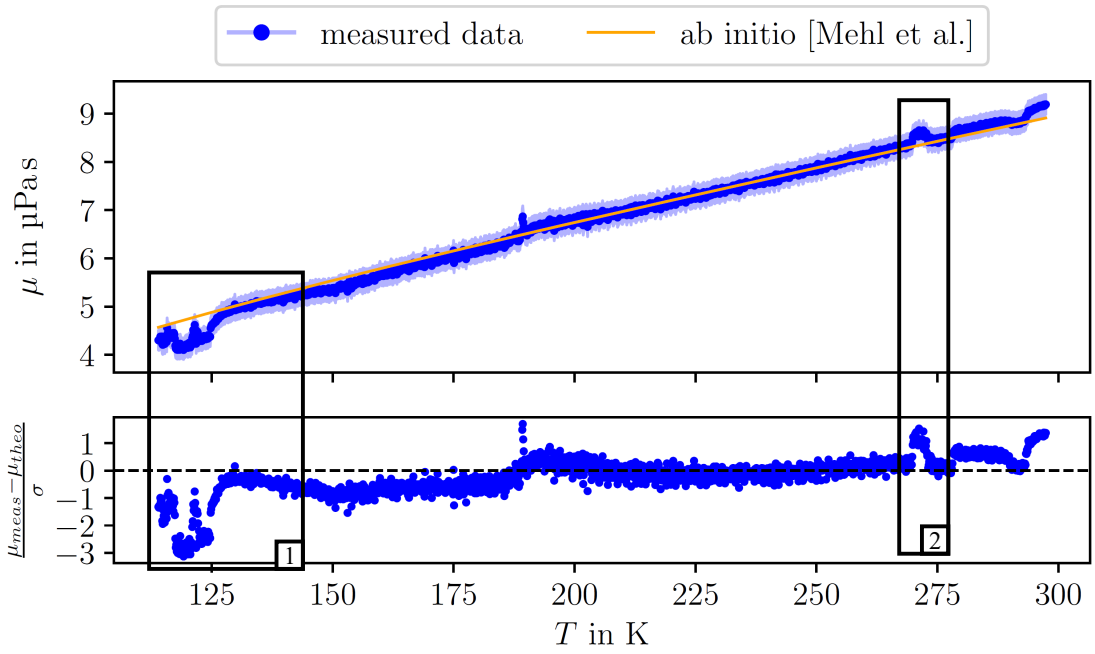

(b)

Figure 6.1.: **Viscosity of protium.** In figure 6.1a the results of the viscosity of protium in dependence of the Temeprature T are shown, generated analog to figure 5.7a, which are calculated directly from the C_0 values, whereas figure 6.1b shows the results calculated from the C_0-fit. In the lower panels the residuals normalized to the uncertainty of the measurement is shown. It can be seen that the artifacts from the calibration measurement marked by boxes 1 and 2 are minimized through the fit.

6.1.2. Deuterium

The results for the measurement with deuterium are shown in figure 6.2. Only the plot for the viscosity values calculated through the linear fit of C_0 are shown. The viscosity data calculated directly from the C_0 values can be found in figure A.1. Contrary to the results of the protium viscosity measurement, there are no upwards edges at temperatures between 275 K to 300 K. This supports the assumption that the edges in the protium data are caused by the additional heating, which has not been done during the measurements with deuterium. The issue with additional heating is that if heated too fast, the temperature gradient inside the sample gas will differ from the non-actively heated measurement, causing problems with the temperature mapping of the fit results. For temperatures from 150 K to lower ones (black box in figure 6.2), the viscosity drifts more downwards than the theory expects, but closes in again from 125 K to 100 K. This is again caused by the mismatch of the measured temperature to the actual temperature of the sample gas around the sphere. Compared to the protium measurements, the residuals are negative over the whole measured temperature range, but still there is a slope to it, which is 35 % smaller than the one for protium. A linear fit of the normalized residuals as shown in figure 6.1 and figure 6.2 in the range from 175 K to 275 K is conducted, excluding any influence from the artifacts at both ends of the temperature range. The results are listed in table 6.1, giving a deviation in the slopes of more than 30 %. This can be an indication that the temperature correction is not sufficient. As already explained in section 5.2, it is not possible to measure the temperature of the sample gas directly around the rotating sphere. The simulations can only give an estimation of the true temperature. If the temperature correction through the simulated temperature range has a different slope than the one implemented within the analysis, this might already explain the slope in the residual. The constant shift towards lower viscosity values cannot be explained through this, as the temperature gradient around the rotating sphere is dependent on the temperature setpoint and not constant over the measured temperature range. Besides this, the values calculated by [AMW87] fit within the uncertainty of the measurement. In contrast to the ab initio values from [MHH10] the ones from [AMW87] are semi empirical. Here the values are calculated by scaling from protium through the mass ratio at temperatures of 350 K and higher, and a correction term gained through comparison with experimental data on the viscosity of deuterium. In other words, these calculated values are, by definition, in good agreement with previous measurements, which indicates a small offset of the viscosity measured with Cryo-ViMA.

Table 6.1.: Fit results of the residuals for the H_2 and D_2 measurements.

Gas	slope in K^{-1}	intercept
H_2	0.0106	−2.3937
D_2	0.0069	−2.3573

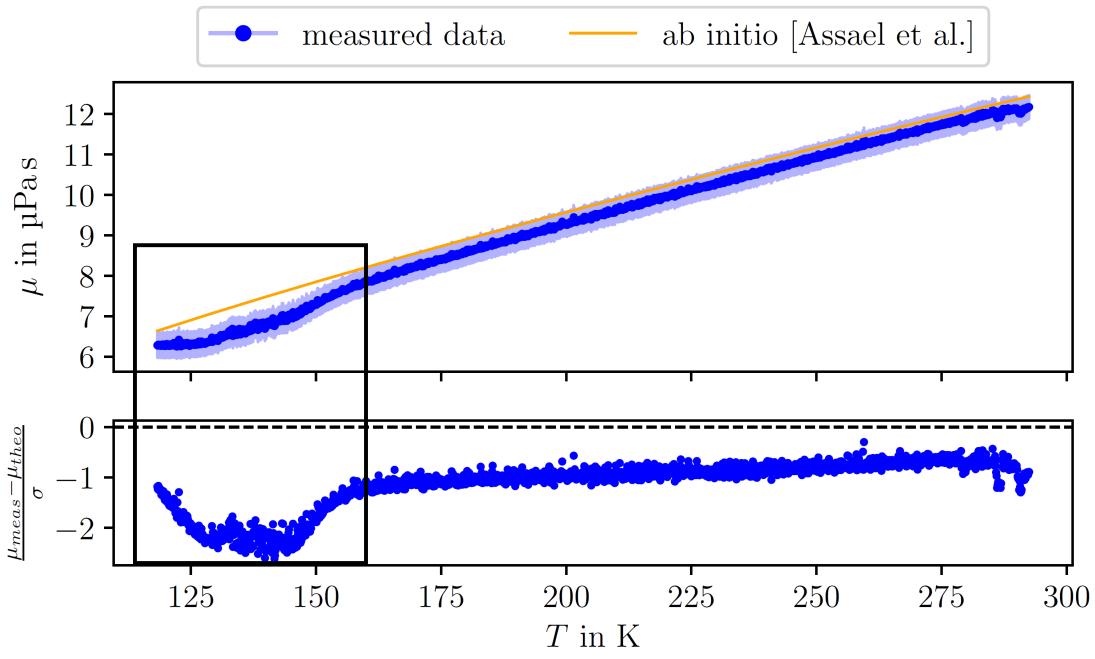

Figure 6.2.: **Viscosity of deuterium.** The measured viscosity values in blue with the uncertainty are shown together with the ab initio calculated viscosity by [AMW87] in dependence of the temperature. It can be seen that for temperatures between 125 K and 150 K (black box) the viscosity seems to drift away from the ab initio values. This behavior is closer described in the text.

6.2. Measurement of the viscosity of T_2

With the Cryo-ViMA experiment the viscosity of gases can be measured with an accuracy between 2 % and 2.3 % in good agreement with literature values. With the knowledge gained from the calibration and characterization measurements, the viscosity of tritium is measured in the same temperature range. To make Cryo ViMA tritium-ready, a T_2 commissioning phase has to be completed. The results of that phase are shown in section 6.2.1 while the other tritium data is shown in section 6.2.2.

6.2.1. T_2 commissioning phase

The commissioning phase is mandatory for every T_2 handling experiment, to reduce the amount of impurities produced mainly in the first weeks of tritium contact to the system, as described in section 4.1 and section 4.1.1. These impurities have an impact on the viscosity of the gas mixture as have been shown in the thesis of T. Poppe[1]. For the commissioning phase, tritium with a purity of 95 % from the buffer vessel of TriHyDe is used. The pressure

[1] Bachelor Thesis: "Impact of chemical equilibrium reactions in hydrogen isotopologue mixtures on viscosity measurements at the Cryo-ViMA experiment", Tim Poppe (02.2024)

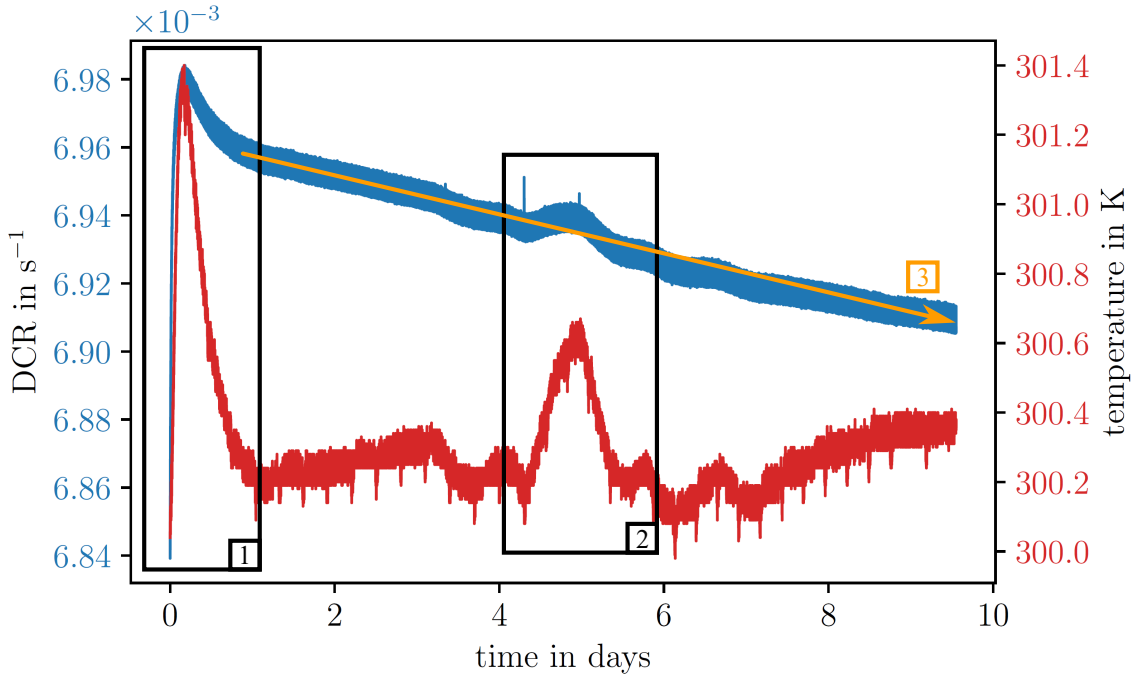

Figure 6.3.: **Commissioning phase of Cryo-ViMA.** In blue, the DCR is plotted against the measurement time in days, whereas in red, the corresponding temperature, measured with the Pt100 sensor, is shown. The black boxes and the orange arrow are regions closer discussed text.

inside the sample gas volume is adjusted to 2500 Pa and the measurement with the SRG is started and ran for nine days. In figure 6.3 the DCR in blue and the temperature in red are depicted over this time period. The peak in the black box with number 1 in the DCR originates from eddy currents causing a heat up of the rotating sphere from the initial acceleration, see section 5.2. The temperature rise caused by this effect is also seen in the same box. This initial acceleration has an effect on the temperature, with the difference that the temperature reaches a plateau, whereas the DCR continues to decrease throughout all measurement days, as indicated by the orange arrow with number 3. This decrease in DCR can have two different causes:

- The gas composition changes due to the radio-chemical reactions induced by T_2
- The surface of the rotor is cleaned from tiny amounts of water or hydrocarbons, leading to a different surface structure, thereby changing the deceleration rate.

Which of these effects has the higher impact will be tested in future experiments, but as long-term measurements with high purity tritium indicate, the first effect is the more likely one.

During measurements with gases like H_2 an increase in temperature normally corresponds to an increase in the DCR, but this cannot be seen in the commissioning phase. This is becoming clearer by looking at the increase in temperature over the fifth day of

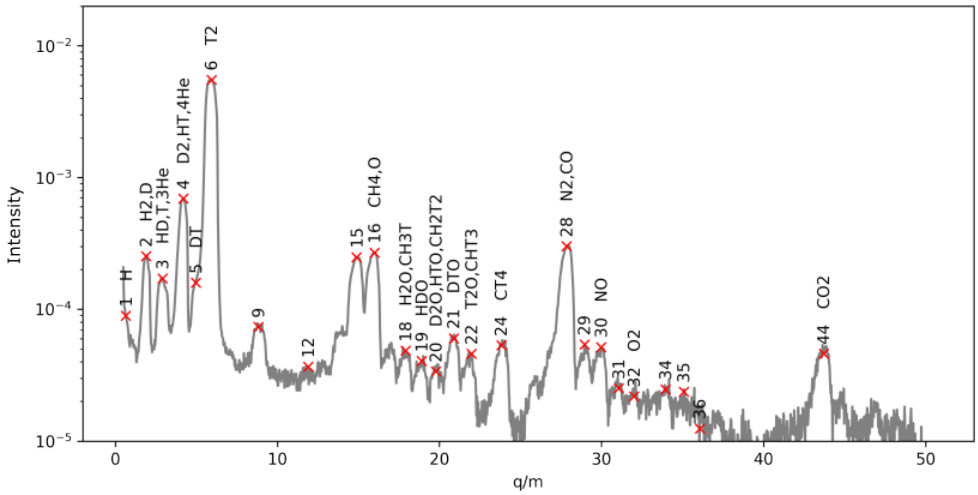

Figure 6.4.: **RGA measurement of Run031.** The signal of the RGA is shown in dependence of the measured ratio of charge and mass q/m. For selected peaks, possible ingredients are listed. As the TriHyDe glovebox is fully inertialized, the presents of oxygen is rather unlikely. The peak height does not directly give the concentration of the labeled ingredients. The initial purity of tritium of this batch was given with 95 %. Nevertheless all hydrogen isotopologues can be found. In addition, tritiated and non-tritiated methane is found within the sample.

measurement in the black box with number 2, which is caused by a temperature change in the laboratory. The DCR also increases along the same curve. The temperature peak is a deviation of ≈0.13 %, while the increase in DCR of ≈0.14 % is in the same order.

Small downward spikes in the temperature occur periodically, and correlate to the injection of nitrogen into the glovebox to maintain an inert atmosphere.

The decrease in DCR cannot be explained by the production of helium through the decay of tritium. The viscosity of helium is higher than the one of tritium, leading to a higher viscosity of the mixture and therefore a higher DCR. An explanation can though be given by the formation of methane of which the viscosity is slightly lower than that of tritium. This effect is already mentioned in section 4.1.

In figure 6.4 the result of the measurement of the gas composition with the residual gas analyzer (RGA) is shown. From the observed line positions, the presence of methane (tritiated and non-tritiated) can be deduced. Some of the lines could also arise from molecules containing oxygen. The only source of oxygen within the experiment is the surfaces of the setup, where small amounts of water molecules cannot be excluded but are very rare, leading to the estimation that these lines are more likely caused by methane. Due to limited resolution of the RGA device, a fully conclusive analysis cannot be given.

To suppress the methane build-up during the high purity tritium measurement and estimate the influence of these impurities on the accuracy of the measurement of the

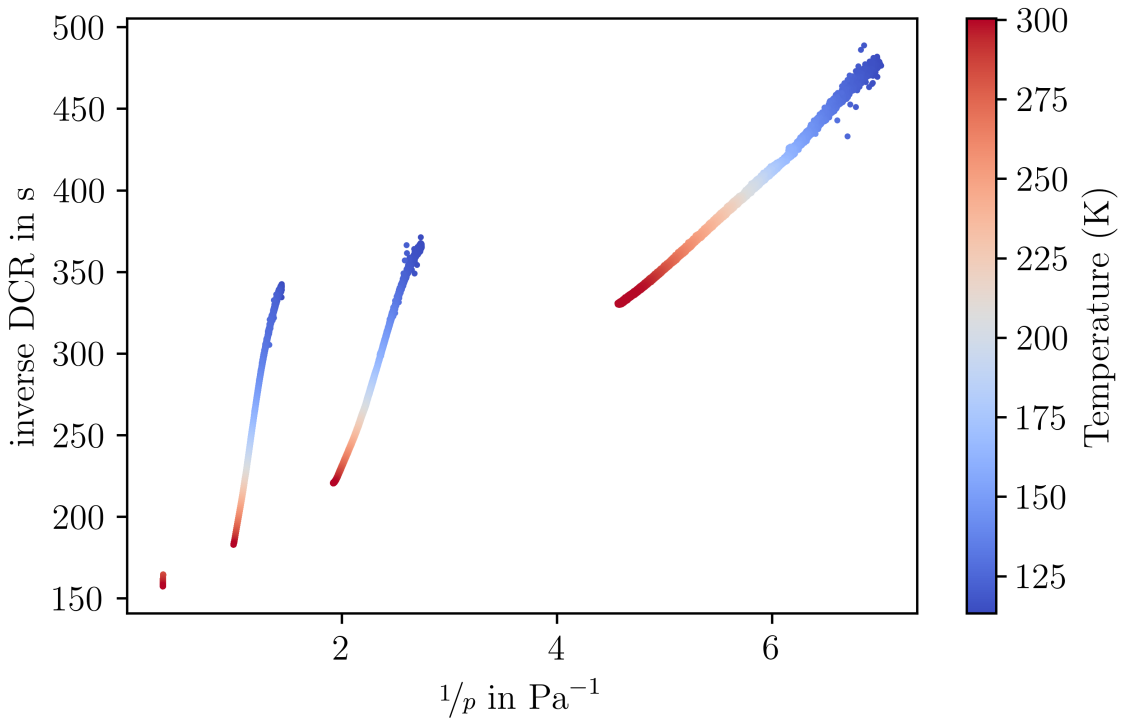

(a)

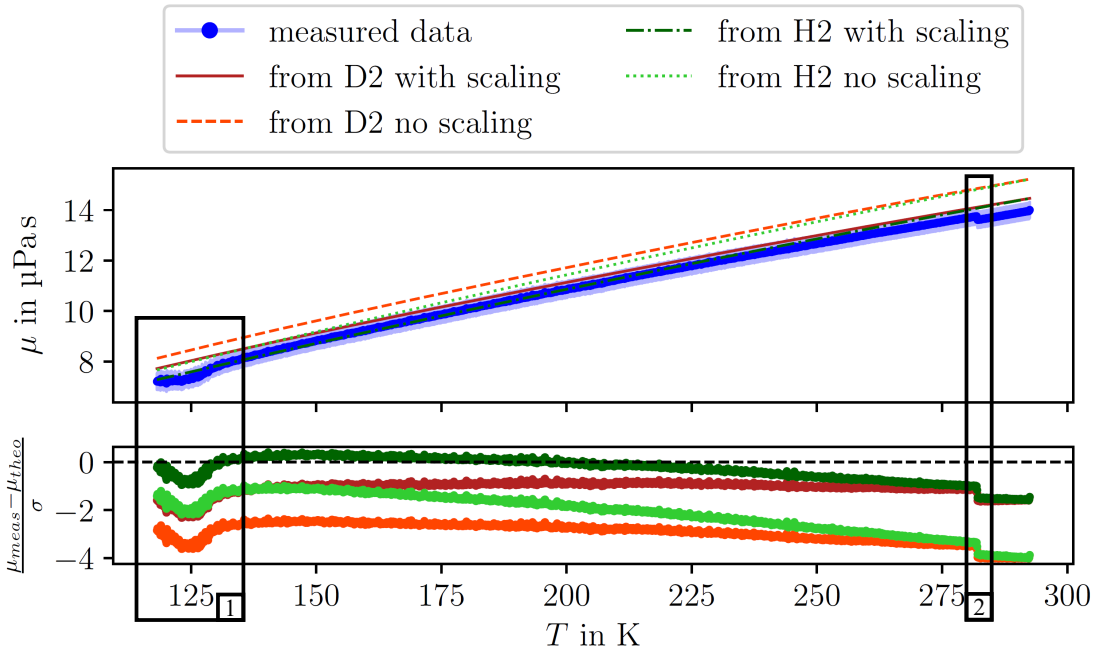

(b)

Figure 6.5.: **Viscosity of tritium - first measurement.** In figure 6.5a, the inverse normalized deceleration rate is plotted against the inverse pressure. The colors indicate the temperature at which the DCR was measured. In figure 6.5b, the viscosity is plotted against the temperature. The dark red and red lines correspond to the extrapolations from D_2 [AMW87] values, the dark and bright green lines to extrapolations from H_2 [MHH10] values, both with and without a scaling factor as described in section 3.4.

viscosity, a first measurement with this mixture is performed. The result can be seen in figure 6.5b. The result of this first measurement seems to fit much better to the extrapolated values, especially the ones extrapolated from H_2, as these are the ones giving the lowest estimated viscosity of T_2. There are two effects at which a closer look needs to be taken.

- In the black box number 1, it is seen that the values for the viscosity differ more from the literature values. This is caused by the setup being not completely thermally equilibrated before the warm-up of the system started. This effect is reduced in the final measurements with high purity T_2.
- In the black box number 2 a small step in the viscosity values is seen. This step is caused by the fact that the analysis is based on the assumption that the inverted normalized deceleration rate changes linear with the inverted pressure in the slip regime. If now measurements are not included completely (shown in figure 6.5a), as the values are not within the Knudsen-range any more, the fit will be slightly tilted to higher or lower values, depending on whether it is the low or the high pressure boundary.

As is seen in the following section, the viscosity values for pure T_2 are lower than the measured values of the commissioning phase, indicating the higher amount of impurities with viscosities higher than tritium, such as ^{3}He from the tritium decay or N_2 from small leakages over the long time during which the tritium has been stored in the system.

6.2.2. Measurement campaign with high purity T_2

The result of the measurement with pure T_2 is shown in figure 6.6, where again the calibration factor C_0 is used from the fit performed in section 5.3. For tritium, measurements have been conducted in the same pressure range as for hydrogen and deuterium but with more pressure setpoints for higher statistics for the fit. In figure 6.6, the influence of the tritium purity and the data selection are compared.

- In green, the viscosity of the gas sample of the commissioning phase is shown. There is a small step at 275 K, which is caused by the Knudsen boundary, as one thermal cycle is not completely integrated in the analysis.
- In orange, the second measurement of the tritium viscosity is plotted with the full measured dataset without any Knudsen boundaries. Steps, as seen in the green line are not present here, as no thermal cycle is cut.
- In blue, the same measurement is analyzed, however in this case, the Knudsen boundaries are set to $0.01 < K_n < 0.5$ as stated in section 3.1.1 and only thermal cycles which are fully within these boundaries are included, to avoid steps in the viscosity distribution, which would disturb the development of an empirical function.

The deviation between the full dataset and Knudsen selected dataset of the second tritium measurement is 0.2 % to 1.8 % and goes up to 5 % between the first and second tritium measurement. As the deviation within one dataset does not exceed the uncertainty of the measurement itself, the Knudsen boundary is no hard limit, as the slip regime is also not strictly distinguishable from the Knudsen regime, meaning the transition between these flow regimes is smooth.

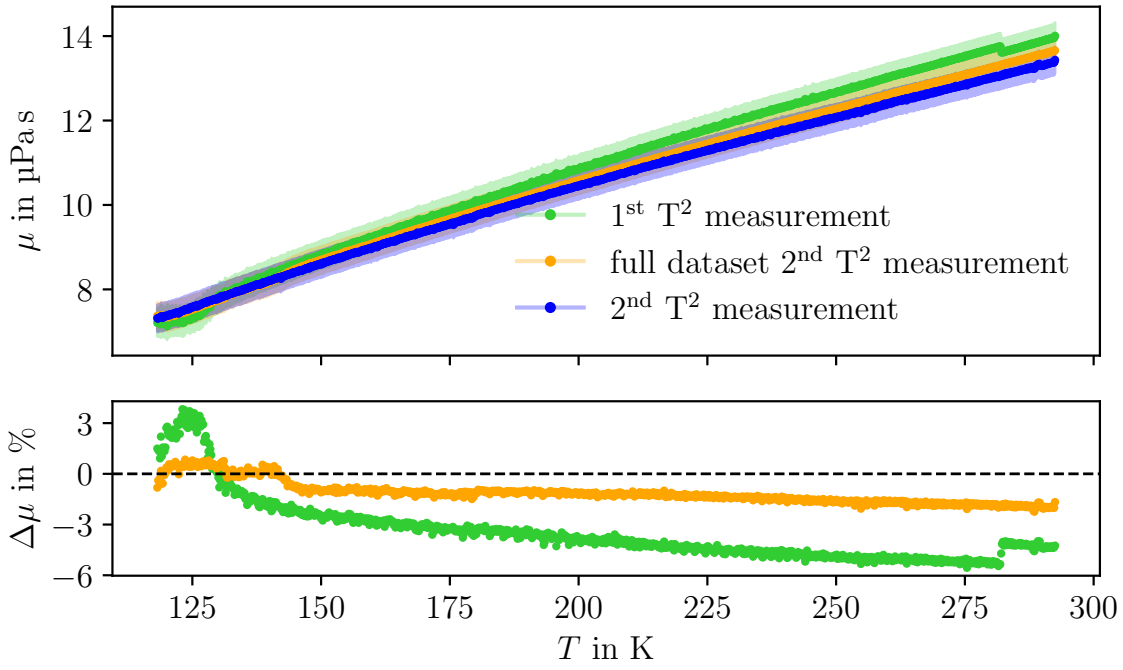

Figure 6.6.: **Viscosity of tritium.** The viscosity is plotted against the temperature. The light bands show the uncertainty of the measurements. In green, the first measurement with T_2 is shown, which was the measurement with the gas sample of the commissioning phase. In orange the result for the viscosity of tritium is shown, if the whole dataset is included in the analysis without any Knudsen boundary conditions. In blue, the final results of the viscosity of T_2 are shown, with adequate Knudsen boundaries. In the lower plot, the deviation between the second T^2 measurement and the other two is given in %.

6.3. Comparison of the measured T_2 viscosity to literature values

The measured values of the viscosity of tritium are compared to the values extrapolated from D_2 ([AMW87]) and H_2 ([MHH10; AMW86]) according to equation (3.12) with and without a correction factor of 5 % as proposed by [Kuc16]. The ab initio calculated values for the viscosity of tritium by classical approach conducted by [Son16] are compared to the measurements. The results are shown in figure 6.7.

In figure 6.7a, the values extrapolated from H_2 are compared to the T_2 measurement. The bright and dark green lines show the extrapolations without any scaling factor, leading to deviations of 5 % to 12 %. The red and orange lines show the values with a scaling factor of 0.95, with deviations to the measured values of 1 % to 6 %. The viscosity of H_2 is taken from two different sources, [AMW86] and [MHH10], with an empirical function of the viscosity of H_2 and ab initio calculated viscosity values, respectively. The extrapolated viscosity values based on the ab initio viscosity of H_2 by [MHH10] show not only an offset,

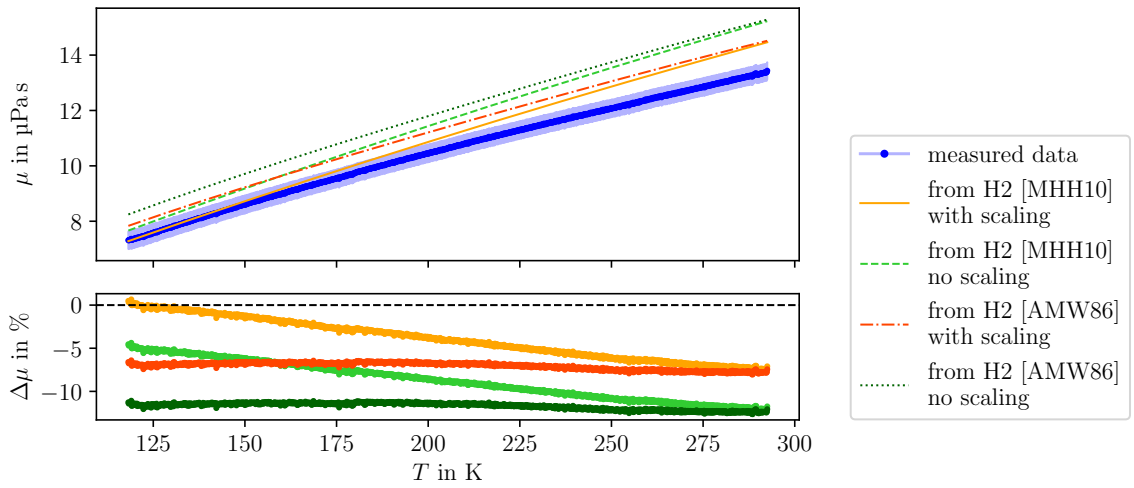

(a) Extrapolated from H_2

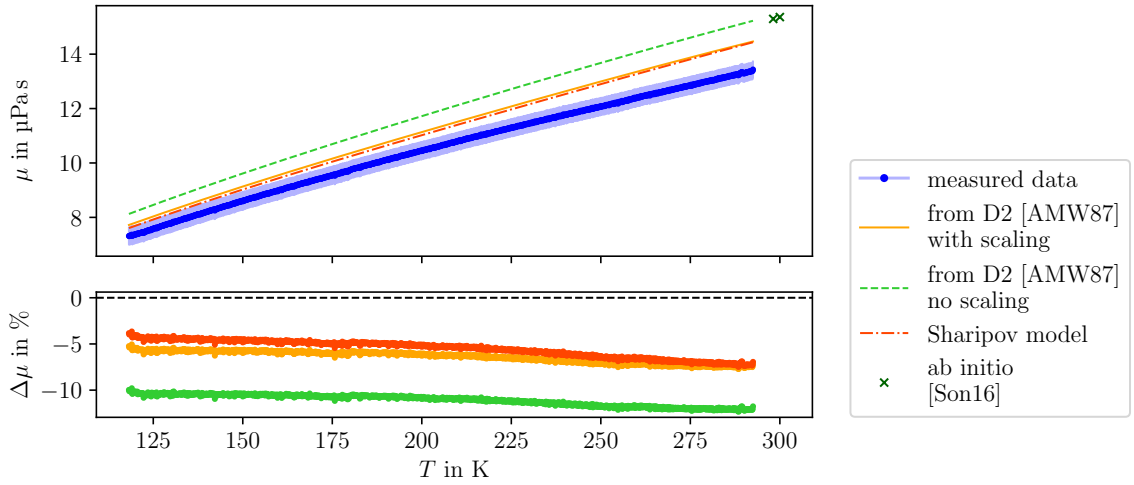

(b) Extrapolated from D_2

Figure 6.7.: **Comparison of extrapolated to measured values for the viscosity of tritium.** In figure 6.7a the measured viscosity of tritium is compared to the viscosity extrapolated from H_2 ([AMW86; MHH10]) with and without scaling factor. In figure 6.7b the same is done for the viscosity values extrapolated from D_2 ([AMW87]) together with the theoretical calculations with the Sharipov model and the ab initio calculated values for the viscosity of tritium from [Son16].

but also a drift with temperature to higher viscosity values. This is not seen in the values calculated from the empirical function by [AMW86]. For the latter values it would be sufficient to chose a better scaling factor, than currently used for example in the KATRIN experiment.

In figure 6.7b the values for the viscosity extrapolated from D_2 with and without scaling factor are shown together with the values generated by the Sharipov model and the ab initio calculated viscosity by [Son16]. The scaling factor of 0.95 improves the accuracy

of the calculations from 10 % to 5 %, a slope in the residuals as for the ab initio values from [MHH10] is not observed. The Sharipov model as it is currently used also shows a deviation of 4 % to 5 %. This can be improved by adjusting the scaling factor form 0.95 to 0.907, which is nearly the doubled 5 % correction one would expect form the doubled extrapolation.

In figure 6.7a, apart from the offset which could be corrected by a proper choice of the scaling factor, the values extrapolated from H_2 with the ab initio calculated values from [MHH10] show a negative slope in the deviations. This cannot be found in the other extrapolations. The measured values of hydrogen fit within the uncertainty of the measurement to the ab initio values, so there are some questions to think about:

1. Is there another systematic uncertainty within the Cryo-ViMA setup which is not fully understood at the moment?
2. Are there any effects that are present in tritium, which are not there in hydrogen?
3. If this slope only occurs in the ab initio calculations, are they truly as accurate as postulated?

To answer the first question, it has to be known that the values calculated by Assael et al. in [AMW86] and [AMW87] were gained from the fit of the kinetic theory (equation (3.7)) to measured data, as it is done within this thesis for T_2. The measurements used for the calculations were conducted with an oscillating disc. If there are any gas-dynamic specific effects, the two setups would not differ enough to make this visible. As the values measured for hydrogen fit to the ab initio values from [MHH10] well, it is not expected that there are additional systematic effects, which would cause the observed deviation.

For the second question, there are different possible ways how tritium might react different than the lighter isotopes, both caused by its radioactivity.

1. The gas composition might change over time, as tritium is held inside the setup for nearly three weeks for one complete measurement. From the first measurement with tritium with a purity of approximately 95 % ^{3}He forming during decay should increase the viscosity. The theoretically extrapolated values are all higher than the measured ones, so if the purity would be the sole cause of the deviation, it should be smaller than the measured deviation, except for impurities caused by the commissioning phase, like methane. These have a lower viscosity than tritium, but only if methane does not change its viscosity much through tritiation. As such effects become less frequent over time, this is a rather unlikely explanation for the deviation, though it cannot be entirely ruled out.

2. The heat produced through the beta decay of tritium. This heat production is two orders of magnitude smaller compared to the heating by the rotating sphere and therefore negligible.

3. Tritium gas produces a plasma. Detailed information about the processes can be found in [Fri20; Kle19]. The basic principle is the production of ions like T^+ or $^3He^+$ caused by the tritium decay, leading to a diversity of molecules such as T_3^+ through scattering. Currently, such effects cannot be implemented in ab initio calculations

on transport properties and are likely to affect the viscosity, leading to the deviation from the current literature values.

This leaves the last question open. As the measurements for hydrogen fit to the ab initio values, the problem will not be the calculation itself, but the extrapolation to tritium. In figure 6.7 the ab initio calculated values for the viscosity of tritium by Song et al. [Son16] are shown for 298.15 K and 300 K. These would fit to the extrapolated values without any scaling factor, so they already differ more than 5 % from the measurement. In both cases, the extrapolation from hydrogen, deuterium and the ab initio calculation, quantum mechanical effects are neglected. With these results at hand, the simple extrapolation of the viscosity of tritium from literature values, or even experimental values of deuterium and hydrogen, is not the most precise way to describe the thermal behavior. There are effects based in the radioactive and/or quantum mechanical nature of tritium affecting macroscopic properties like the viscosity.

6.4. Model development for the tritium viscosity at low pressures

The empirical function for the viscosity of tritium cannot be extracted from the whole temperature range, as the deviations at low temperatures would disturb the fit. The temperature range for fitting an empirical function is fixed to 125 K to 270 K. From the definition of the viscosity in the zero density limit (equation (3.7)), the temperature dependence is in first approximation in the order of $T^{1/2}$. Throughout the whole temperature range of the data-set, quantum effects can be neglected compared to the influence below 100 K. A fit in the form of $\mu = a \cdot \sqrt{T} + b$ is used, where a is the scaling factor and b is the offset of the fit function, since the viscosity will not vanish at 0 K. For better results, b can be temperature dependent according to the Chapman-Enskog theory [Cha16]. As described in equation (3.8), there are four terms in total to describe the viscosity, of which only the first one corresponds to the viscosity in the zero-density limit. The second term is called the initial viscosity and normally dependent on the temperature and the density. As the density in the case under estimation is very low, the correction of this term will also be low. Nevertheless it is implemented, but with the exponent of the temperature left as a free fit parameter. The fitting function is then described by

$$\mu = a \cdot \sqrt{T} + b \cdot T^d \,, \tag{6.1}$$

with d being the exponent of the temperature in the offset-term. This function is referenced to as the $\sqrt{T}$-fit within this thesis.

The second approach is referred to as the "Sharipov model" within this work. For the calculations of the column density profile of the KATRIN experiment, the viscosity of tritium is extracted from the ab initio calculated viscosity of hydrogen according to equation (3.12). The extrapolation is done in two steps. First, the viscosity of D_2 is extrapolated without any correction factor from the viscosity of H_2. Second, the viscosity

of T_2 is extrapolated from the extrapolated viscosity of deuterium, with a scaling factor of 0.95[2]. In the original code by F. Sharipov[3] it is suggested to use the scaling factor for the extrapolations of the viscosity of tritium from experimental values of deuterium measured by [AMW87]. But the underlying equation used is the theoretical potential of hydrogen, so that the viscosity reads

$$\begin{aligned}\mu &= 0.95 \cdot \sqrt{3/2} \cdot \mu_{D_2} \\ &= 0.95 \cdot \sqrt{3/2} \cdot \mu_{H_2} \cdot \sqrt{2/1} \cdot \left(1 - \exp^{(-2.8105(T/\epsilon)^{1/3})}\right) ,\end{aligned} \tag{6.2}$$

with the temperature T and the well-depth of the potential ϵ from hydrogen, as listed in [AMW86]. As the values for the viscosity used in this equation are the values for hydrogen, the scaling factor should be used two times, changing to 0.9025. The factor -2.8105 in the exponent arises from a fit conducted by [AMW87] and can be left as a free parameter for the fit within this thesis, named d. This model shall be fitted to the measured values, hence the scaling factor of 0.95 is left as a free fitting parameter as well as the well-depth ϵ.
In figure 6.8 the results of the two fits are shown. The calculated values according to the Sharipov model are displayed in orange while the $\sqrt{T}$-fit results are plotted in green. The $\sqrt{T}$-model resembles the measurement data very good, while the Sharipov-model only resembles the shape below 200 K before it starts to deviate significantly. By taking a closer look at the fit results in table 6.2, it is clear that the fit is not able to find the right parameters. This is independent of the optimization method used. From all four parameters of the Sharipov model, only three give reasonable results, while one parameter is close to or at the boundary. The $\sqrt{T}$-model is the best choice to describe the thermal behavior of the viscosity of tritium, which is in good agreement with the kinetic gas theory.

[2] KATRIN internal column density calculator (A. Marsteller, 2018)
[3] F. Sharipov (2003), KATRIN internal report.

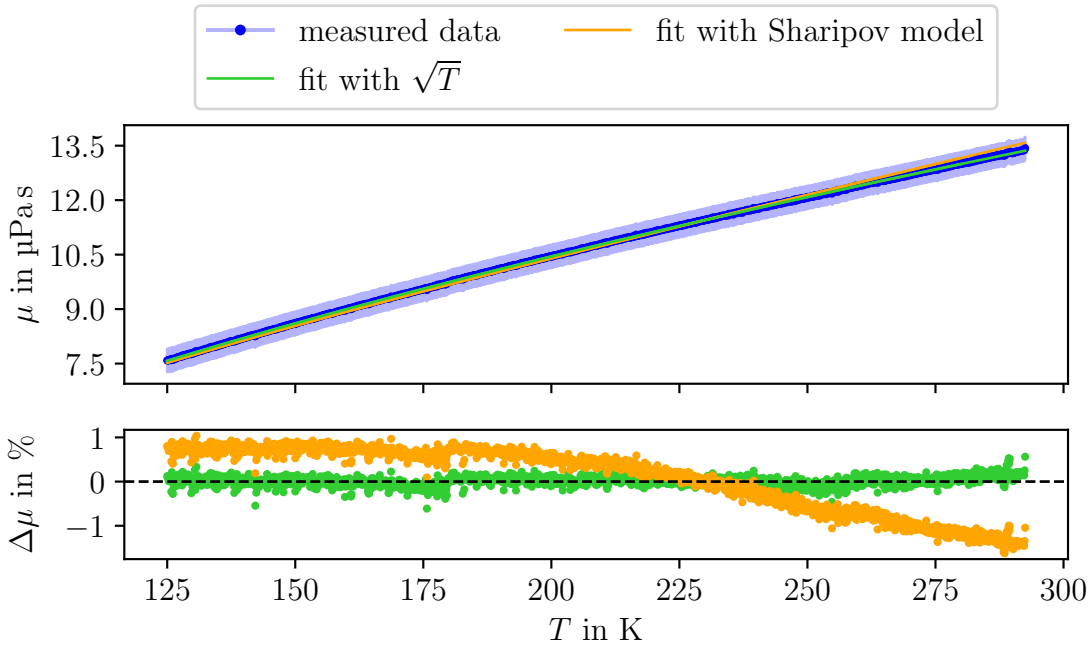

Figure 6.8.: **Theory comparison of the viscosity of tritium.** In the upper plot the measured viscosity of tritium is plotted as blue dots with an error-bars of around 2 % against the temperature. The green line shows the fitted $\sqrt{T}$-Model, the orange line shows the fitted Sharipov model. The red line corresponds to the Sharipov model without any fitting, except for changing the scaling parameter from 0.95 to 0.907, which is best fitting by eye to the measured values. In the lower plot the deviation between the measured values and the theory is shown in percent.

Within this chapter the measurements of the viscosity of H_2, D_2 and T_2 are analysed and discussed. The measurements for H_2 and D_2 fit to ab initio and empirically calculated literature values within the uncertainty of the measurement. In contrast to this, the measurements of the viscosity of T_2 show high deviations from 5 % to 12 % depending on the chosen starting values for extrapolations and the choice of correction factors. As the measurement for H_2 and D_2 give reasonable results, it is unlikely that the measurements with T_2 are much more off the true values for the viscosity. To be able to describe the temperature dependence of the viscosity of T_2 an empirical function is fitted to the measured data, resulting in

$$\mu = 0.78\sqrt{T} + 0.009 \cdot T^{-2.26} \tag{6.3}$$

with the viscosity μ and the temperature T.

Table 6.2.: Fit results for the Sharipov method for different optimization methods. None of the fit methods was able to fit all four parameters. From comparison of the results for the parameters to the start values, as they occur for hydrogen, the results of the Powell method or the L-BFGS-B method fit best. The last column shows the results for the $\sqrt{T}$-fit, where only three parameters had to be fitted.

	Sharipov-fit				$\sqrt{T}$-fit
Parameter	Least-Squares	Nelder-Mead	Powell	L-BFGS-B	Least-Square
a	4.580	4.995	2.956	3.562	0.775
b	1.000	1.002	28.151	33.279	0.009
c	0.330	0.415	1e-05	1.360	-
d	0.891	0.891	0.940	0.891	-2.263
χ^2	80.493	80.493	80.500	80.493	0.308
χ^2_{red}	0.052	0.052	0.052	0.052	2.94e-04
Akaike	-4580.6	-4580.6	-4580.5	-4580.6	-8544.4
Bayesian	-4559.2	-4559.2	-4559.1	-4559.2	-8529.6
R^2	0.979	0.979	0.979	0.979	0.9997

7. Impact of viscosity measurements on current and future science

As described in section 6.3, tritium viscosity from extrapolation of H_2 and D_2 data deviates approx 5 % from measurements, scaling factors already considered. This deviation cannot be explained by any mass or temperature effect from the measurement, but has to be caused by the different nature of tritium compared to hydrogen or deuterium. The impact of the overestimation of the viscosity on vacuum and fusion science, as well as on the KATRIN experiment will be explained in this chapter.

7.1. Impact on vacuum science

In vacuum science, the viscosity of gases is an important material property to describe the movement and momentum transfer in fluids. Therefore, for many different gases, the viscosity has been measured, while for noble gases like helium [HM00] or neon [Egg92], ab initio calculations have been conducted. For small molecules like hydrogen these calculations become more unreliable, as the underlying theory for collisions between molecules is very complex to calculate. The potentials needed for these calculations are approximations under specific boundary conditions, yet with high accuracy. Such calculations have been conducted for example, for hydrogen as the smallest and simplest molecule [MHH10], and show good agreement with measured values. However, already for deuterium, calculations found are based on measured data, meaning the viscosity equation gained from this procedure is only an empirical function. Nevertheless, with such an approach, available theoretical calculations can be validated and information about the potential energy and the collision integral can be extracted. As shown in section 6.1.2, the empirical viscosity function for deuterium fits to the ones measured within this work, leading to the estimation that the measurements for tritium would also fit to such empirical calculations, if available. If T_2 interacts in the same way as H_2 and D_2, the shape of the temperature dependence should only be shifted, not tilted or distorted in any kind. As displayed in figure 6.7, the extrapolated values from ab initio calculations for hydrogen are not only shifted, but also tilted, compared to the measured values, indicating that the theory for the viscosity of tritium is not fully understood. The function for the temperature dependent viscosity of tritium developed within this work can therefore be used to compare to corresponding theoretical calculations for tritium. As such, these measurements are the first to test the influence of quantum-mechanical and radioactive effects on viscosity and to refine current existing ab initio potentials and collision parameters for tritium.

7.2. Impact on fusion science

In section 2.2, it is explained that the most efficient way to achieve fusion energy is the use of a mixture of deuterium and tritium. Tritium accountancy is needed to guarantee the safety of the people and the environment [NYH06; Kle15], which needs best possible knowledge on the properties of tritium.

For the improvement of the tritium inventory management it is crucial to know the viscosity of tritium for simulations of the efficiency of the different systems of a fusion reactor. Even for simulations where the viscosity does not enter the calculations directly, as done in [TD21], the viscosity is needed for the calculation of input parameters like the reference diameter of the molecule. The current extrapolated values overestimate the viscosity of tritium. A lower viscosity in the gas phase causes for example, pressure profiles to flatten. As viscosity decreases, momentum transport between molecules also decreases. Therefore, the velocity of molecules does change less over collisions. This has a direct impact on the pumping efficiency as faster gases are easier to pump than slower ones and hence influences the tritium inventory management.

For inertial confinement fusion the viscosity of tritium and the fusion plasma play a role in the simulation of shock waves in the targets as described in [MKF14]. For such calculations, the viscosity is not only needed in the zero-density limit, but also for dense matter. The current results can be regarded as the first starting point to improve these simulations to get a better impression of the energy needed for the plasma to ignite and its evolution until it is burned.

Another problem is given by the tritium accountancy, needed as safety requirement to run a fusion reactor. The following information is recieved through personal communication with Dr. Robin Größle. For the accountancy, the trueness of the measurement on the tritium inventory is needed, which is normally measured through volumetric setups combined with inline analytic tools like Laser-Raman systems. These measurements naturally contain uncertainties. For a hypothetical uncertainty of 1 % on the inventory one has to consider the following:

- T_2 is produced inside the breeding blankets
- T_2 is lost through
  - fusion ($\approx$400 g d^{-1}),
  - decay (5 % a^{-1}) and
  - diffusion through all materials with unknown amount.

This means that by only regarding the burn-up fraction of tritium of 1 %, a throughput of 40 kg d^{-1} is needed, leading to an uncertainty of 400 g d^{-1}. This means that 400 g T_2 could be lost through an unknown leak, without further notice. At TLK the tritium accountancy is done by collecting all tritium from the experiments at once and measure the total amount of tritium, for example through calorimeters. For a fusion reactor, this is not feasible. The only chance is to get as much information on T_2 as possible, to improve measurements and simulations. [1] With these measurements, a first step towards better knowledge on

[1] p.c. Dr. Robin Größle, KIT IAP-TLK

T_2 is made, showing that it is not sufficient, to extrapolate data from the other hydrogen isotopologues.

7.3. Impact on the KATRIN experiment

In section 2.3.3, the influence of tritium viscosity on the column density of the WGTS is explained. Figure 2.4 shows the simulated column density profile along the WGTS beam tube with the estimated tritium viscosity and a variation of ±7 %. The measurements conducted in this work indicate that the viscosity of tritium is approximately 5 % lower than previously estimated from the Sharipov model. Consequently, the actual column density profile is expected to be closer to the blue curve in figure 7.1, where

$$\Delta\left(p/p_{inj}\right) = \left(p/p_{inj}\right)_{expected} - \left(p/pinj\right)_{true} \tag{7.1}$$

with $\left(p/p_{inj}\right)_{expected}$ representing the normalized pressure along the beam tube calculated with the estimated tritium viscosity, and $\left(p/p_{inj}\right)_{true}$ representing the same value calculated with the true tritium viscosity.

This result implies that, for a given measured integral column density, the profile is flatter than expected, exhibiting a lower CD in the injection region and higher CD at both ends of the beam tube. This shift not only affects the CD in the standard beta-scanning mode of the KATRIN experiment, but also in the so-called krypton mode, where a small fraction of krypton (Kr) is injected into the source for calibration purposes. Because krypton is significantly heavier than tritium, mass effects influence the gas density distribution along the beam tube, causing a separation in the density distributions of T_2 and Kr. Their distributions are also calculated using gas dynamic formulas that require the rarefaction parameter, which in turn depends on the viscosity of the gas mixture[2]. For an improvement of these simulations, it is planned to also measure the viscosity of a gas mixture of T_2 and Kr as it is used in this mode in future. According to [Sei19] the impact of the gas dynamics model on the neutrino mass shift is 0.5 % but here, only the uncertainty of 2.5 % on the tritium viscosity caused by possible impurities inside the source is accounted for. In the measurement within this thesis, the gas mixture is comparable to the one in the KATRIN experiment, so these 2.5 % can be neglected, while the true value for the tritium viscosity is 5 % lower than expected. As demonstrated in [Kuc16], the neutrino mass shift Δm_ν^2 is on the order of 10^{-4} eV^2 for a CD profile deviation of 2 % to 10 %, depending on the source's gas dynamics model, where viscosity is only one of several parameters. The change in the CD profile caused by the viscosity is slightly below 0.5 %, leading to a neutrino mass shift smaller than the previously stated 10^{-4} eV^2.

[2] F. Sharipov (2010), internal KATRIN report.

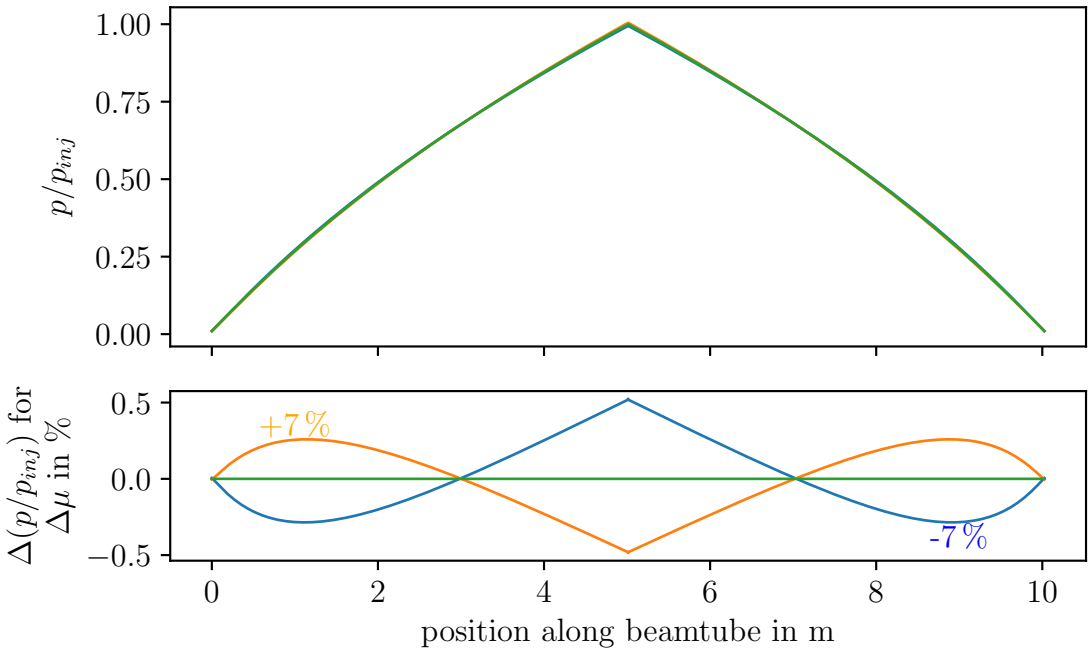

Figure 7.1.: **The Column Density Profile of the WGTS.** The CD profile is plotted in terms of the pressure along the beamtube normalized to the injection pressure. In the lower graph the difference in the density profile is shown once for the estimated viscosity in green and the viscosity with ±7 % difference.

8. Summary and Outlook

Summary The viscosity is an important parameter to describe the behavior of fluids and needed in many different scientific topics. For vacuum science and experiments and technologies in need of vacuum systems, the viscosity of gases is of special interest. Also fundamental science has a great interest in transport properties of light elements, like helium and hydrogen, to test current available ab initio calculations and to improve standard values for calibration issues. In these cases mostly helium is used, whereas ab initio calculations of hydrogen also yield reasonable results. But already for deuterium, there are no complete ab initio calculations available which also include quantum mechanic properties. For tritium neither quantum mechanical ab initio calculations needed for temperatures below 300 K, nor experimental values are known in literature.

Tritium is the heaviest hydrogen isotopologue and radioactive, so measuring the viscosity of T_2 and tritiated and deuterated hydrogen is a highly valuable test bed for model validation and improvement. Since tritium is a radioactive isotope legal regulations apply when working with it. The Tritium Laboratory Karlsruhe is a unique facility in Europe, which has a license to handle up to 40 g of tritium and therefore has enough tritium on site to measure its properties like the viscosity. There are two major missions the TLK is working on. First the Karlsruhe Tritium Neutrino Experiment (KATRIN), which is the leading experiment in search for the neutrino mass, where the spectrum of the decay electrons from the tritium beta decay is measured. The imprint of the neutrino mass is a small change in the spectral shape of the electron spectrum of tritium, mainly influencing the region around the endpoint of 18.6 keV. The second mission is the support for fusion research and development, where a variety of experiments ranging from small scale experiments like the viscosity measurement as it is done with this thesis, up to technical scale systems to test isotope separation and water detritiation are developed. With such measurements, not only technical improvements on, for example, fusion power system can be achieved, but also the test bed for theoretical ab initio calculations is increased. Basic tritium physics and properties are always an important starting point and input to scale up from small scale to full scale integration later on in a fusion power plant.

The currently existing values for the viscosity of tritium are given with high uncertainties in the order of 2 % to 10 % [Kuc18; Son16], and are often just extrapolated from hydrogen or deuterium, as it is done in [Kuc16]. The goal of this work was to measure the viscosity of tritium in a temperature range of 100 K to 300 K in the zero-density limit with an accuracy of around 2 %, to be able to test currently existing values.

To reach this goal the measurement setup had to be compatible to tritium and cryogenic temperatures, leaving the spinning rotor gauge (SRG) as the only possible method. This measurement device is tritium compatible without any adjustments and the compatibility with cryogenic temperatures has been approved in pretests with measurements inside a liquid nitrogen bath [Wyd22]. The Cryogenic Viscosity Measurement Apparatus (Cryo-

ViMA) is based on a spinning rotor gauge from MKS Instruments and cooled with a cold-gas system utilizing nitrogen as coolant. The setup has been calibrated with helium and tested with hydrogen and deuterium, to see if any systematic effects occur which would disturb the measurement or reduce its accuracy. From all studies concerning uncertainties of the measurement including isotopic purity, dimensions of the SRG, deceleration rate, pressure, temperature and calibration factor, it has been shown that the two main contributions come from the radius of the rotating sphere and the temperature measurement, caused by a temperature gradient around the sphere.

For hydrogen, it was observed that the ab initio calculated viscosity by [MHH10] has a slightly flatter temperature dependence than the measured viscosity, but stays within the uncertainty of the measurement over the whole temperature range. For deuterium, where the literature values are calculated with an empirical equation by [AMW87], this tilt of the measured values compared to the literature is 35 % smaller than for H_2 measurement and the theoretical values are also within the uncertainty of the measurement. With this result, it has been concluded that there are no major systematic effects which had not been accounted for, and the measurement can be trusted within its uncertainty of 2.5 %. The measurements with tritium were done in two steps, first the burn-in phase measurement, where it was expected that radiochemical effects cause impurities which influence the accuracy of the measurement. Through these effects methane and other hydrocarbons are built, but the rate with which impurities are produced decreases with tritium exposure time. For the second step, tritium with a purity of 99 % is used, resulting in the final measurement for the tritium viscosity.

It has been shown in section 6.4 that the kinetic gas theory equation can be adjusted to the measurement with deviations in the sub-percent region. However, currently used extrapolated viscosity values show deviations to the measurement of 4 % to 12 % in the temperature range from 100 K to 300 K, even with correction factors arising from the comparison of extrapolated deuterium viscosity values to measured ones. It has been shown that such a high deviation cannot be explained by small fractions of impurities in the region of 1 % to 2 %. Impurities through hydrogen or deuterium cause deviations well below the uncertainty limit of the measurement. Other impurities like ^{3}He or methane have a higher impact, but are not present in a significant amount. This indicates that there are some effects, most likely quantum mechanical ones, which are ignored in the current ab initio calculations or in the extrapolations, as the three hydrogen isotopologues differ in their quantum states.

With these measurements it is now possible to improve simulations concerning tritium gas flows, pumping efficiency and development, and tritium inventory management. In addition, the testbed for quantum mechanical effects and their impact on macroscopic material property calculations is increased. With tritium being not only one of the smallest molecules like hydrogen, but also being radioactive, the influence of the decay products on the transport properties can be examined. So with the end of this thesis project there is now complete empirical data and a model available for research and development that describes the T_2 viscosity within the temperature range from 100 K to 300 K within an accuracy of 2.5 %.

Outlook Currently, there are different projects planned, to improve the accuracy of the measurements, extend the temperature range and explore the feasibility to examine additional phenomenons with the Cryo-ViMA setup.

To improve the accuracy of the measurement there are different possibilities available. The Tritium Hydrogen Deuterium experiment (TriHyDe) is able to supply Cryo-ViMA with all hydrogen isotopologues and helium, however, with small adjustments it is possible to also use other noble gases for cross-calibration. In addition, the measurements can be evaluated relative to helium, giving only the quotient of the viscosities relative to helium. Thereby the main uncertainty source of the rotor radius can be deleted, improving the accuracy to approximately 1 %.

Another aspect to be optimized is the thermal cycle. The slower the thermal cycle is conducted, the smaller the temperature gradient will be within the gas. The current measurement show deviations in the measurements of the different sensors of 1 K to 4 K, depending on the temperature, which has to be accounted for in the analysis. In addition, it is planned to exchange parts of the cooling system, enabling the use of liquid nitrogen to measure the viscosity down to 77 K.

Another phenomenon which is still not fully understood are the exchange reactions between the hydrogen isotopologues. The equilibrium states are known, but the reaction rates for tritium containing reactions are not completely known. With Cryo-ViMA a setup is available, where the change of the gas composition with time is observable through the change in the deceleration rate of the rotating sphere. With knowledge of the gas composition at the beginning and end of the measurement, which can be analyzed with TriHyDe, the deceleration rate gives information of the speed at which the educts react.

These advancements not only enhance our understanding of tritium's unique transport properties but also provide a robust foundation for future experiments and theoretical work, supporting both fusion technology development and fundamental quantum mechanical studies.

A. Appendix

A.1. Reynolds number

For the setup used in this work the Reynolds number is not needed, but shall be shortly explained to understand a different type of viscometer in section 3.2 and why this type of viscometer was not chosen for the present measurements. The Reynolds number Re is used to describe the flow behavior of fluids, defined as

$$Re = \frac{\rho_g \cdot v \cdot 2r}{\mu}, \tag{A.1}$$

with ρ_g being the density of the sample gas, v being the averaged velocity of the gas flowing through, in this case, the tube with radius r and the gas viscosity μ, as based on the definition in [Jou18]. The Reynolds-number is used as an estimation to discriminate between laminar and turbulent flows. Like with the Knudsen-number, the border between those two flow types is not strictly fixed to one value, but deviates for each setup individually, depending on the boundary conditions of the part of interest.

A.2. Additional plots for the viscosity measurements

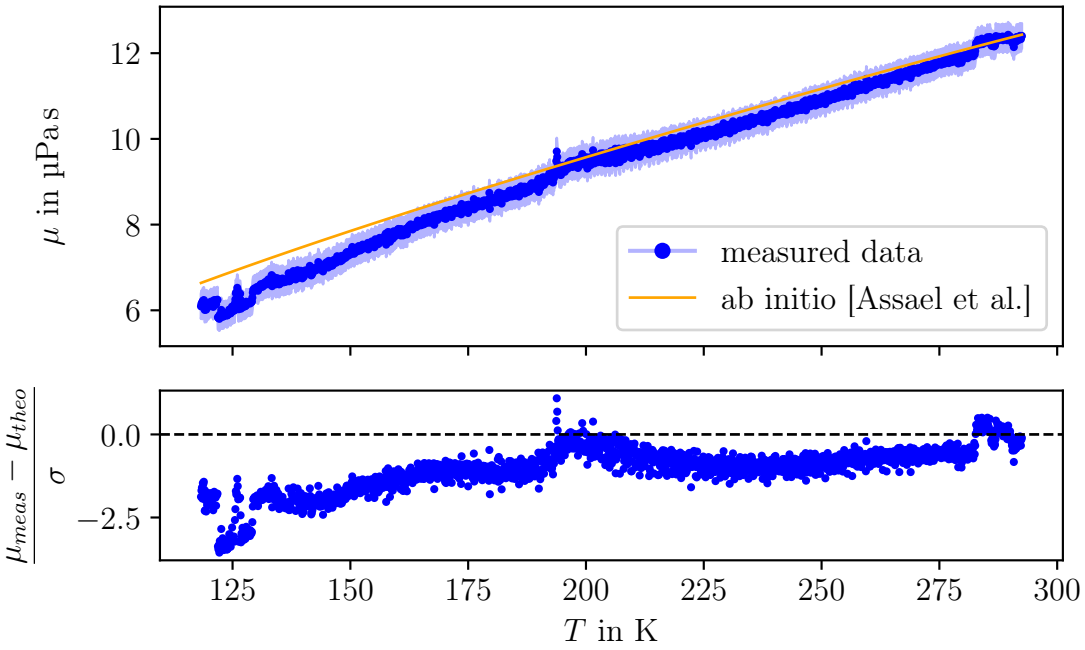

Figure A.1.: **Viscosity of deuterium from directly measured C_0 values.** The measured viscosity in blue with the uncertainty is shown together with the ab initio calculated viscosity by [AMW87] in dependence of the temperature. It can be seen that a temperatures between 125 K and 150 K the viscosity seems to drift away from the ab initio values. This behavior is described more closely in section 6.1.1.

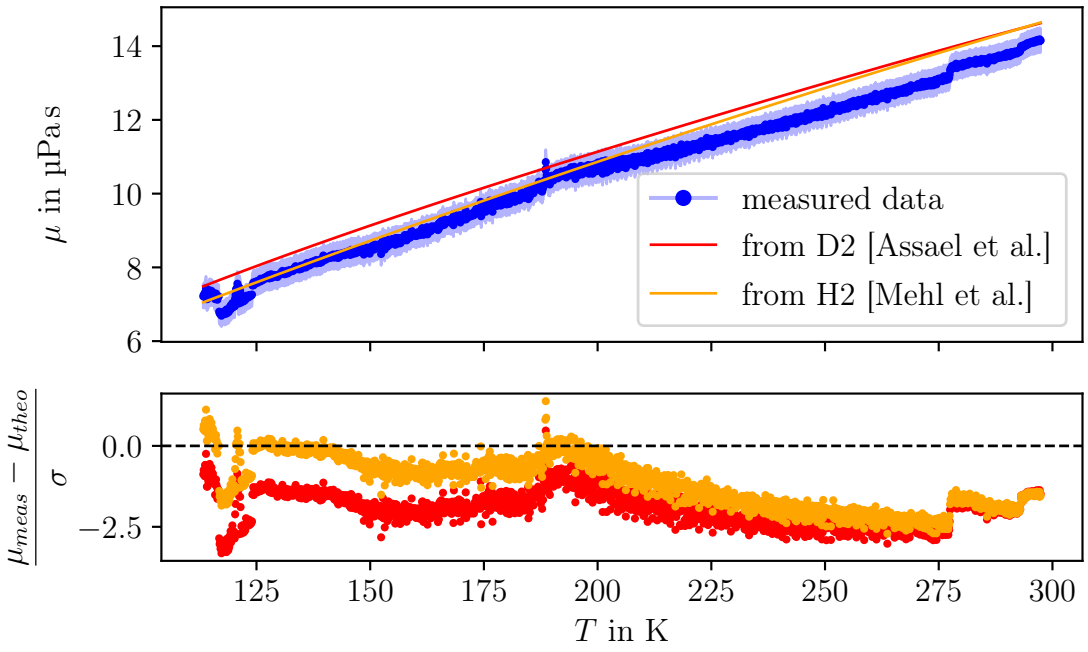

Figure A.2.: **Viscosity of tritium from directly measured C_0 values.** The measured viscosity in blue with the uncertainty is shown together with the extrapolated viscosity from ab initio values of deuterium by [AMW87] and protium by [MHH10] in dependence of the temperature.

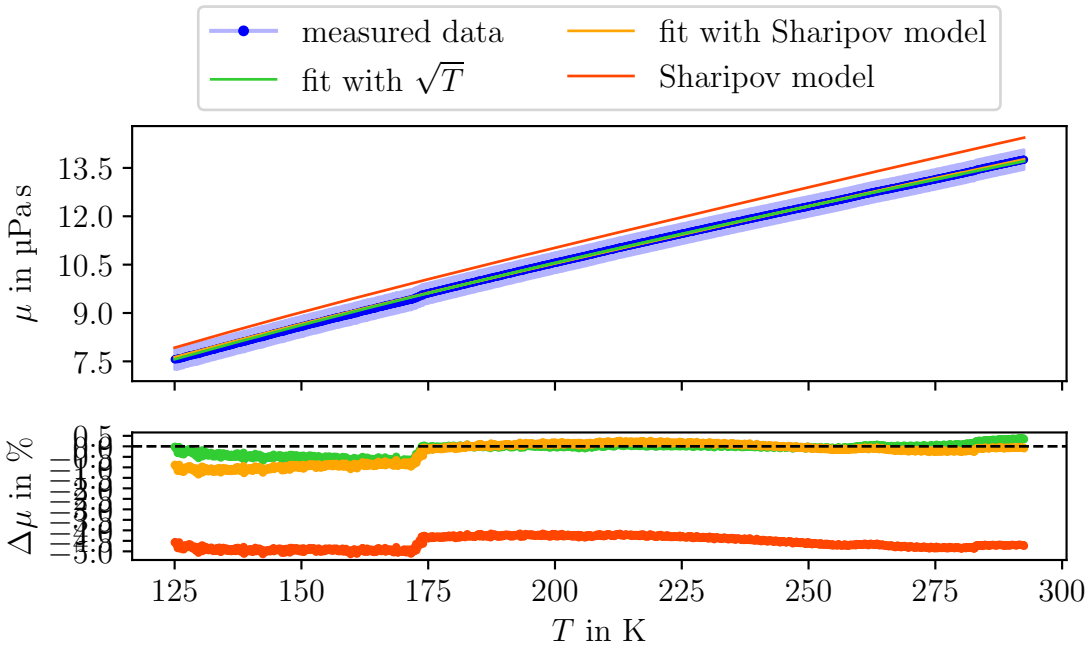

(a)

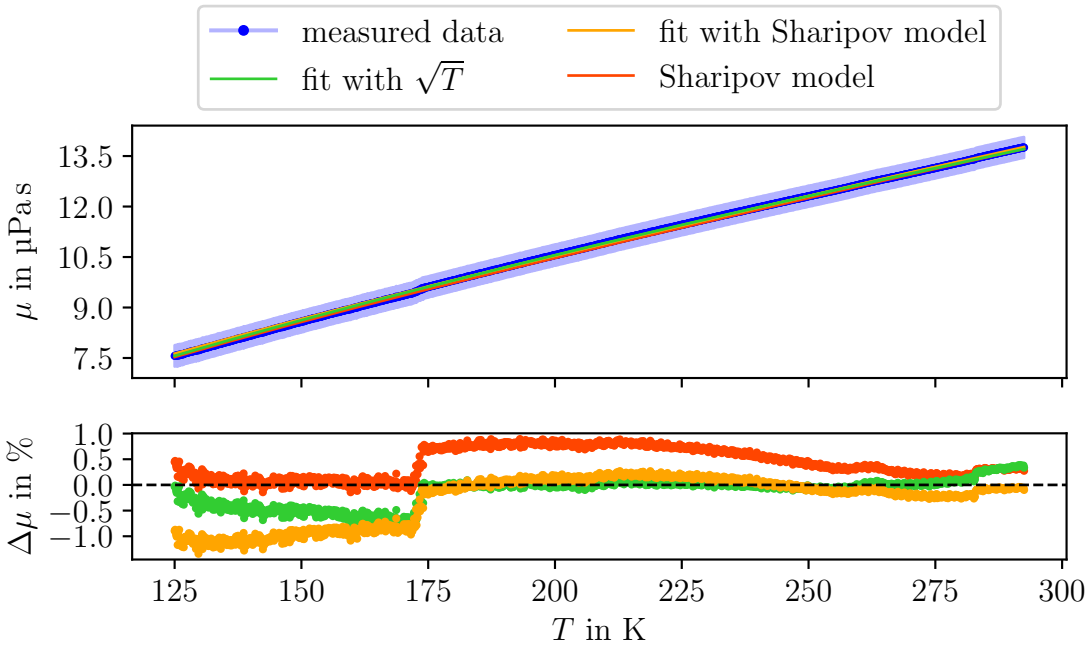

(b)

Figure A.3.: **Comparison of the theories for fitting the tritium viscosity.** Figure A.3a shows the Sharipov model with a scaling factor of 0.95 as used in the calculations for the KATRIN CD, figure A.3b shows the Sharipov model with a scaling factor of 0.9025.

A.3. Velocity slip coefficient and tangential momentum accommodation coefficient

Apart from the viscosity, with the measurements shown in chapter 6, also the velocity slip coefficient and the tangential momentum accommodation coefficient can be calculated. The velocity slip coefficient describes the behavior of a fluid close to a boundary. It is mostly needed in rarefied gases, where in contrast to continuum flow, the velocity of the boundary layer of the fluid is not set to zero, but has a finite velocity in dependence of the surface material of the boundary, the gas and the mean free path of the gas. More information on the velocity slip coefficient can be found for example in [Hua68; Sha11; Gib12]. The tangential momentum accommodation coefficient is a measure to describe the reflection of gas particles on the surface. Values close to 1 indicate that the whole tangential momentum of the gas particle is lost on the surface, leading to a complete diffuse reflection according to the Maxwell-Boltzmann distribution [AP08]. From the results in figure A.4a it seems that the velocity slip of tritium will be smaller than that of H_2 and D_2, while the tangential momentum accommodation coefficient indicates a higher amount of diffusely reflected gas particles. In addition the mass scaling, as it is done for the viscosity, does not work, as this would mean that the velocity slip coefficient of tritium should be higher than that of the other two species, while its tangential momentum accommodation coefficient should be lower. Currently it can only be suggested that this is caused by a different behavior in the surface interactions of tritium, which needs further investigation.

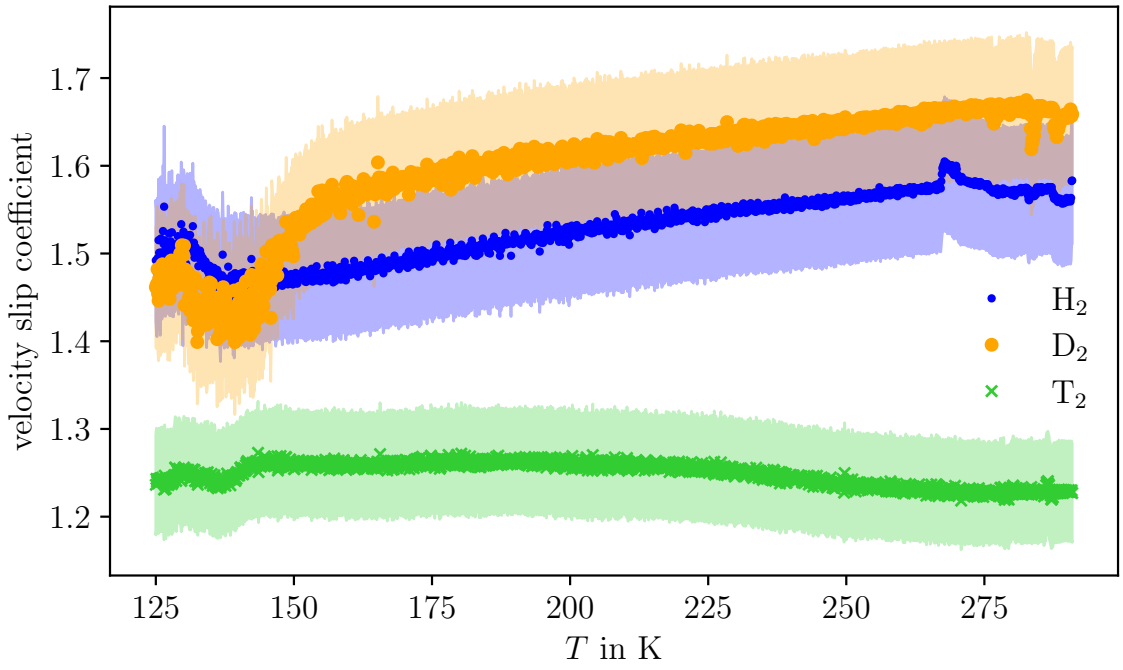

(a)

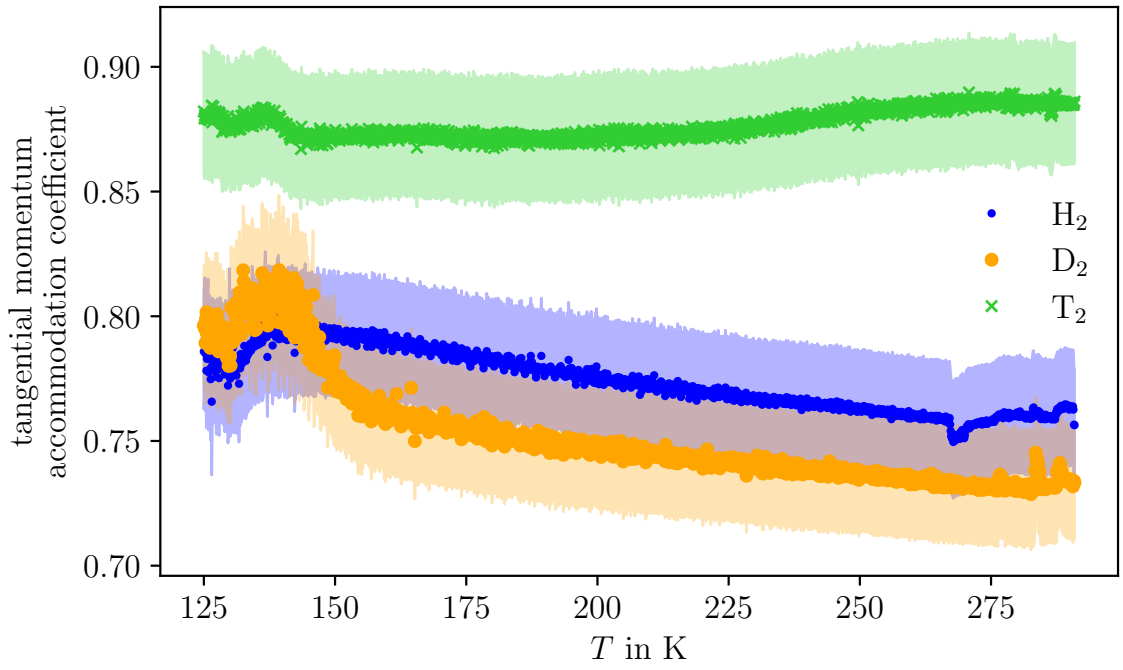

(b)

Figure A.4.: **Velocity slip coefficient and tangential momentum accomodation coefficient.** In figure A.4a the velocity slip coefficient for H_2, D_2 and T_2 is shown, while in figure A.4b the tangential momentum accommodation coefficient of the same isotopologues is shown in dependence of the temperature T. It can be seen that the values for H_2 and D_2 fit within the uncertainty limit, but tritium significantly deviates from these values. The uncertainty on these values is in the range of 5 %.

Bibliography

[Ake20] Max Aker et al. “Quantitative Long-Term Monitoring of the Circulating Gases in the KATRIN Experiment Using Raman Spectroscopy”. en. In: *Sensors* 20.17 (Jan. 2020). Number: 17 Publisher: Multidisciplinary Digital Publishing Institute, p. 4827. ISSN: 1424-8220. DOI: 10.3390/s20174827. URL: https://www.mdpi.com/1424-8220/20/17/4827 (visited on 03/22/2024).

[Ake21a] M. Aker et al. *First direct neutrino-mass measurement with sub-eV sensitivity.* eprint: 2105.08533. 2021.

[Ake21b] M. Aker et al. “The design, construction, and commissioning of the KATRIN experiment”. In: *Journal of Instrumentation* 16.08 (Aug. 2021). Publisher: IOP Publishing, T08015. DOI: 10.1088/1748-0221/16/08/t08015.

[Ake22a] M Aker et al. “Direct neutrino-mass measurement with sub-electronvolt sensitivity”. In: *Nature Physics* 18.2 (2022). Publisher: Nature Publishing Group UK London, pp. 160–166. DOI: https://doi.org/10.1038/s41567-021-01463-1.

[Ake22b] M. Aker et al. “Improved eV-scale sterile-neutrino constraints from the second KATRIN measurement campaign”. In: *Physical Review D* 105.7 (2022). Publisher: APS, p. 072004. DOI: https://doi.org/10.1103/PhysRevD.105.072004.

[Ake24] M. Aker et al. *Direct neutrino-mass measurement based on 259 days of KATRIN data.* arXiv:2406.13516. June 2024. DOI: 10.48550/arXiv.2406.13516. URL: http://arxiv.org/abs/2406.13516 (visited on 10/14/2024).

[AMW86] M. J. Assael et al. “The Viscosity and Thermal Conductivity of Normal Hydrogen in the Limit of Zero Density”. In: *Journal of Physical and Chemical Reference Data* 15.4 (Oct. 1986), pp. 1315–1322. ISSN: 0047-2689. DOI: 10.1063/1.555764. URL: https://doi.org/10.1063/1.555764 (visited on 09/02/2024).

[AMW87] M. J. Assael et al. “The Viscosity of Normal Deuterium in the Limit of Zero Density”. In: *Journal of Physical and Chemical Reference Data* 16.2 (Apr. 1987), pp. 189–192. ISSN: 0047-2689. DOI: 10.1063/1.555778. URL: https://doi.org/10.1063/1.555778 (visited on 09/02/2024).

[Ang05] J. Angrik et al. “KATRIN Design Report 2004”. In: Feb. 2005. URL: https://api.semanticscholar.org/CorpusID:117547488 (visited on 06/14/2024).

[AP08] A. Agrawal et al. “Survey on measurement of tangential momentum accommodation coefficient”. In: *Journal of Vacuum Science & Technology A* 26.4 (June 2008), pp. 634–645. ISSN: 0734-2101. DOI: 10.1116/1.2943641. URL: https://doi.org/10.1116/1.2943641 (visited on 11/18/2024).

[Ass14] Marc J Assael et al., eds. *Experimental Thermodynamics Volume IX Advances in Transport Properties of Fluids*. en. Cambridge: Royal Society of Chemistry, 2014. ISBN: 978-1-84973-677-0. DOI: 10.1039/9781782625254-FP001. URL: http://ebook.rsc.org/?DOI=10.1039/9781782625254-FP001 (visited on 07/17/2024).

[Ass18] M. J. Assael et al. "Reference Values and Reference Correlations for the Thermal Conductivity and Viscosity of Fluids". en. In: *Journal of Physical and Chemical Reference Data* 47.2 (June 2018), p. 021501. ISSN: 0047-2689, 1529-7845. DOI: 10.1063/1.5036625. URL: https://pubs.aip.org/jpr/article/47/2/021501/242182/Reference-Values-and-Reference-Correlations-for (visited on 03/20/2024).

[Atz22] S. Atzeni et al. "Breakthrough at the NIF paves the way to inertial fusion energy". en. In: *Europhysics News* 53.1 (2022). Number: 1 Publisher: EDP Sciences, pp. 18–23. ISSN: 0531-7479, 1432-1092. DOI: 10.1051/epn/2022106. URL: https://www.europhysicsnews.org/articles/epn/abs/2022/01/epn2022531p18/epn2022531p18.html (visited on 09/19/2024).

[BB01] Hans-Stephan Bosch et al. "Energie: Kernfusion als Energiequelle der Zukunft: Der International Thermonuclear Experimental Reactor ITER ist der nächste Schritt auf dem Weg zum Fusionskraftwerk". de. In: *Physikalische Blätter* 57.11 (2001), pp. 55–60. ISSN: 1521-3722. DOI: 10.1002/phbl.20010571118. URL: https://onlinelibrary.wiley.com/doi/abs/10.1002/phbl.20010571118 (visited on 09/17/2024).

[Bel20] Ian H. Bell. "Entropy Scaling of Viscosity—I: A Case Study of Propane". en. In: *Journal of Chemical & Engineering Data* 65.6 (June 2020), pp. 3203–3215. ISSN: 0021-9568, 1520-5134. DOI: 10.1021/acs.jced.0c00209. URL: https://pubs.acs.org/doi/10.1021/acs.jced.0c00209 (visited on 07/30/2024).

[BM55] E. W. Becker et al. "Die Zähigkeit von HD und He3 zwischen 14 K und 20 K". In: *Zeitschrift für Physik* 140.5 (Sept. 1955). Publisher: Springer Science and Business Media LLC, pp. 535–539. DOI: 10.1007/bf01337559.

[Bor08] B. Bornschein. "Determination of Neutrino Mass from Tritium Beta Decay". In: *Fusion Science and Technology* 54.1 (July 2008). Publisher: American Nuclear Society _eprint: https://doi.org/10.13182/FST54-59, pp. 59–66. ISSN: 1536-1055. DOI: 10.13182/FST54-59. URL: https://doi.org/10.13182/FST54-59 (visited on 11/08/2024).

[Bor26] Max Born. "Zur Quantenmechanik der Stoßvorgänge". de. In: *Zeitschrift für Physik* 37.12 (Dec. 1926), pp. 863–867. ISSN: 0044-3328. DOI: 10.1007/BF01397477. URL: https://doi.org/10.1007/BF01397477 (visited on 09/16/2024).

[BS52] E. W. Becker et al. "Difference in Viscosity of *Ortho* - and *Para* -Hydrogen at Low Temperatures". en. In: *Physical Review* 87.3 (Aug. 1952), pp. 525–525. ISSN: 0031-899X. DOI: 10.1103/PhysRev.87.525. URL: https://link.aps.org/doi/10.1103/PhysRev.87.525 (visited on 03/20/2024).

[BS64] H. BRENNER et al. “SLOW VISCOUS ROTATION OF A SPHERE IN A CIRCULAR CYLINDER”. In: *The Quarterly Journal of Mechanics and Applied Mathematics* 17.1 (Feb. 1964), pp. 55–63. ISSN: 0033-5614. DOI: 10.1093/qjmam/17.1.55. URL: https://doi.org/10.1093/qjmam/17.1.55 (visited on 06/25/2024).

[Bsc18] Sabine Bschorer. “Grundbegriffe”. In: *Technische Strömungslehre: Lehr- und Übungsbuch*. Ed. by Sabine Bschorer. Wiesbaden: Springer Fachmedien, 2018, pp. 1–32. ISBN: 978-3-658-20037-4. DOI: 10.1007/978-3-658-20037-4_1. URL: https://doi.org/10.1007/978-3-658-20037-4_1 (visited on 12/04/2024).

[BTL97] J.A. Bentz et al. “The spinning rotor gauge: measurements of viscosity, velocity slip coefficients, and tangential momentum accommodation coefficients for N2 and CH4”. en. In: *Vacuum* 48.10 (Oct. 1997), pp. 817–824. ISSN: 0042207X. DOI: 10.1016/S0042-207X(97)00031-6. URL: https://linkinghub.elsevier.com/retrieve/pii/S0042207X97000316 (visited on 03/20/2024).

[Bul93] NM Bulgakova et al. “Study of a diffusion pump ejector”. In: *Vacuum*. Special Issue Selected Proceedings of the 12th International Vacuum Congress (IVC-12) 8th International Conference on Solid Surfaces (ICSS-8) 44.5 (May 1993), pp. 749–752. ISSN: 0042-207X. DOI: 10.1016/0042-207X(93)90140-6. URL: https://www.sciencedirect.com/science/article/pii/0042207X93901406 (visited on 09/02/2024).

[CDL19] Claude Cohen-Tannoudji et al. *Quantenmechanik. Band 1*. ger. Trans. by Joachim Streubel et al. 5. Auflage. De Gruyter Studium. Berlin Boston: De Gruyter, 2019. ISBN: 978-3-11-063873-8 978-3-11-062600-1.

[Cer00] Carlo Cercignani. *Rarefied gas dynamics: from basic concepts to actual calculations*. eng. Cambridge texts in applied mathematics. Cambridge: Cambridge University Press, 2000. ISBN: 978-0-521-65992-5 978-0-521-65008-3.

[Cha16] Sydney Chapman. “VI. On the law of distribution of molecular velocities, and on the theory of viscosity and thermal conduction, in a non-uniform simple monatomic gas”. en. In: *Philosophical Transactions of the Royal Society of London. Series A, Containing Papers of a Mathematical or Physical Character* 216.538-548 (Jan. 1916), pp. 279–348. ISSN: 0264-3952, 2053-9258. DOI: 10.1098/rsta.1916.0006. URL: https://royalsocietypublishing.org/doi/10.1098/rsta.1916.0006 (visited on 10/17/2024).

[Cis20] F. Cismondi et al. “Progress of the conceptual design of the European DEMO breeding blanket, tritium extraction and coolant purification systems”. In: *Fusion Engineering and Design* 157 (Aug. 2020). Publisher: Elsevier BV, p. 111640. DOI: 10.1016/j.fusengdes.2020.111640.

[Cla23] Michel Claessens. *ITER: The Giant Fusion Reactor: Bringing a Sun to Earth*. en. Copernicus Books. ISSN: 2731-8982, 2731-8990. Cham: Springer International Publishing, 2023. ISBN: 978-3-031-37761-7 978-3-031-37762-4. DOI: 10.1007/978-3-031-37762-4. URL: https://link.springer.com/10.1007/978-3-031-37762-4 (visited on 09/17/2024).

[Cle] Daniel Clery. “European fusion reactor sets record for sustained energy”. In: (). URL: h%20t%20t%20p%20s%20:%20/%20/%20w%20w%20w%20.%20s%20c%20i%20e%20n%20c%20e%20.%20o%20r%20g.

[Cor58] J. M. J. Coremans et al. “The viscosity of gaseous He, Ne, H2 and D2 below 80°K”. In: *Physica* 24.6 (Jan. 1958), pp. 557–576. ISSN: 0031-8914. DOI: 10.1016/S0031-8914(58)80070-1. URL: https://www.sciencedirect.com/science/article/pii/S0031891458800701 (visited on 07/15/2024).

[Cri06] Ioana-R. Cristescu et al. “Tritium inventory assessment for ITER using TRIMO”. In: *Fusion Engineering and Design*. Proceedings of the Seventh International Symposium on Fusion Nuclear Technology 81.1 (Feb. 2006), pp. 763–769. ISSN: 0920-3796. DOI: 10.1016/j.fusengdes.2005.06.367. URL: https://www.sciencedirect.com/science/article/pii/S0920379605005831 (visited on 09/18/2024).

[Cri20] Ion Cristescu et al. “Overview of the Tritium Technologies for the EU DEMO Breeding Blanket”. In: *Fusion Science and Technology* 76.4 (May 2020). Publisher: Informa UK Limited, pp. 446–457. DOI: 10.1080/15361055.2020.1716456.

[Dem24] Leszek Demkowicz. *Mathematical theory of finite elements*. eng. Computational science and engineering 28. Philadelphia, PA: SIAM, Society for Industrial and Applied Mathematics, 2024. ISBN: 978-1-61197-772-1.

[DG13] Christian Day et al. “The Direct Internal Recycling concept to simplify the fuel cycle of a fusion power plant”. In: *Fusion Engineering and Design*. Proceedings of the 27th Symposium On Fusion Technology (SOFT-27); Liège, Belgium, September 24-28, 2012 88.6 (Oct. 2013), pp. 616–620. ISSN: 0920-3796. DOI: 10.1016/j.fusengdes.2013.05.026. URL: https://www.sciencedirect.com/science/article/pii/S0920379613004663 (visited on 09/19/2024).

[Doe02] L. Doerr et al. “Upgrade of the Isotope Separation System at the Tritium Laboratory Karlsruhe”. In: *Fusion Science and Technology* 41.3P2 (May 2002). Publisher: American Nuclear Society _eprint: https://doi.org/10.13182/FST02-A22765, pp. 1155–1159. ISSN: 1536-1055. DOI: 10.13182/FST02-A22765. URL: https://doi.org/10.13182/FST02-A22765 (visited on 11/14/2024).

[Ede04] Dörrenberg Edelstahl. *Material Properties*. Nov. 2004. URL: https://www.finemetal.ro/wp-content/uploads/2020/09/1.4034-R45-X46Cr13-1.pdf (visited on 08/09/2024).

[Egg92] Rolf Eggenberger et al. “Ab initio calculation of the shear viscosity of neon in the liquid and hypercritical state over a wide pressure and temperature range”. In: *Chemical Physics* 164.3 (Aug. 1992), pp. 321–329. ISSN: 0301-0104. DOI: 10.1016/0301-0104(92)87071-G. URL: https://www.sciencedirect.com/science/article/pii/030101049287071G (visited on 10/29/2024).

[Fam24] Francesca R. Famà et al. “Thermodynamic and economic analyses of the retrofit of existing electric power plants with fusion reactors”. In: *Energy Conversion and Management: X* 23 (July 2024), p. 100668. ISSN: 2590-1745. DOI: 10.1016/j.ecmx.2024.100668. URL: https://www.sciencedirect.com/science/article/pii/S2590174524001466 (visited on 10/22/2024).

[Fie92] A Fiege. *Tritium.* 5055. Publication Title: Kernforschungszentrum Karlsruhe. 1992.

[Fre85] J. K. Fremerey. “The spinning rotor gauge”. In: *Journal of Vacuum Science & Technology A* 3.3 (May 1985), pp. 1715–1720. ISSN: 0734-2101. DOI: 10.1116/1.573007. URL: https://doi.org/10.1116/1.573007 (visited on 03/28/2024).

[Fri20] Fabian Ruben Friedel. “Ion and plasma systematics during the first KATRIN neutrino mass measurements”. PhD Thesis. Karlsruher Institut für Technologie (KIT), 2020. DOI: 10.5445/IR/1000126837. URL: https://publikationen.bibliothek.kit.edu/1000126837 (visited on 11/14/2024).

[FW23] Johann Fischer et al. “On the history of key empirical intermolecular potentials”. In: *Fluid Phase Equilibria* 573 (Oct. 2023), p. 113876. ISSN: 0378-3812. DOI: 10.1016/j.fluid.2023.113876. URL: https://www.sciencedirect.com/science/article/pii/S0378381223001565 (visited on 07/30/2024).

[Geb18] Christof Gebhardt. *Praxisbuch FEM mit ANSYS Workbench: Einführung in die lineare und nichtlineare Mechanik.* ger. 3., aktualisierte Auflage. München: Hanser, 2018. ISBN: 978-3-446-45001-1.

[Gi20] Keii Gi et al. “Potential contribution of fusion power generation to low-carbon development under the Paris Agreement and associated uncertainties”. In: *Energy Strategy Reviews* 27 (Jan. 2020), p. 100432. ISSN: 2211-467X. DOI: 10.1016/j.esr.2019.100432. URL: https://www.sciencedirect.com/science/article/pii/S2211467X19301257 (visited on 09/19/2024).

[Gib12] Livio Gibelli. “Velocity slip coefficients based on the hard-sphere Boltzmann equation”. In: *Physics of Fluids* 24.2 (Feb. 2012), p. 022001. ISSN: 1070-6631. DOI: 10.1063/1.3680873. URL: https://doi.org/10.1063/1.3680873 (visited on 11/18/2024).

[Gil80] John T. Gill. “Effect of container preparation on the growth of protium and methane impurities into tritium gas”. In: *Journal of Vacuum Science and Technology* 17.2 (Mar. 1980), pp. 645–654. ISSN: 0022-5355. DOI: 10.1116/1.570532. URL: https://doi.org/10.1116/1.570532 (visited on 03/22/2024).

[Glu00] M Glugla et al. “Experience gained during the modification of the Caprice system to Caper”. In: *Fusion Engineering and Design* 49-50 (Nov. 2000), pp. 811–816. ISSN: 0920-3796. DOI: 10.1016/S0920-3796(00)00206-4. URL: https://www.sciencedirect.com/science/article/pii/S0920379600002064 (visited on 09/18/2024).

[Glu88] M. Glugla et al. “On the Synthesis, Selfradiolysis, and Catalytic Decomposition of Tritiated Ammonia and Methane”. In: *Fusion Technology* 14.2P2A (Sept. 1988). Publisher: Taylor & Francis _eprint: https://doi.org/10.13182/FST88-A25213, pp. 683–688. ISSN: 0748-1896. DOI: 10.13182/FST88-A25213. URL: https://doi.org/10.13182/FST88-A25213 (visited on 03/22/2024).

[GME83] J. T. Gill et al. “Chemically polished stainless steel tubing for tritium service”. In: *Journal of Vacuum Science & Technology A* 1.2 (Apr. 1983), pp. 869–873. ISSN: 0734-2101. DOI: 10.1116/1.572012. URL: https://doi.org/10.1116/1.572012 (visited on 03/22/2024).

[Gro06] Horst-W. Grollius. *Grundlagen der Pneumatik: mit 16 Tafeln und 20 Aufgaben*. ger. München Wien: Fachbuchverl. Leipzig im Hanser-Verl, 2006. ISBN: 978-3-446-22977-8.

[Grö15] Robin Größle. “Das TapIR Experiment - IR-Absorptionsspektren flüssiger Wasserstoffisotopologe”. German. PhD Thesis. Karlsruher Institut für Technologie (KIT), 2015. DOI: 10.5445/IR/1000055643.

[HCB64] Joseph O. Hirschfelder et al. *The Molecular Theory of Gases and Liquids*. en. Google-Books-ID: dvvcEAAAQBAJ. John Wiley & Sons, Jan. 1964. ISBN: 978-0-471-40065-3.

[HD86] A. A. Haasz et al. “Synergistic methane formation kinetics for hydrogen impact on carbon”. In: *The Journal of Chemical Physics* 85.6 (Sept. 1986), pp. 3293–3299. ISSN: 0021-9606. DOI: 10.1063/1.450999. URL: https://doi.org/10.1063/1.450999 (visited on 03/22/2024).

[Hei19] Florian Heizmann. “Analysis tools and methods for tritium data taking with the KATRIN experiment”. PhD Thesis. Karlsruher Institut für Technologie (KIT), 2019. DOI: 10.5445/IR/1000093536.

[Hil24] David Hillesheimer et al. “Four Years of Tritium Operation of the KATRIN Experiment at TLK”. In: *Fusion Science and Technology* 80.3-4 (May 2024). Publisher: Taylor & Francis _eprint: https://doi.org/10.1080/15361055.2023.2209691, pp. 465–471. ISSN: 1536-1055. DOI: 10.1080/15361055.2023.2209691. URL: https://doi.org/10.1080/15361055.2023.2209691 (visited on 04/08/2024).

[HM00] J.J. Hurly et al. “Ab initio values of the thermophysical properties of helium as standards”. en. In: *Journal of Research of the National Institute of Standards and Technology* 105.5 (Sept. 2000), p. 667. ISSN: 1044677X. DOI: 10.6028/jres.105.054. URL: https://nvlpubs.nist.gov/nistpubs/jres/105/5/j55hur.pdf (visited on 03/20/2024).

[Hu15] Xunxiang Hu et al. “Hydrogen permeation in FeCrAl alloys for LWR cladding application”. In: *Journal of Nuclear Materials* 461 (June 2015), pp. 282–291. ISSN: 0022-3115. DOI: 10.1016/j.jnucmat.2015.02.040. URL: https://www.sciencedirect.com/science/article/pii/S002231151500135X (visited on 04/09/2024).

[Hua68] A. Ben Huang. “Slip Coefficient of a Gas”. en. In: *The Physics of Fluids* 11.1 (Jan. 1968), pp. 61–63. ISSN: 0031-9171. DOI: 10.1063/1.1691779. URL: https://pubs.aip.org/pfl/article/11/1/61/894535/Slip-Coefficient-of-a-Gas (visited on 11/18/2024).

[IDV] Yu Igitkhanov et al. “A new concept for a higher burn-up fraction improvement in DEMO reactor”. In: ().

[Ili93] NV Iliasova et al. “Computational optimization of diffusion pump parameters”. In: *Vacuum*. Special Issue Selected Proceedings of the 12th International Vacuum Congress (IVC-12) 8th International Conference on Solid Surfaces (ICSS-8) 44.5 (May 1993), pp. 745–747. ISSN: 0042-207X. DOI: 10.1016/0042-207X(93)90139-2. URL: https://www.sciencedirect.com/science/article/pii/0042207X93901392 (visited on 09/02/2024).

[ITE] ITER. *Advantages of fusion*. en. URL: http://www.iter.org/sci/fusion (visited on 09/19/2024).

[Jou07] Karl Jousten. “Gauges for fine and high vacuum”. In: *CAS 2006 - CERN Accelerator School: Vacuum in Accelerators, Proceedings* (Jan. 2007).

[Jou18] Karl Jousten, ed. *Handbuch Vakuumtechnik*. de. Springer Reference Technik. Wiesbaden: Springer Fachmedien Wiesbaden, 2018. ISBN: 978-3-658-13385-6 978-3-658-13386-3. DOI: 10.1007/978-3-658-13386-3. URL: http://link.springer.com/10.1007/978-3-658-13386-3 (visited on 03/20/2024).

[KIT23] KIT. *The Tritium Laboratory Karlsruhe (TLK)*. Sept. 2023. URL: https://www.iap.kit.edu/tlk/english/index.php.

[Kle15] J. E. Klein et al. “Tritium Accountancy in Fusion Systems”. In: *Fusion Science and Technology* 67.2 (Mar. 2015). Publisher: American Nuclear Society _eprint: https://doi.org/10.13182/FST14-T44, pp. 420–423. ISSN: 1536-1055. DOI: 10.13182/FST14-T44. URL: https://doi.org/10.13182/FST14-T44 (visited on 11/26/2024).

[Kle19] Manuel Klein. “Tritium ions in KATRIN: blocking, removal and detection”. PhD Thesis. Karlsruher Institut für Technologie (KIT), 2019. DOI: 10.5445/IR/1000093526. URL: https://publikationen.bibliothek.kit.edu/1000093526 (visited on 11/14/2024).

[KN64] J Kestin et al. “Viscosity of the Isotopes of Hydrogen and their Intermolecular Force Potentials”. In: *The Physics of Fluids* 7.5 (1964), pp. 730–734. DOI: 10.1063/1.1711275.

[Kra23] Bennet Krasch. “Spectroscopic Investigations of Intermolecular Effects in the KATRIN Tritium Source Loop”. PhD Thesis. Karlsruher Institut für Technologie (KIT), 2023. DOI: 10.5445/IR/1000158844. URL: https://publikationen.bibliothek.kit.edu/1000158844 (visited on 07/23/2024).

[KRW72] J. Kestin et al. "Viscosity of the isotopes of hydrogen and their intermolecular force potentials". In: *Journal of the Chemical Society, Faraday Transactions 1: Physical Chemistry in Condensed Phases* 68.0 (1972). Publisher: Royal Society of Chemistry (RSC), p. 2316. DOI: 10.1039/f19726802316.

[Kuc18] Laura Kuckert et al. "Modelling of gas dynamical properties of the Katrin tritium source and implications for the neutrino mass measurement". In: *Vacuum* 158 (Dec. 2018), pp. 195–205. ISSN: 0042-207X. DOI: 10.1016/j.vacuum.2018.09.036. URL: https://www.sciencedirect.com/science/article/pii/S0042207X18310972 (visited on 03/20/2024).

[Kuc16] Laura Kuckert. "The windowless gaseous tritium source of the KATRIN experiment - characterisation of gas dynamical and plasma properties". PhD Thesis. Karlsruhe: Karlsruher Institut für Technologie (KIT), 2016. DOI: 10.5445/IR/1000065077. URL: http://dx.doi.org/10.5445/IR/1000065077.

[Loy96] S. K. Loyalka. "Theory of the spinning rotor gauge in the slip regime". en. In: *Journal of Vacuum Science & Technology A: Vacuum, Surfaces, and Films* 14.5 (Sept. 1996), pp. 2940–2945. ISSN: 0734-2101, 1520-8559. DOI: 10.1116/1.580248. URL: https://pubs.aip.org/jva/article/14/5/2940/242969/Theory-of-the-spinning-rotor-gauge-in-the-slip (visited on 03/20/2024).

[LSH24] Johannes Lenhard et al. "On the History of the Lennard-Jones Potential". en. In: *Annalen der Physik* 536.6 (2024), p. 2400115. ISSN: 1521-3889. DOI: 10.1002/andp.202400115. URL: https://onlinelibrary.wiley.com/doi/abs/10.1002/andp.202400115 (visited on 07/30/2024).

[LU00] L.L. Lucas et al. "Comprehensive review and critical evaluation of the half-life of tritium". en. In: *Journal of Research of the National Institute of Standards and Technology* 105.4 (July 2000), p. 541. ISSN: 1044677X. DOI: 10.6028/jres.105.043. URL: https://nvlpubs.nist.gov/nistpubs/jres/105/4/j54luc2.pdf (visited on 04/09/2024).

[Mal13] Oleg B. Malyshev et al. "Electron stimulated desorption from the 316L stainless steel as a function of impact electron energy". In: *Journal of Vacuum Science & Technology A* 31.3 (Apr. 2013), p. 031601. ISSN: 0734-2101. DOI: 10.1116/1.4798256. URL: https://doi.org/10.1116/1.4798256 (visited on 03/22/2024).

[Mar21] A. Marsteller et al. "Neutral tritium gas reduction in the KATRIN differential pumping sections". In: *Vacuum* 184 (Feb. 2021), p. 109979. ISSN: 0042-207X. DOI: 10.1016/j.vacuum.2020.109979. URL: https://www.sciencedirect.com/science/article/pii/S0042207X2030837X (visited on 10/23/2024).

[Mar21] Alexander Marsteller. "Characterization and optimization of the KATRIN tritium source". PhD Thesis. Karlsruhe: Karlsruher Institut für Technologie (KIT), 2021. DOI: 10.5445/IR/1000127553. URL: http://dx.doi.org/10.5445/IR/1000127553.

[Mat03] M. Matsuyama et al. “Non-destructive tritium measurements of Mk IIA divertor tile by BIXS”. In: *Journal of Nuclear Materials*. Plasma-Surface Interactions in Controlled Fusion Devices 15 313-316 (Mar. 2003), pp. 491–495. ISSN: 0022-3115. DOI: 10.1016/S0022-3115(02)01380-6. URL: https://www.sciencedirect.com/science/article/pii/S0022311502013806 (visited on 10/21/2024).

[Mat76] A G Mathewson. *Ion induced desorption coefficients for titanium alloy, pure aluminium and stainless steel*. Geneva, 1976. DOI: 10.17181/CERN-ISR-VA-76-5. URL: https://cds.cern.ch/record/314510 (visited on 03/22/2024).

[Max] Max-Planck-Gesellschaft. *Brennpunkte der Kernfusion*. de. URL: https://www.mpg.de/22167704/kernfusion-fusionsreaktor (visited on 09/19/2024).

[MBM07] Eric F. May et al. “Reference viscosities of H_2, CH_4, Ar, and Xe at low densities”. en. In: *International Journal of Thermophysics* 28.4 (Oct. 2007), pp. 1085–1110. ISSN: 0195-928X, 1572-9567. DOI: 10.1007/s10765-007-0198-7. URL: http://link.springer.com/10.1007/s10765-007-0198-7 (visited on 03/20/2024).

[McC90] Frederick R. W. McCourt et al. *Nonequilibrium Phenomena in Polyatomic Gases: Volume 1: Dilute Gases*. English. Oxford: Clarendon Press, Sept. 1990. ISBN: 978-0-19-855631-2.

[McC99] Frederick R. W. McCourt et al. *Nonequilibrium Phenomena in Polyatomic Gases: Volume 2: Cross-sections, Scattering, and Rarefied Gases*. English. Oxford: Clarendon Press, Apr. 1999. ISBN: 978-0-19-855648-0.

[MHH10] James B. Mehl et al. “Ab Initio Transport Coefficients of Gaseous Hydrogen”. en. In: *International Journal of Thermophysics* 31.4-5 (May 2010), pp. 740–755. ISSN: 0195-928X, 1572-9567. DOI: 10.1007/s10765-009-0697-9. URL: http://link.springer.com/10.1007/s10765-009-0697-9 (visited on 03/20/2024).

[MKF14] R. J. Mason et al. “Real viscosity effects in inertial confinement fusion target deuterium–tritium micro-implosions”. In: *Physics of Plasmas* 21.2 (Feb. 2014), p. 022705. ISSN: 1070-664X. DOI: 10.1063/1.4864641. URL: https://doi.org/10.1063/1.4864641 (visited on 10/29/2024).

[MKS09] MKS. *Spinning Rotor Vacuum Gauge - Instruction Manual*. 2009. URL: https://www.npl.washington.edu/TRIMS/sites/sand.npl.washington.edu.TRIMS/files/manuals-documentation/MKS-SRG-3-manual.pdf.

[Mor77] G. A. Morris. *Methane formation in tritium gas exposed to stainless steel*. English. Tech. rep. UCRL-52262. Lawrence Livermore National Lab. (LLNL), Livermore, CA (United States), Mar. 1977. DOI: 10.2172/7320371. URL: https://www.osti.gov/biblio/7320371 (visited on 03/22/2024).

[MRS79] J.R. Jr. McNally et al. *Fusion reactivity graphs and tables for charged particle reactions*. en. Tech. rep. ORNL/TM-6914, 5992170. Aug. 1979, ORNL/TM–6914, 5992170. DOI: 10.2172/5992170. URL: http://www.osti.gov/servlets/purl/5992170/ (visited on 10/24/2024).

[MS66] S Mathur et al. “Relations between thermal conductivity and diffusion coefficients of pure and mixed polyatomic gases”. en. In: *Proceedings of the Physical Society* 89.3 (Nov. 1966), pp. 753–764. ISSN: 0370-1328. DOI: 10.1088/0370-1328/89/3/331. URL: https://iopscience.iop.org/article/10.1088/0370-1328/89/3/331 (visited on 08/28/2024).

[NB24] Simon Niemes et al. “Speed of Sound Measurement of Hydrogen Isotopologues Containing Tritium for Reference Gas Sample Verification”. In: *Fusion Science and Technology* 80.3-4 (May 2024). Publisher: American Nuclear Society _eprint: https://doi.org/10.1080/15361055.2023.2209087, pp. 558–562. ISSN: 1536-1055. DOI: 10.1080/15361055.2023.2209087. URL: https://doi.org/10.1080/15361055.2023.2209087 (visited on 11/14/2024).

[Nie21] Simon Niemes. “Calibration of a Laser-Raman-System using gas samples of all hydrogen isotopologues for KATRIN”. PhD Thesis. Karlsruher Institut für Technologie (KIT), 2021. DOI: 10.5445/IR/1000128966.

[NIS22] NIST. *Thermophysical Properties of Fluid Systems*. Feb. 2022. URL: https://webbook.nist.gov/chemistry/fluid/ (visited on 02/09/2022).

[NYH06] Masataka Nishi et al. “Study on tritium accountancy in fusion DEMO plant at JAERI”. In: *Fusion Engineering and Design*. Proceedings of the Seventh International Symposium on Fusion Nuclear Technology 81.1 (Feb. 2006), pp. 745–751. ISSN: 0920-3796. DOI: 10.1016/j.fusengdes.2005.08.052. URL: https://www.sciencedirect.com/science/article/pii/S0920379605005818 (visited on 11/26/2024).

[Öch23] Andreas Öchsner. *Computational Statics and Dynamics: An Introduction Based on the Finite Element Method*. eng. 3rd ed. 2023. Cham: Springer International Publishing, 2023. ISBN: 978-3-031-09673-0. DOI: 10.1007/978-3-031-09673-0.

[Pád96] A. A. H. Pádua et al. “Validation of an accurate vibrating-wire densimeter: Density and viscosity of liquids over wide ranges of temperature and pressure”. en. In: *International Journal of Thermophysics* 17.4 (July 1996), pp. 781–802. ISSN: 1572-9567. DOI: 10.1007/BF01439190. URL: https://doi.org/10.1007/BF01439190 (visited on 07/18/2024).

[PBG24] Florian Priester et al. “Comparison of Three Compact Raman Systems with Excitation Laser Wavelengths of 405, 532, and 660 nm (μRA-RGB)”. In: *Fusion Science and Technology* 80.3-4 (May 2024). Publisher: American Nuclear Society _eprint: https://doi.org/10.1080/15361055.2023.2166779, pp. 571–575. ISSN: 1536-1055. DOI: 10.1080/15361055.2023.2166779. URL: https://doi.org/10.1080/15361055.2023.2166779 (visited on 10/21/2024).

[RHC98] Warren M. Rohsenow et al., eds. *Handbook of heat transfer*. en. 3rd ed. McGraw-Hill handbooks. New York: McGraw-Hill, 1998. ISBN: 978-0-07-053555-8.

[Ros16] Informationsstelle Edelstahl Rostfrei. *Rauheitsmaße bei Oberflächen von nichtrostendem Stahl*. 2016. URL: https://www.edelstahl-rostfrei.de/fileadmin/user_upload/ISER/downloads/MB_984_Rauheitsmasse.pdf (visited on 08/20/2024).

[Röt23] C. Röttele et al. “Characterization of the KATRIN cryogenic pumping section”. In: *Vacuum* 208 (Feb. 2023), p. 111699. ISSN: 0042-207X. DOI: 10.1016/j.vacuum.2022.111699. URL: https://www.sciencedirect.com/science/article/pii/S0042207X22008211 (visited on 10/23/2024).

[RV57] A.O. Rietveld et al. “Viscosity of mixtures of H2 and HD between 300 and 14 °K”. en. In: *Physica* 23.6-10 (Jan. 1957), pp. 838–842. ISSN: 00318914. DOI: 10.1016/S0031-8914(57)94957-1. URL: https://linkinghub.elsevier.com/retrieve/pii/S0031891457949571 (visited on 03/20/2024).

[RWW10] Annika Richmann et al. “Polieren optischer Präzisionsoberflächen mit Laserstrahlung”. de. In: *Deutsche Gesellschaft für angewandte Optik e.V.* (2010). ISSN: 1614-8436.

[Sch13] Magnus Schlösser et al. “Accurate calibration of the laser Raman system for the Karlsruhe Tritium Neutrino Experiment”. In: *Journal of Molecular Structure*. MOLECULAR SPECTROSCOPY AND MOLECULAR STRUCTURE 2012 1044 (July 2013), pp. 61–66. ISSN: 0022-2860. DOI: 10.1016/j.molstruc.2012.11.022. URL: https://www.sciencedirect.com/science/article/pii/S0022286012010629 (visited on 10/21/2024).

[Sch01] Uwe Schumacher. “Status and problems of fusion reactor development”. en. In: *Naturwissenschaften* 88.3 (Mar. 2001), pp. 102–112. ISSN: 1432-1904. DOI: 10.1007/s001140100214. URL: https://doi.org/10.1007/s001140100214 (visited on 09/19/2024).

[Sei19] Hendrik Seitz-Moskaliuk. “Characterisation of the KATRIN tritium source and evaluation of systematic effects”. de. PhD thesis. 2019. DOI: 10.5445/IR/1000090748. URL: https://publikationen.bibliothek.kit.edu/1000090748.

[SH11] Uwe Schumacher et al. “Nuclear Technology, 4. Nuclear Fusion”. en. In: *Ullmann’s Encyclopedia of Industrial Chemistry*. ISSN: 1435-6007 _eprint: https://onlinelibrary.wiley.com/doi/pdf/10.1002/14356007.o17_o07. John Wiley & Sons, Ltd, 2011. ISBN: 978-3-527-30673-2. DOI: 10.1002/14356007.o17_o07. URL: https://onlinelibrary.wiley.com/doi/abs/10.1002/14356007.o17_o07 (visited on 09/18/2024).

[Sha11] Felix Sharipov. “Data on the Velocity Slip and Temperature Jump on a Gas-Solid Interface”. en. In: *J. Phys. Chem. Ref. Data* 40.2 (2011).

[Sha16] Felix Sharipov. *Rarefied gas dynamics : fundamentals for research and practice*. Backup Publisher: Wiley-VCH. Weinheim: Wiley-VCH Verlag GmbH & Co. KGaA, 2016. ISBN: 3-527-41326-X 978-3-527-41326-3.

[Sha96] Felix Sharipov. “Rarefied gas flow through a long tube at any temperature ratio”. In: *Journal of Vacuum Science & Technology A: Vacuum, Surfaces, and Films* 14.4 (1996). Publisher: American Vacuum Society, pp. 2627–2635. DOI: https://doi.org/10.1116/1.579991.

[She92] R. H. Sherman et al. “Radiochemical Reaction Studies of Tritium Mixed Gases by Laser Raman Spectroscopy at TSTA”. In: *Fusion Technology* 21.2P2 (Mar. 1992). Publisher: Taylor & Francis _eprint: https://doi.org/10.13182/FST92-A29788, pp. 457–461. ISSN: 0748-1896. DOI: 10.13182/FST92-A29788. URL: https://doi.org/10.13182/FST92-A29788 (visited on 03/22/2024).

[Son16] Bo Song et al. “Ab Initio Values of the Gas Transport Properties of Hydrogen Isotopologues and Helium–Hydrogen Mixtures at Low Density”. In: *Journal of Chemical & Engineering Data* 61.5 (May 2016). Publisher: American Chemical Society (ACS), pp. 1910–1916. DOI: 10.1021/acs.jced.6b00076.

[Sou86] P. C. Souers. *Hydrogen Properties for Fusion Energy*. en. University of California Press, Jan. 1986. ISBN: 978-0-520-05500-1.

[Sta12] Weston M. Stacey. *Fusion Plasma Physics*. en. John Wiley & Sons, Oct. 2012. ISBN: 978-3-527-41134-4.

[TD21] Tim Teichmann et al. “Particle Simulation of Linear Diffusion Pumps for DEMO Torus Exhaust Pumping”. en. In: *Fusion Engineering and Design* 169 (Aug. 2021), p. 112694. ISSN: 09203796. DOI: 10.1016/j.fusengdes.2021.112694. URL: https://linkinghub.elsevier.com/retrieve/pii/S0920379621004701 (visited on 09/02/2024).

[Tek96] P. Tekasakul et al. “The spinning rotor gauge: Measurements of viscosity, velocity slip coefficients, and tangential momentum accommodation coefficients”. en. In: *Journal of Vacuum Science & Technology A: Vacuum, Surfaces, and Films* 14.5 (Sept. 1996), pp. 2946–2952. ISSN: 0734-2101, 1520-8559. DOI: 10.1116/1.580249. URL: https://pubs.aip.org/jva/article/14/5/2946/243003/The-spinning-rotor-gauge-Measurements-of-viscosity (visited on 03/20/2024).

[Unr13] W. Unrath. *The Vacuum Technology Book*. Vol. 2. PI 0355_2 PDE. Backup Publisher: Pfeiffer Vacuum GmbH. Asslar: Pfeiffer Vacuum GmbH, Apr. 2013.

[Unr18] W. Unrath. *Grundlagen der Vakuumtechnik*. Kat.-Nr. 199 90. Cologne: Leybold GmbH, 2018.

[VC38] A Van Itterbeek et al. “Measurements on the viscosity of hydrogen-and deuterium gas between 293 K and 14 K”. In: *Physica* 5.10 (1938). Publisher: Elsevier, pp. 938–944. DOI: https://doi.org/10.1016/S0031-8914(38)80036-7.

[VV40] A. Van Itterbeek et al. “Measurements on the viscosity of neon, hydrogen, deuterium and helium as a function of the temperature, between room temperature and liquid hydrogen temperatures”. en. In: *Physica* 7.3 (Mar. 1940), pp. 265–272. ISSN: 00318914. DOI: 10.1016/S0031-8914(40)90115-X. URL: https://linkinghub.elsevier.com/retrieve/pii/S003189144090115X (visited on 03/20/2024).

[Wel15] S. Welte et al. “Tritium Laboratory Karlsruhe: Administrative and Technical Framework for Isotope Laboratory Operation”. In: *Fusion Science and Technology* 67.3 (Apr. 2015). Publisher: Informa UK Limited, pp. 635–638. DOI: 10.13182/fst14-t98.

[Wil50] C. R. Wilke. “A Viscosity Equation for Gas Mixtures”. en. In: *The Journal of Chemical Physics* 18.4 (Apr. 1950), pp. 517–519. ISSN: 0021-9606, 1089-7690. DOI: 10.1063/1.1747673. URL: https://pubs.aip.org/jcp/article/18/4/517/314304/A-Viscosity-Equation-for-Gas-Mixtures (visited on 03/20/2024).

[Wyd22] Johanna Wydra et al. “Towards the first direct measurement of the dynamic viscosity of gaseous tritium at cryogenic temperatures”. In: *Vacuum* 203 (Sept. 2022), p. 111237. ISSN: 0042-207X. DOI: 10.1016/j.vacuum.2022.111237. URL: https://www.sciencedirect.com/science/article/pii/S0042207X2200361X (visited on 03/22/2024).

[Wyd23] Johanna Wydra et al. “ViMA – The Spinning Rotor Gauge to Measure the Viscosity of Tritium Between 77 and 300 K”. en. In: (Sept. 2023). ISSN: 1536-1055. URL: https://www.tandfonline.com/doi/epdf/10.1080/15361055.2023.2238170?needAccess=true (visited on 03/22/2024).

[Wyd24] Johanna Wydra et al. “Thermal simulations on a spinning rotor gauge to improve systematic uncertainties for viscosity measurements”. In: *Fusion Engineering and Design* 202 (May 2024), p. 114367. ISSN: 0920-3796. DOI: 10.1016/j.fusengdes.2024.114367. URL: https://www.sciencedirect.com/science/article/pii/S0920379624002205 (visited on 03/22/2024).

[Yan24] Sojeong Yang et al. “Improved reliability and availability of fundamental properties for all hydrogen isotopologues by Gaussian process regression using data from experiments and path-integral simulations”. In: *International Journal of Hydrogen Energy* 73 (July 2024), pp. 392–401. ISSN: 0360-3199. DOI: 10.1016/j.ijhydene.2024.06.054. URL: https://www.sciencedirect.com/science/article/pii/S0360319924022535 (visited on 08/05/2024).

[Zyl21] A. B. Zylstra et al. “Record Energetics for an Inertial Fusion Implosion at NIF”. In: *Physical Review Letters* 126.2 (Jan. 2021). Publisher: American Physical Society, p. 025001. DOI: 10.1103/PhysRevLett.126.025001. URL: https://link.aps.org/doi/10.1103/PhysRevLett.126.025001 (visited on 09/19/2024).

Danksagung

Zunächst möchte ich mich bei Frau Prof. Dr. Kathrin Valerius bedanken. Sie war bereit, meine Arbeit zu betreuen, und stand stets sofort zur Verfügung – sei es, um eine von mir vorgeschlagene Abschlussarbeit zu begleiten oder um mich bei der Organisation von Seminaren oder Arbeitsmitteln zu unterstützen und das trotz überquellendem Terminplan.

Herrn Professor Dr. Ulrich Husemann möchte ich danken, dass er sich als Zweitkorrektor bereit gestellt hat und dabei noch viele kleine Feinheiten zur Verbesserung der Arbeit gefunden hat.

Außerdem möchte ich mich bei Dr. Beate Bornschein bedanken. Als sie mir die Stelle zusagte, sagte sie: „Wir schreiben uns immer groß auf die Fahne Familienfreundliches KIT, und wir machen das jetzt einfach." Über die letzten Jahre hat sie zusammen mit dem ganzen Team bewiesen, dass das tatsächlich "einfach" möglich ist.

Vor allem möchte ich mich auch bei allen am TLK bedanken, nicht nur für die fachliche Unterstützung, sondern auch für die schönen Gespräche und die vielen Freizeitaktivitäten, der nächste Kino-Abend kommt bestimmt. Um das hier einmal in aller Deutlichkeit zu sagen: Beate sagte zwar "wir machen das jetzt", aber ihr habt gezeigt, dass es geht und wie es geht. Ihr habt mir nie das Gefühl gegeben, mehr oder weniger leisten zu müssen, nur weil ich Frau und Mutter bin. Stattdessen war immer nur wichtig, was ich kann und wie ich bin. Ihr seid einfach eine wahnsinns tolle Gruppe.

Ein ganz besonderer Dank geht dabei auch an Nancy Tuchscherer und Albert Braun, ohne die mein Aufbau nie so schnell maßgenau in der Box eingebaut worden wäre, an Dr. Florian Priester für die vielen CAD-Zeichnungen und das Cryo-Design meines Aufbaus, an Dr. Robin Größle und Dr. Alexander Marsteller für die vielen Diskussionen zur Datenanalyse und den Messergebnissen, an Dr. Simon Niemes und Stefan Welte für die Unterstützung, um im Dokumentations-Dschungel bei der Vorbereitung für den Einbau in die Handschuhbox nicht den Überblick zu verlieren, und natürlich an Dr. Michael Sturm. Er hat mich nicht nur als Gruppenleiter unterstützt und geführt, sondern war auch meine erste Anlaufstelle in Sachen Bauteillager (ich denke hier vor allem an die hunderte Dichtscheiben, die ich mir „geliehen" habe). Ihr seid eine großartige Gruppe, sodass ich auch jetzt noch sehr gerne zur Arbeit komme.

Zusätzlich möchte ich mich noch bei Dr. Max Aker, meinem Leidensgenossen in so vielen Lebensbereichen, bedanken für die schöne Zeit. Das Wettrennen ist vorbei, das Einhorn sitzt beim Pferdchen im Goldtopf. Ich denke, das war eine der besten Ideen, die wir hatten, um uns gegenseitig anzuspornen, trotz Umzug, Renovierung, Familie und all der kleinen Krisen nicht den Kopf zu verlieren und „einfach" fertig zu werden.

Ein weiterer Dank geht an Dr. Valentin Hermann. Wir haben uns im ersten Semester getroffen und uns gegenseitig bis hierhin begleitet. Ich denke, es gibt nicht viele Menschen, die so viel über mich wissen und so viel mit mir erlebt haben wie du. Ich bin einfach glücklich, einen Freund wie dich zu haben.

Und das bringt mich auch zu den wichtigsten Personen in meinem Leben: meiner Familie.

Meinen Eltern, die mich immer unterstützt haben, mich nie gefragt haben, ob ich wirklich Physik studieren will, sondern einfach an mich geglaubt haben und mir alles Erdenkliche ermöglicht haben, damit mein Traum wahr wird.

Meiner Schwester, die für mich meine engste Vertraute, meine beste Freundin und die unglaublichste Tante ist, die ich mir für meine Kinder wünschen könnte.

Meinen beiden Kindern, die mir gezeigt haben, was wirklich wichtig ist – einfach, weil sie da sind, weil sie sind, wie sie sind. Durch sie habe ich gelernt, auch mal „Nein“ zu sagen, wenn ich merke, dass es so nicht geht, dass es zu viel ist, und mich für das einzusetzen, was mir wichtig ist.

Und natürlich geht mein größter Dank an meinen Mann Marco Wydra. Vor über 16 Jahren haben wir zueinander gefunden. Er hat mich durch das Abitur, das Bachelor- und das Masterstudium begleitet, und er hat mir die beiden schönsten Geschenke gemacht, die es gibt. Die letzten Jahre waren anstrengend, und es gab viele Stolpersteine, um nicht zu sagen Felsbrocken auf unserem Weg, aber ich weiß, dass ich mit dir alles schaffen kann. Danke, dass du da bist.